patterns that occur around a wheel [13]. The sharp edges of the wheel cutout provide opportunities to induce flow in the horizontal plane, while the rotating wheel tends to induce circulation in the vertical plane. These effects allow the wheel to influence more flow than simply that which is seen because of its frontal area presented to the flow. The obvious improvement is aerodynamic shielding of the wheels and wheel well areas. While this is possible to some extent on rear wheels, steer rotation on the front wheels complicates the use of such treatment at the front. Experimental research has shown that decreasing the clearance between the underside and the ground and minimizing the wheel cavity decreases the total aerodynamic drag contribution from the wheel [12].

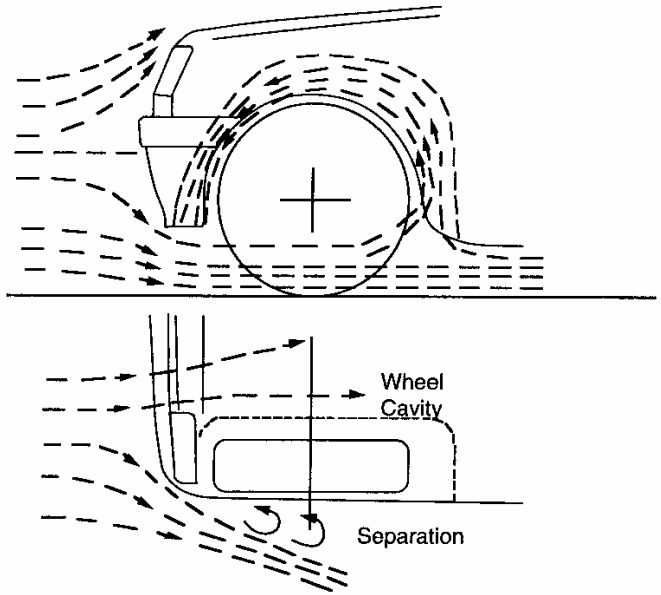

Fig 4.15 Air flow recirculation in a wheel well.

The cooling system is the last major contributor to drag. Air flow passing through the radiator impacts on the engine and the firewall, exerting its dynamic pressure as drag on the vehicle. The air flow pattern inside a typical engine compartment may be very chaotic due to the lack of aerodynamic treatment in this area. Figure 4.16 illustrates this situation [12]. With no attention to the need for air flow management, the air entering through the radiator dissipates much of its forward momentum against the vehicle compo-

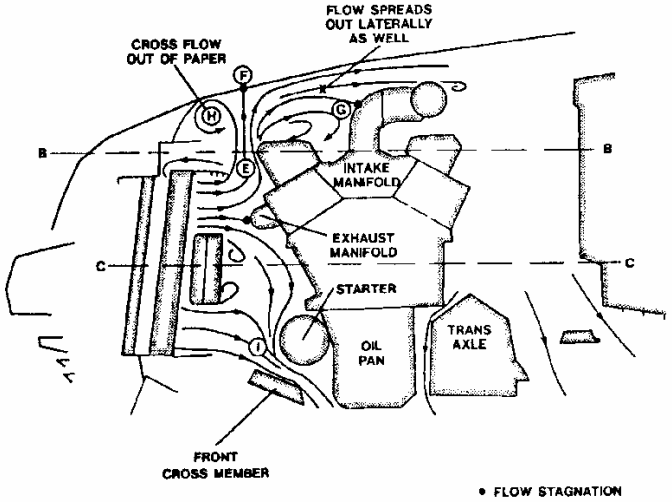

Fig 4.16 Air flow pattern inside a typical engine compartment. (Source: Williams, J., Ohler, W., Hackett, J., and Hammar, L., "Water Flow Simulation of Automotive Underhood Air Flow Phenomena," SAE Paper No. 910307, SP-855, 1991, 31 p.)

nents in the engine compartment before spilling out through the underside openings. The momentum exchange translates directly into increased drag.

Flow management in the cooling system can affect the drag coefficient by as much as 0.025 [10]. The drag contribution from this source is normally taken to be the difference in drag measured with the cooling system inlets open and covered. As seen in Figure 4.17, careful design to direct the flow (allowing it to maintain its velocity so that the static pressure remains low) can reduce the drag produced. Although these various arrangements may not be feasible within the styling theme of a given car, the potential for aerodynamic improvements is evident in the drag reductions shown. In order to reduce drag on modern cars, cooling inlet size is held to the practical minimum.

Aerodynamic Aids

Bumper Spoilers

Front bumper spoilers are aerodynamic surfaces extending downward from the bumper to block and redirect the shear flow that impacts on the underbody components. While the spoiler contributes pressure drag, at least

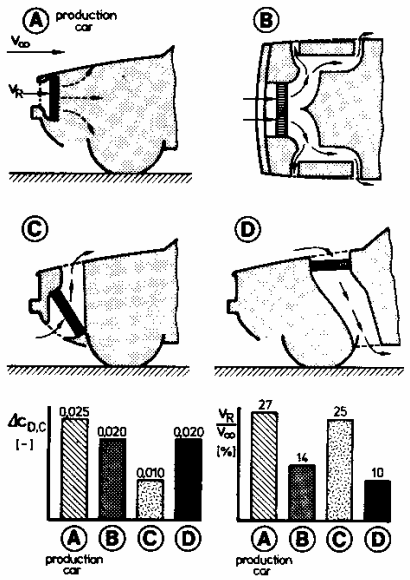

Fig. 4.17 Influence of cooling system on drag.

with a shallow depth the reduction in underbody drag is more significant. As spoiler depth is increased, eventually the increasing pressure drag outweighs further reduction in underbody drag and the overall drag increases. The low pressure produced also has the effect of reducing front-end lift.

Air Dams

Air dams are flow-blocking surfaces installed at the perimeter of the radiator to improve flow through the radiator at lower vehicle speeds. The improvement derives from the decreased pressure behind the radiator/fan, and may reduce drag by reduction of pressure on the firewall.

Deck Lid Spoilers

Spoilers and air foils on the rear deck may serve several purposes. By deflecting the air upward, as shown in Figure 4.18, the pressure is increased on the rear deck creating a down force at the most advantageous point on the vehicle to reduce rear lift. The spoilers may also serve to stabilize the vortices in the separation flow, thus reducing aerodynamic buffeting. In general, they tend to increase drag.

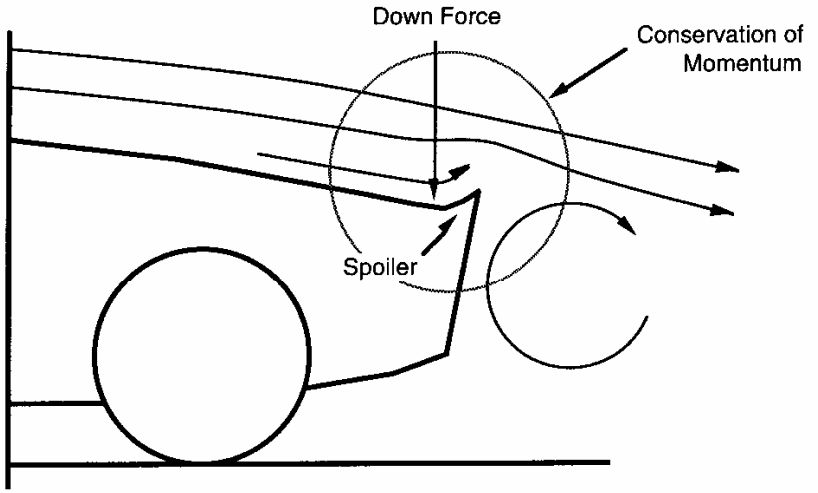

Fig. 4.18 Influence of a spoiler on flow over the rear.

Window and Pillar Treatments

Drip rails and offsets between windows and pillars on a car body are always sources of drag. Disturbance to the air flow in these regions may cause small separation zones. The disturbance to the air in the high-velocity air stream causes momentum loss which creates drag. Smooth contours are important not only for drag reduction, but also for reduction of aerodynamic noise.

Optimization

The development of automotive aerodynamics has been described as occurring in three stages [14]:

1) Adaptation of streamlined shapes from other disciplines (e.g., ship-building) at the turn of the century.

2) Application of the knowledge of fluid mechanics from aircraft aero-dynamics around the 1930s.

3) Current efforts to optimize the numerous details of the design to obtain good air flow characteristics.

The optimization is founded on the premise that the styling concept of the car is established and aerodynamic improvement can only be attempted in the

form of changes to detail in the styling. An example of the optimization is shown in Figure 4.19. The sketches show minor modifications in detail such as a change in the air dam (A), hood line (B), A-pillar shape (C) and D-pillar shape (D and E). The graph illustrates the magnitude of drag reduction obtained from various combinations of these changes. The power of drag reduction by attention to details is illustrated by the fact that an overall drag reduction of 21% is achieved.

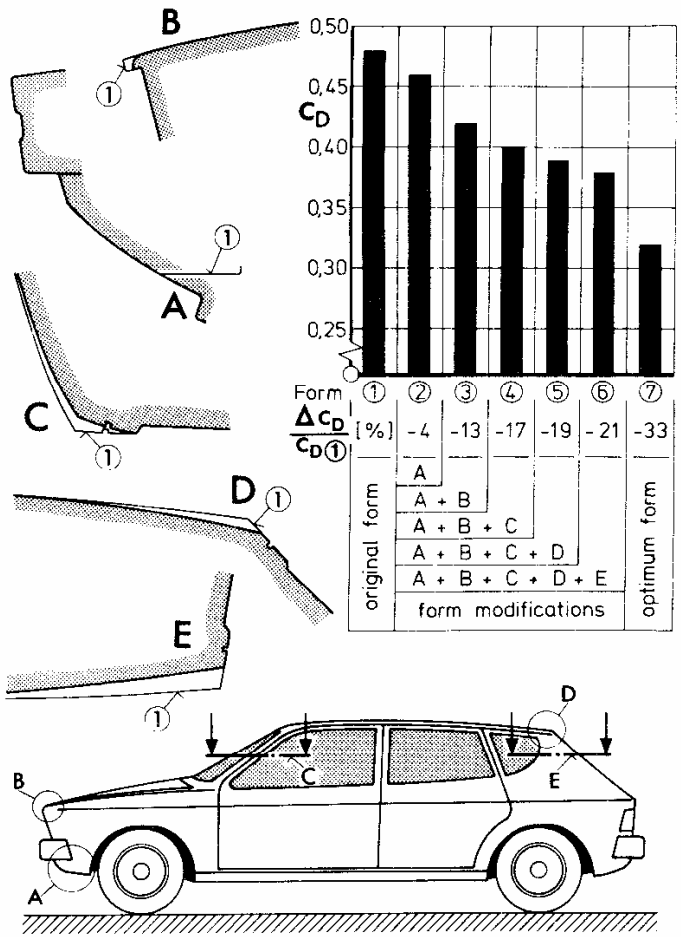

Fig. 4.19 Optimization of body detail.

Drag

Because air flow over a vehicle (or any other body for that matter) is so complex, it is necessary to develop semi-empirical models to represent the effect. Therefore, aerodynamic drag is characterized by the equation:

$$D_A = 1/2\ \rho\ V^2\ C_D\ A \qquad (4\text{-}2)$$

where:

C_D = Aerodynamic drag coefficient
A = Frontal area of the vehicle
ρ = Air density

(Note: The SAE symbol for drag, "D," is subscripted with an "A" in the text to denote it as aerodynamic drag to distinguish it from symbols used elsewhere in the text. The same convention will be used with aerodynamic lift and side force.)

The term $1/2\ \rho\ V^2$ in the above equation is the dynamic pressure of the air, and is often referred to as the "q," typically expressed in units of pounds per square foot. The drag coefficient, C_D, is determined empirically for the car. The frontal area, A, is the scale factor taking into account the size of the car. (A half-scale model of a car, which has one-fourth of the area, will have one-fourth of the drag.) Because the size of a vehicle has a direct influence on drag, the drag properties of a car are sometimes characterized by the value of "C_D A."

Air Density

The air density is variable depending on temperature, pressure, and humidity conditions. At standard conditions (59°F and 29.92 inches of Hg) the density is 0.076 lb/ft^3. As used in this equation, the air density must be expressed as mass density, obtained by dividing by the acceleration of gravity; thus the value for standard atmospheric conditions is $\rho = 0.076/32.2 = 0.00236$ lb-sec^2/ft^4. Density at other conditions can be estimated for the prevailing pressure, P_r, and temperature, T_r, conditions by the equation:

$$\rho = 0.00236\ \left(\frac{P_r}{29.92}\right)\left(\frac{519}{460 + T_r}\right) \qquad (4\text{-}3a)$$

where:

P_r = Atmospheric pressure in inches of mercury
T_r = Air temperature in degrees Fahrenheit

In the metric system the equivalent equation for air density in kg/m^3 is:

$$\rho = 1.225 \left(\frac{P_r}{101.325}\right)\left(\frac{288.16}{273.16 + T_r}\right) \quad (4\text{-}3b)$$

where:

P_r = Atmospheric pressure in kiloPascals
T_r = Air temperature in degrees Celsius

Drag Coefficient

The drag coefficient is determined experimentally from wind tunnel tests or coast down tests. The definition of C_D comes from Eq. (4-2):

$$C_D = \frac{D_A}{\frac{1}{2}\rho V^2 A} = \frac{\text{Drag force}}{(\text{Dynamic pressure})\,(\text{area})} \quad (4\text{-}4)$$

The drag coefficient varies over a broad range with different shapes. Figure 4.20 shows the coefficients for a number of shapes. In each case it is presumed that the air approaching the body has no lateral component (i.e., it is straight along the longitudinal axis of the vehicle). Note that the simple flat plate has a drag coefficient of 1.95. This coefficient means that the drag force

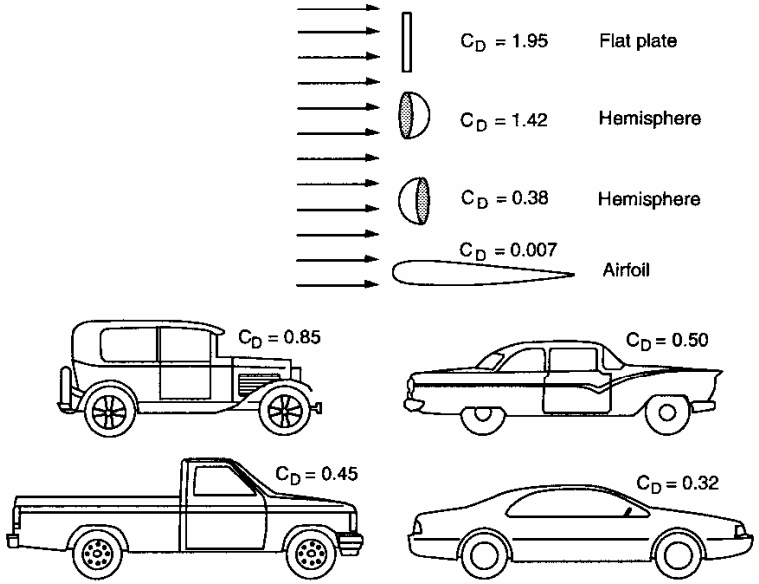

Fig. 4.20 Drag coefficients of various bodies.

is 1.95 times as large as the dynamic pressure acting over the area of the plate. The extreme drag produced by the plate results from the fact that the air spilling around the plate creates a separation area much larger than the plate itself.

In practice, a vehicle driving along a road experiences atmospheric winds in addition to the wind component arising from its speed. Atmospheric winds vary in intensity throughout the United States, with typical mean values of 10-20 mph, and gusty winds to 50 and 60 mph. The atmospheric wind will be random in direction with respect to the vehicle's direction of travel. Thus the relative wind seen by the vehicle will consist of the large component due to its speed, plus a smaller atmospheric wind component in any direction. Figure 4.21 illustrates how the relative wind will vary randomly.

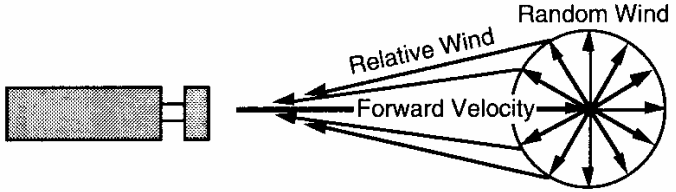

Fig. 4.21 Relative wind seen by a motor vehicle on the road.

When the atmospheric wind blows toward the vehicle a "headwind" is present, and the total velocity used in Eq. (4-2) is:

$$V = V_v + V_w \quad (4\text{-}5)$$

where:

V_v = Vehicle speed

V_w = Wind speed

Blowing in the direction of travel is a "tailwind," and the velocities are subtracted. Because the velocity is squared in Eq. (4-2), the increase in drag from a headwind is much greater than the decrease in drag from a tailwind of the same velocity.

In an average sense, the relative wind can be represented as a vector emanating from any point on the perimeter of the circle, and the average drag on the road will not be equivalent to simply the mean speed of the vehicle. Particularly important in this regard is the way in which the drag coefficient varies with a side wind component. On tractor-trailers side winds are

particularly important because they disturb the aerodynamic flow field. Figure 4.22 shows the air flow around a tractor-trailer when the relative wind is at a 30-degree angle. Note that the flow is well attached on the right side of the vehicle, but a huge separation region occurs on the downwind side. In addition to the drag created by the wind impinging on the front of the truck, the large momentum change of the wind hitting the trailer adds another large drag component. Thus with trucks and cars, the change in drag coefficient with yaw angle of the wind is very important.

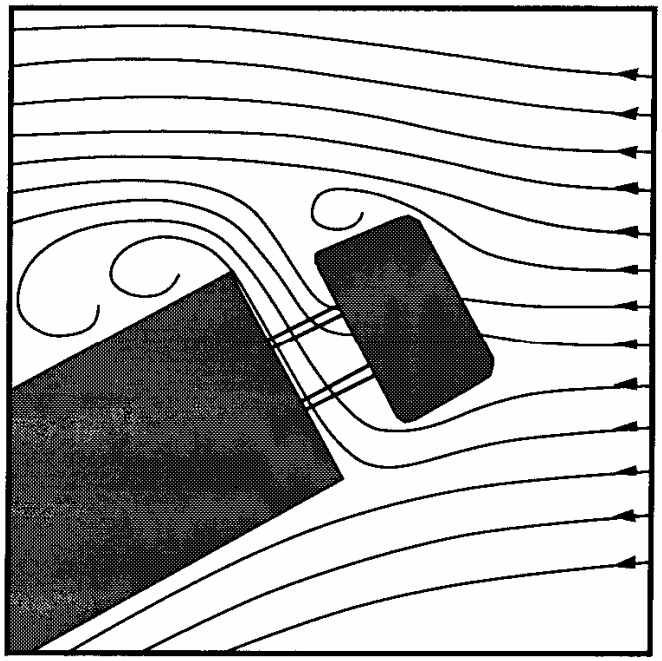

Fig. 4.22 Air flow around a tractor-semitrailer with 30-degree wind angle.

In contrast, with the much better aerodynamic design of cars, their drag coefficient is not as sensitive to yaw angle because the flow will not separate so readily. Normally, the drag coefficient increases by 5 to 10% with yaw angles in the range typical of on-road driving for passenger cars. Figure 4.23 shows the typical influence of yaw angle on the drag coefficients of several different types of vehicles.

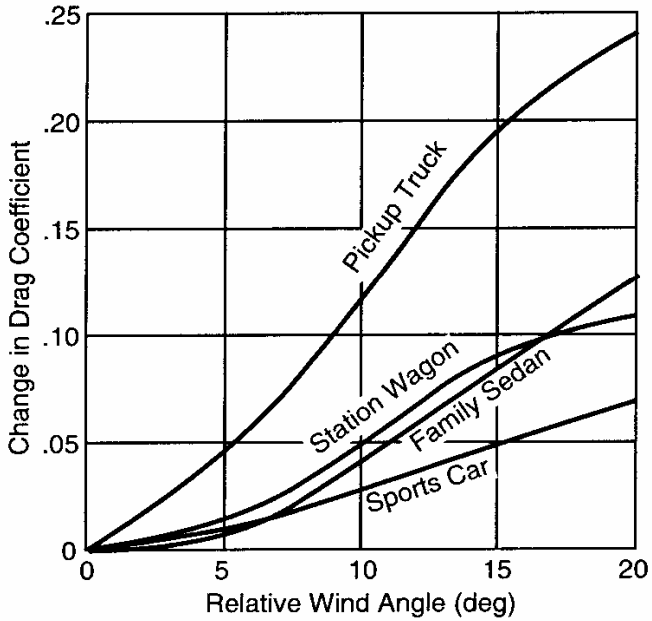

Fig. 4.23 Influence of yaw angle on drag coefficients of typical vehicle types.

Side Force

The lateral wind components will also impose a side force on the vehicle attempting to change its direction of travel. The exact effect depends both on the vehicle and the nature of the wind. In strong crosswinds, the side force is typically greater than the drag force, such that the angle of the overall wind force is much greater than the relative wind angle [15].

When the vehicle first encounters a crosswind condition on the road (a transient crosswind), the lateral force is first imposed on the front of the vehicle and may divert it in the downwind direction. The aerodynamic shape of the vehicle and even the steering system characteristics affect performance in this sense. Crosswind behavior is an important enough aspect of aerodynamics that it is discussed separately in a later section.

Under steady-state wind conditions, the side force imposed on a vehicle in a crosswind is given by:

$$S_A = 1/2\ \rho\ V^2\ C_S\ A \qquad (4\text{-}6)$$

where:

S_A = Side force
V = Total wind velocity
C_S = Side force coefficient (function of the relative wind angle)
A = Frontal area

Note that the frontal area, rather than the side area, is used in the equation. Figure 4.24 shows typical characteristics of C_S as a function of wind angle. The side force coefficient is zero at zero relative wind angle, and grows nearly linearly with the angle for the first 20 to 40 degrees. The slope of the gradient varies somewhat with vehicle type, but will typically be in the range of 0.035/deg to 0.06/deg [16].

The side force acts on the body at the center of pressure, which is normally located ahead of the center of gravity such that the vehicle is turned away from the wind. In wind tunnel measurements the side force is measured in the ground plane at the mid-wheelbase position. The difference between this location and the center of pressure results in an overturning moment and a yaw moment whenever a side force is present.

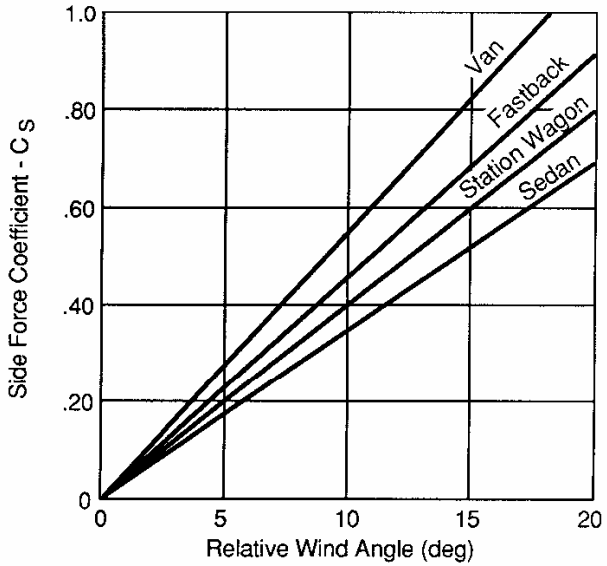

Fig. 4.24 Side force coefficient as a function of yaw angle for typical vehicles.

Lift Force

The pressure differential from the top to the bottom of the vehicle causes a lift force. These forces are significant concerns in aerodynamic optimization of a vehicle because of their influence on driving stability. The lift force is measured at the centerline of the vehicle at the center of the wheelbase. The force, L_A, is quantified by the equation:

$$L_A = 1/2\ \rho\ V^2\ C_L\ A \qquad (4\text{-}7)$$

where:

L_A = Lift force
C_L = Lift coefficient
A = Frontal area

As was seen in Figure 4.8, the lift force is dependent on the overall shape of the vehicle. At zero wind angle, lift coefficients normally fall in the range of 0.3 to 0.5 for modern passenger cars [17], but under crosswind conditions the coefficient may increase dramatically reaching values of 1 or more [18].

In aerodynamic studies the combined effect of lift and the pitching moment may be taken into account simultaneously by determining a lift coefficient for both the front and rear wheels [15]. In that case an equation similar to Eq. (4-7) is used to describe the lift effect at each axle.

Lift can have a negative impact on handling through the reduced control forces available at the tires. Front lift, which reduces steering controllability, is reduced by front bumper spoilers and by rearward inclination of front surfaces. Lift at the rear of the vehicle, which also reduces stability, is the most variable with vehicle design. In general, designs that cause the flow to depart with a downward angle at the rear of the vehicle create rear lift. Lift can be decreased by use of underbody pans, spoilers, and a change in the angle of attack of the body (a 3-degree cant on the body can decrease lift force by 40 percent).

Pitching Moment

While the lift force acts to decrease (or increase) the weight on the axles, the pitching moment acts to transfer weight between the front and rear axles. Pitching moment arises from the fact that the drag does not act at the ground plane (thus it accounts for the elevation of the drag force) and the lifting force

may not act exactly at the center of the wheelbase. Pitching moment is described by the equation:

$$PM = 1/2\ \rho\ V^2\ C_{PM}\ A\ L \qquad (4\text{-}8)$$

where:

PM = Pitching moment
C_{PM} = Pitching moment coefficient
A = Frontal area
L = Wheelbase

Because it is a moment equation, a characteristic length is needed to achieve dimensional consistency in the equation. The vehicle wheelbase is used for this purpose. A moment can be translated about without changing its effect, so there is no need for a "point of action." Most modern cars have a pitching moment in the range of 0.05 to 0.2, and it is quite sensitive to the angle of attack on the vehicle. Figure 4.25 shows how the pitching moment coefficient varies with body pitch angle on several vehicles.

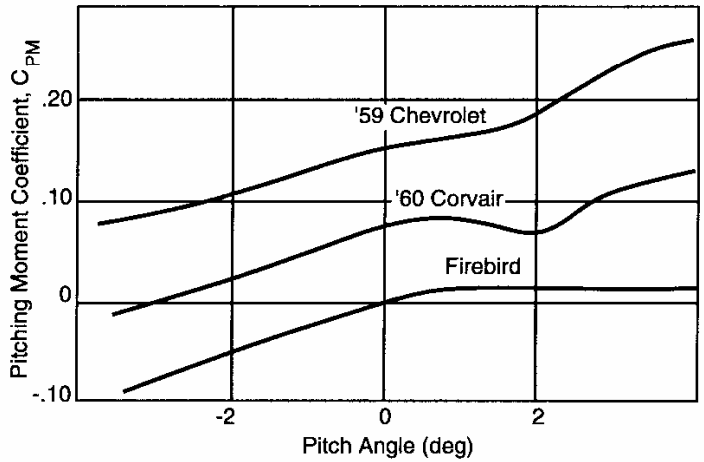

Fig. 4.25 Variation of Pitching Moment Coefficient with body pitch angle [16].

Yawing Moment

The lateral force caused by a side wind does not normally act at the mid-wheelbase position. Thus a yawing moment, YM, is produced. The yawing

moment is quantified by the equation:

$$YM = 1/2\ \rho\ V^2\ C_{YM}\ A\ L \qquad (4\text{-}9)$$

where:

YM = Yawing moment
C_{YM} = Yawing moment coefficient
A = Frontal area
L = Wheelbase

The yawing moment coefficient varies with wind direction, starting at zero with zero relative wind angle and growing almost linearly up to 20-degree angle. Figure 4.26 shows the coefficient for some typical vehicles. The slope of the coefficient at small angles ranges from 0.007/deg to 0.017/deg [18].

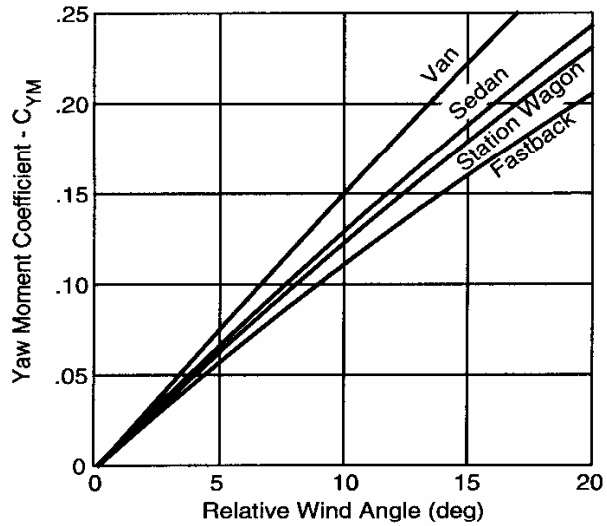

Fig 4.26 Yawing Moment Coefficient for typical vehicles.

Rolling Moment

The lateral force caused by a side wind acts at an elevated point on the vehicle. Thus a rolling moment, RM, is produced. The moment has only a minor influence on vehicle stability, depending largely on the roll steer

properties of the suspensions. The rolling moment is quantified by the equation:

$$RM = 1/2\ \rho\ V^2\ C_{RM}\ A\ L \qquad (4\text{-}10)$$

where:

RM = Rolling moment
C_{RM} = Rolling moment coefficient
A = Frontal area
L = Wheelbase

The rolling moment coefficient is sensitive to wind direction much like the yawing moment coefficient, being quite linear over the first 20 degrees of relative wind angle. The slope of the rolling moment coefficient ranges from 0.018/deg to 0.04/deg [18].

Crosswind Sensitivity

The growing sophistication of aerodynamic design in motor vehicles in combination with the increased sensitivities to crosswinds often accompanying drag reductions has stimulated interest in understanding and controlling the factors that affect behavior in a crosswind [19, 20, 21, 22]. "Crosswind sensitivity" generally refers to the lateral and yawing response of a vehicle in the presence of transverse wind disturbances which affect the driver's ability to hold the vehicle in position and on course.

Crosswind sensitivity is dependent on more than just the aerodynamic properties of the vehicle. In the literature [19] the key elements that have been identified are:

- Aerodynamic properties
- Vehicle dynamic properties (weight distribution, tire properties, and suspensions)
- Steering system characteristics (compliances, friction and torque assist)
- Driver closed-loop steering behavior and preferences

Crosswind behavior is studied using instrumented vehicles in natural random (ambient) wind conditions, under exposure to crosswind generators (fans that produce a crosswind in an experimental test area), and in driving simulators. The primary variables of interest are the yaw response, lateral

acceleration response, steering corrections when holding a specified course, and the subjective judgments of test drivers.

Good crosswind behavior is most strongly correlated with yaw rate response. Figure 4.27 illustrates the correlation that has been obtained between subjective ratings in a "gauntlet" crosswind (fans alternately blowing in opposite directions) and yaw rate response [19]. The high degree of correlation in these particular tests suggests that yaw rate response in a crosswind nearly explains all variation in subjective ratings from vehicle to vehicle. Other measures of response that correlate well with subjective ratings in order of importance are lateral acceleration at the driver's seat headrest, steering wheel displacement, and lateral acceleration.

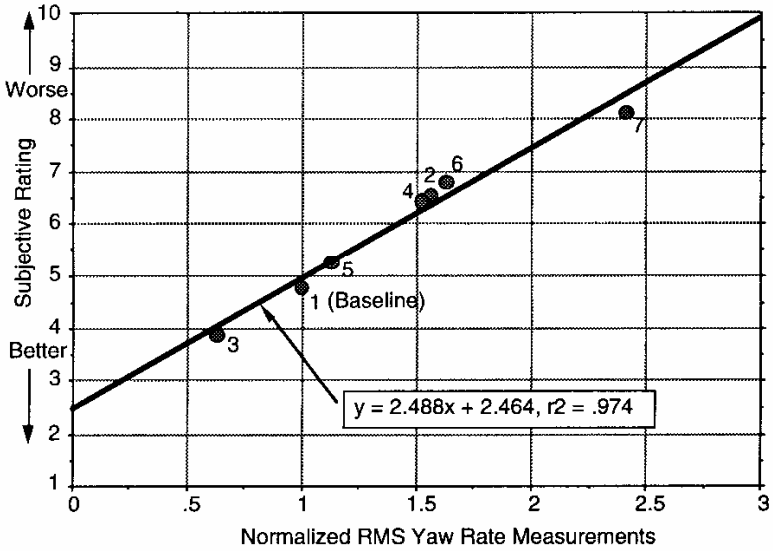

Fig. 4.27 Correlation of subjective ratings with normalized RMS yaw rate response [19].

The aerodynamic property of primary importance to crosswind sensitivity is the center of pressure (CP) location and its relative distance ahead of the vehicle's neutral steer point. The neutral steer point (NSP) is the point on the vehicle at which a lateral force produces equal sideslip angles at both front and rear axles.

The CP is the resultant action point of the combined lateral force and yaw moment reactions on the vehicle. In general, more rearward center of pressure locations, which are closer to the NSP, minimize lane deviations in a crosswind and are subjectively more acceptable. The effect of fore/aft CP location is seen in the lateral acceleration responses of three vehicles given in Figure 4.28. A forward CP location induces a large lateral acceleration response because the effective action point is near the front of the vehicle and the vehicle is turned strongly away from the wind. With a rearward CP position, the vehicle yaws less and resists the tendency to be displaced sideways.

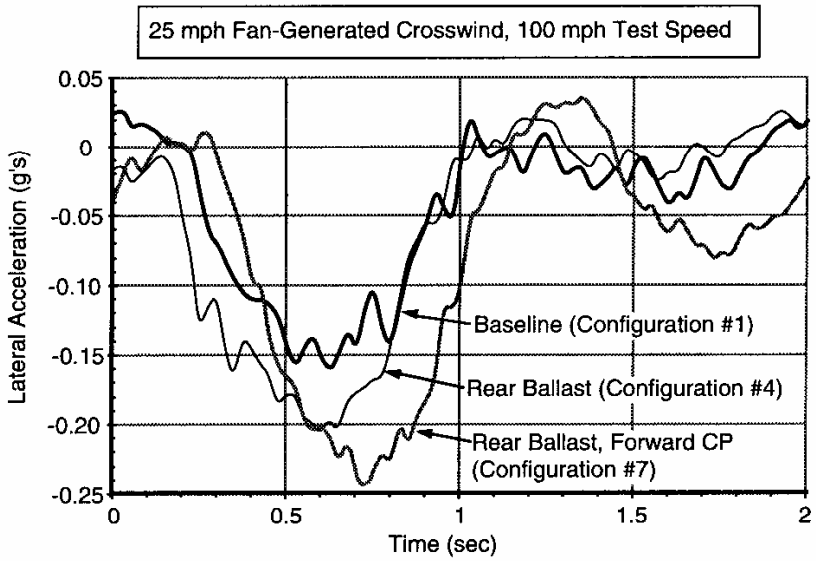

Fig. 4.28 Crosswind lateral acceleration response with variation of CP location [19].

Other vehicle dynamic properties come into play in determining how the vehicle responds to a given crosswind force. For example, the weight distribution on the front and rear axles determines the center of gravity location and the NSP location. Tire properties (such as cornering stiffness) also affect

the location of the NSP and, hence, the degree to which the vehicle resists the yawing moment disturbance from the aerodynamic side force.

A first estimate of crosswind sensitivity can be obtained from a calculation of static yaw rate response to a steady crosswind with no steering input [19]. Under static conditions, a vehicle's passive crosswind response is given by:

$$\frac{r}{\alpha_{cw}} = \frac{q\,C_y\,A}{M\,V}\left[\frac{d_{ns} + (b - L/2 + L\,C_{YM})}{d_{ns} + \zeta_d}\right] \qquad (4\text{-}11)$$

where:

- r = Yaw rate
- α_{cw} = Aerodynamic wind angle
- q = Dynamic pressure = $\rho V^2/2$
- C_y = Side force coefficient
- C_{YM} = Yawing moment coefficient
- A = Frontal area
- M = Mass of the vehicle
- V = Forward velocity
- d_{ns} = Distance from center of mass to neutral steer point
- b = Distance from front axle to center of mass
- L = Wheelbase
- ζ_d = Moment arm proportional to the tire force yaw damping moment about the neutral steer point

$$= \frac{L^2}{M\,V^2}\,\frac{C_f C_r}{(C_f + C_r)}$$

- C_f = Effective total tire cornering stiffness of the front axle
- C_r = Effective total tire cornering stiffness of the rear axle

As noted above, the neutral steer point identifies that fore/aft point on the vehicle where an external side force will not cause the vehicle to yaw. This point is affected by tire force properties, steering system compliance, suspension kinematics and weight distribution. The numerator in the second term on the right-hand side of Eq. (4-11) is the distance from the neutral steer point to the aerodynamic center of pressure. Thus a large distance between these points contributes to crosswind sensitivity.

The denominator in this same term contains the moment arm of the tire force yaw damping moment. This term can be increased to reduce crosswind sensitivity by increasing wheelbase or the effective tire cornering stiffness.

Effective tire cornering stiffness is favorably influenced directly by using tires with high cornering stiffness and by eliminating compliances in the steering or suspension which allow the vehicle to yield to the crosswind. However, the moment arm is strongly diminished by forward speed, thereby tending to increase crosswind sensitivity as speed goes up.

The static analysis discussed above may overlook certain other vehicle dynamic properties that can influence crosswind sensitivity. Roll compliance, particularly when it induces suspension roll steer effects, may play a significant role not included in the simplified analysis. Thus a more comprehensive analysis using computer models of the complete dynamic vehicle and its aerodynamic properties may be necessary for more accurate prediction of a vehicle's crosswind sensitivity.

ROLLING RESISTANCE

The other major vehicle resistance force on level ground is the rolling resistance of the tires. At low speeds on hard pavement, the rolling resistance is the primary motion resistance force. In fact, aerodynamic resistance becomes equal to the rolling resistance only at speeds of 50-60 mph. For off-highway, level ground operation, the rolling resistance is the only significant retardation force.

While other resistances act only under certain conditions of motion, rolling resistance is present from the instant the wheels begin to turn. Rolling resistance, in addition, has another undesirable property—a large part of the power expended in a rolling wheel is converted into heat within the tire. The consequent temperature rise reduces both the abrasion resistance and the flexure fatigue strength of the tire material, and may become the limiting factor in tire performance.

There are at least seven mechanisms responsible for rolling resistance:

1) Energy loss due to deflection of the tire sidewall near the contact area
2) Energy loss due to deflection of the tread elements
3) Scrubbing in the contact patch
4) Tire slip in the longitudinal and lateral directions
5) Deflection of the road surface
6) Air drag on the inside and outside of the tire
7) Energy loss on bumps

Considering the vehicle as a whole, the total rolling resistance is the sum of the resistances from all the wheels:

$$R_x = R_{xf} + R_{xr} = f_r W \qquad (4\text{-}12)$$

where:

R_{xf} = Rolling resistance of the front wheels

R_{xr} = Rolling resistance of the rear wheels

f_r = Rolling resistance coefficient

W = Weight of the vehicle

For theoretically correct calculations, the dynamic weight of the vehicle, including the effects of acceleration, trailer towing forces and the vertical component of air resistance, is used. However, for vehicle performance estimation, the changing magnitude of the dynamic weight complicates the calculations without offering significant improvements in accuracy. Furthermore, the dynamic weight transfer between axles has minimal influence on the total rolling resistance (aerodynamic lift neglected). For these reasons, static vehicle weight is sufficiently accurate for computation of rolling resistance in most cases.

All of these considerations apply, in a strict sense, only for straight-line motion. For vehicles which are subjected to lateral forces (cornering or aerodynamic loading), the direction of rolling resistance deviates from the direction of actual travel, and the tractive force must overcome the vectorial resultant of the side force and rolling resistance.

Factors Affecting Rolling Resistance

The coefficient of rolling resistance, f_r, is a dimensionless factor that expresses the effects of the complicated and interdependent physical properties of tire and ground. Establishment of standardized conditions for measurement of the effects of variables like the structure of the ground material, composition of the rubber, design elements of the tire, temperature, etc., proves difficult if not impossible. Some of the more important factors are discussed below.

Tire Temperature

Because much of the rolling resistance on paved surfaces arises from deflection and energy loss in the tire material, the temperature of the tire can

have a significant effect on the resistance experienced. In the typical situation where a tire begins rolling from a cold condition, the temperature will rise and the rolling resistance will diminish over a first period of travel. Figure 4.29 shows the relative changes in temperature and rolling resistance that will occur [18]. In the figure the tire must roll a distance of at least 20 miles before the system approaches stable operation. In typical tire tests it is therefore common to warm up the tire for 20 minutes or more before taking measurements that may be affected by the warm-up condition. For the short trips representative of much automotive travel, the tires never warm up to benefit from the lowest possible levels of rolling resistance.

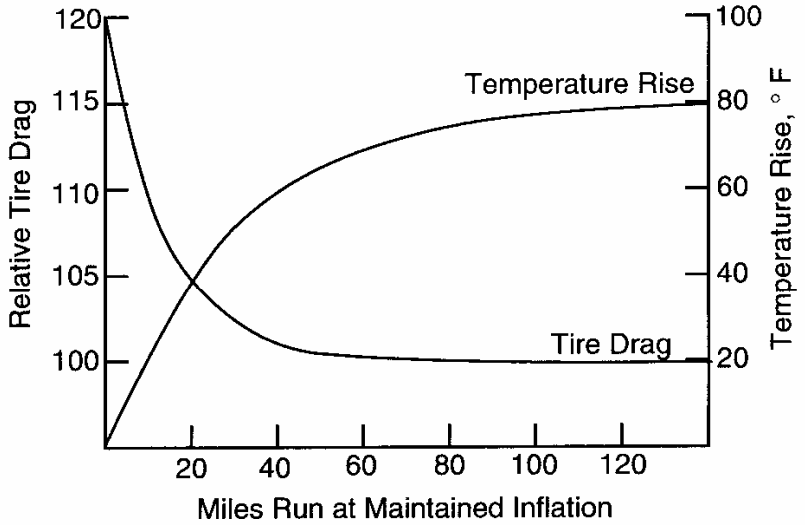

Fig. 4.29 Relative tire temperature and rolling resistance during warm-up.

Tire Inflation Pressure/Load

To a large extent, the tire inflation pressure determines the tire elasticity and, in combination with the load, determines the deflection in the sidewalls and contact region. The overall effect on rolling resistance also depends on the elasticity of the ground. Figure 4.30 shows how the coefficient changes with inflation pressure on different types of surfaces.

On soft surfaces like sand, high inflation pressures result in increased ground penetration work and therefore higher coefficients. Conversely, lower

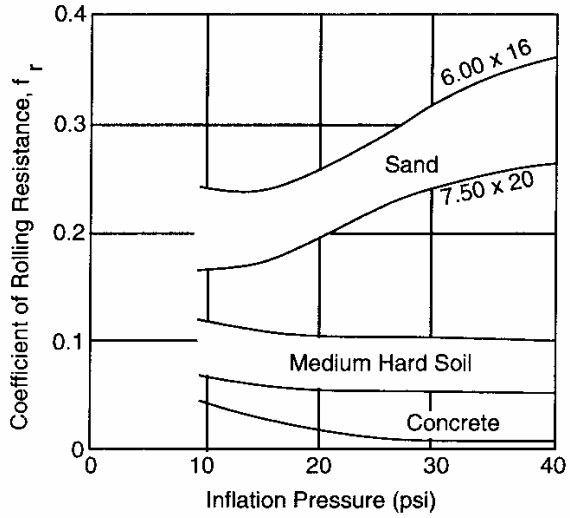

Fig. 4.30 Coefficient of rolling resistance versus inflation pressure [16].

inflation pressure, while decreasing ground penetration, increases tire-flexure work. Thus the optimum pressure depends on the surface deformation characteristics. In general, the "increased traction" obtained by lowering tire pressure on a sand surface is actually achieved through a reduction in rolling resistance.

On medium plastic surfaces such as dirt, the effects of inflation pressure on tire and ground approximately balance, and the coefficient remains nearly independent of inflation pressure. On hard (paved) surfaces, the coefficient decreases with higher inflation pressure since flexure work of the tire body will be greatly reduced.

Velocity

The coefficient is directly proportional to speed because of increased flexing work and vibration in the tire body, although the effect is small at moderate and low speeds and is often assumed to be constant for calculation. The influence of speed becomes more pronounced when speed is combined with lower inflation pressure. Figure 4.31 shows the rolling resistance versus speed for a radial, bias-belted, and bias-ply tires [23]. The sharp upturn in coefficient at high speeds is caused by a high-energy standing wave developed

in the tire carcass just behind the tire contact patch. If allowed to persist for even moderate periods of time, catastrophic failure can result. Thus formation of a standing wave is one of the primary effects limiting a tire's rated speed. Modern tires rated for high speed normally include stabilizers in the shoulder area to control the development of standing waves.

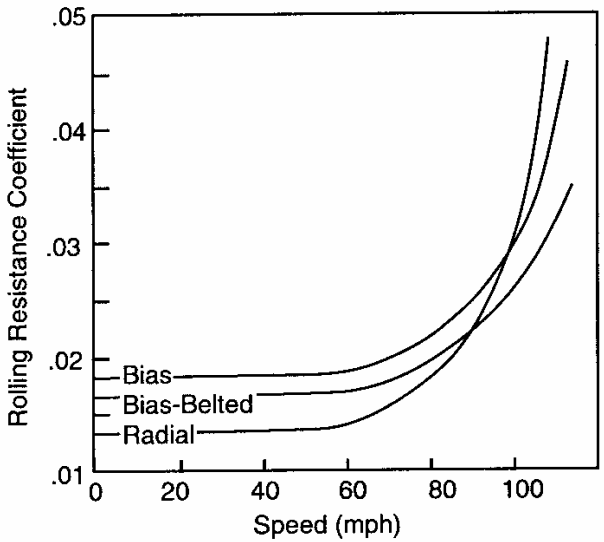

Fig. 4.31 Rolling resistance versus speed.

Tire Material and Design

The materials and thickness of both the tire sidewalls (usually expressed in plies) and the tread determine the stiffness and energy loss in the rolling tire. Figure 4.32 shows the rolling resistance of experimental tires constructed of different types of rubber in the sidewalls and tread areas [23]. The plot vividly illustrates the losses deriving from hysteresis in the tread material. Although hysteresis in the tread rubber is important for good wet traction, it degrades rolling resistance performance.

Worn-out, smooth-tread tires show coefficient values up to 20 percent lower than new tires. Fine laminations, on the other hand, increase the coefficient as much as 25 percent. The cord material in the sidewall has only a small effect, but the cord angle and tire belt properties (belted versus radial-ply tires) have a significant influence.

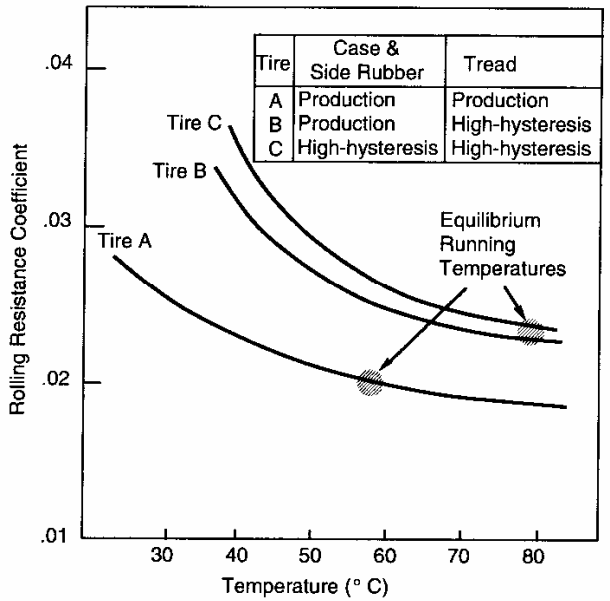

Fig. 4.32 Rolling resistance versus temperature for tires with different polymers.

Tire Slip

Wheels transferring tractive or braking forces show higher rolling resistance due to wheel slip and the resulting frictional scuffing. Cornering forces produce the same effects. Figure 4.33 shows the rolling resistance effects as a function of slip angle [23]. At a few degrees of slip, equivalent to moderate-high cornering accelerations, the rolling resistance coefficient may nearly double in magnitude. The effect is readily observed in normal driving when one will "scrub" off speed in a corner.

Typical Coefficients

The multiple and interrelated factors affecting rolling resistance make it virtually impossible to devise a formula that takes all variables into account. Before a value for rolling resistance coefficient can be chosen for a particular application, the overall degree of accuracy required for the calculations should be established.

Several equations for estimating rolling resistance have been developed over the years. Studies on the rolling loss characteristics of solid rubber tires

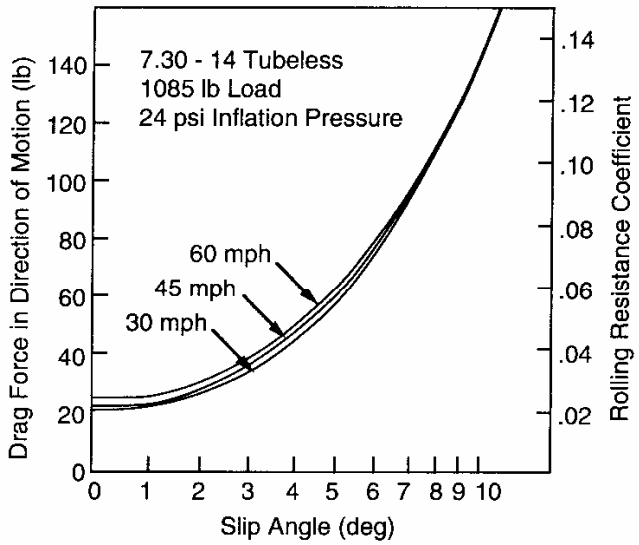

Fig. 4.33 Rolling resistance coefficient versus slip angle.

[23] led to an equation of the form:

$$f_r = \frac{R_X}{W} = C\,\frac{W}{D}\sqrt{\frac{h_t}{w}} \qquad (4\text{-}13)$$

where:

R_X = Rolling resistance force
W = Weight on the wheel
C = Constant reflecting loss and elastic characteristics of the tire material
D = Outside diameter
h_t = Tire section height
w = Tire section width

From this formulation, rolling resistance is seen to be load sensitive, increasing linearly with load. Larger tires reduce rolling resistance, as do low aspect ratios (h/w). Some confirmation of the general trends from this equation appear in the literature from studies of the rolling resistance of conventional passenger car tires of different sizes under the same load conditions [23].

Other equations for the rolling resistance coefficient for passenger car tires rolling on concrete surfaces have been developed. The variables in these

equations are usually inflation pressure, speed and load. The accuracy of a calculation is naturally limited by the influence of factors that are neglected.

At the most elementary level, the rolling resistance coefficient may be estimated as a constant. The table below lists some typical values that might be used in that case.

		Surface	
Vehicle Type	Concrete	Medium Hard	Sand
Passenger cars	0.015	0.08	0.30
Heavy trucks	0.012	0.06	0.25
Tractors	0.02	0.04	0.20

At lower speeds the coefficient rises approximately linearly with speed. Thus equations have been developed which include a linear speed dependence, such as below:

$$f_r = 0.01\,(1 + V/100) \qquad (4\text{-}14)$$

where:

V = Speed in mph

Over broader speed ranges, the coefficient rises in a manner that is closer to a speed-squared relationship. The Institute of Technology in Stuttgart has developed the following equation for rolling on a concrete surface [16]:

$$f_r = f_o + 3.24\,f_s\,(V/100)^{2.5} \qquad (4\text{-}15)$$

where:

V = Speed in mph

f_o = Basic coefficient

f_s = Speed effect coefficient

The two coefficients, f_o and f_s, depend on inflation pressure and are determined from the graph shown in Figure 4.34.

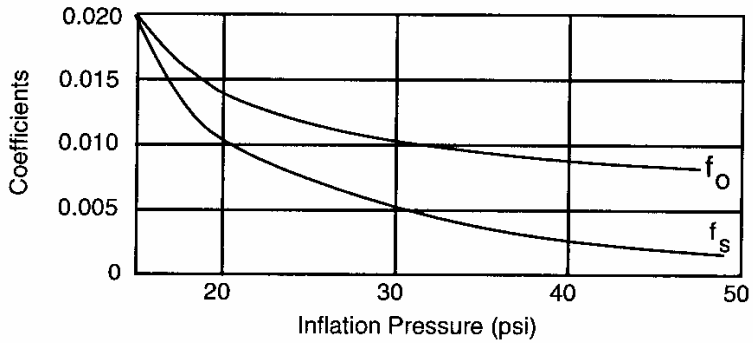

Fig. 4.34 Coefficients for Eq. (4-15).

At the University of Michigan Transportation Research Institute, similar equations for estimating rolling resistance of heavy truck tires of both the radial and bias-ply types were developed [24]. These are:

$$f_r = (0.0041 + 0.000041\ V)\ C_h \quad \text{Radial tires} \qquad (4\text{-}16a)$$

$$f_r = (0.0066 + 0.000046\ V)\ C_h \quad \text{Bias-ply tires} \qquad (4\text{-}16b)$$

where:

V = Speed in mph

C_h = Road surface coefficient

= 1.0 for smooth concrete

= 1.2 for worn concrete, brick, cold blacktop

= 1.5 for hot blacktop

Rolling resistance is clearly a minimum on hard, smooth, dry surfaces. A worn-out road almost doubles rolling resistance. On wet surfaces, higher rolling resistance is observed probably due to the cooler operating temperature of the tire which reduces its flexibility.

TOTAL ROAD LOADS

The summation of the rolling resistance and aerodynamic forces (and grade forces, if present) constitutes the propulsion load for the vehicle, and is

normally referred to as "road load." The road load force is thus:

$$R_{RL} = f_r\ W + 1/2\ \rho\ V^2\ C_D\ A + W \sin\theta \qquad (4\text{-}17)$$

The sum of these forces is plotted for a typical large vehicle in Figure 4.35. The rolling resistance has been assumed constant with a coefficient of 0.02 and a vehicle weight of 3650 lb. The aerodynamic drag assumes a vehicle of 23.3 ft^2 frontal area and a drag coefficient of 0.34. The total road load curve rises with the square of the speed due to the aerodynamic component. Rolling resistance and grade simply slide the whole curve upward in proportion to their size.

The road load horsepower is computed by multiplying Eq. (4-16) by the vehicle velocity and applying the appropriate conversion factor to obtain horsepower. In that case:

$$HP_{RL} = R_{RL}\ V/550 = (f_r\ W + 1/2\ \rho\ V^2\ C_D\ A + W \sin\theta)\ V/550 \qquad (4\text{-}18)$$

The road load power corresponding to the road load forces in Figure 4.35 is shown in Figure 4.36 for a level road condition. Note that the power increases much more rapidly with velocity due to the cubic relationship in Eq. (4-18). Thus at high speeds a small increase in speed results in a large increase in vehicle power required, with an associated penalty to fuel economy.

Fuel Economy Effects

Today, aerodynamic and rolling resistance forces are of particular interest for their effect on fuel consumption. Aerodynamic drag, of course, is the most

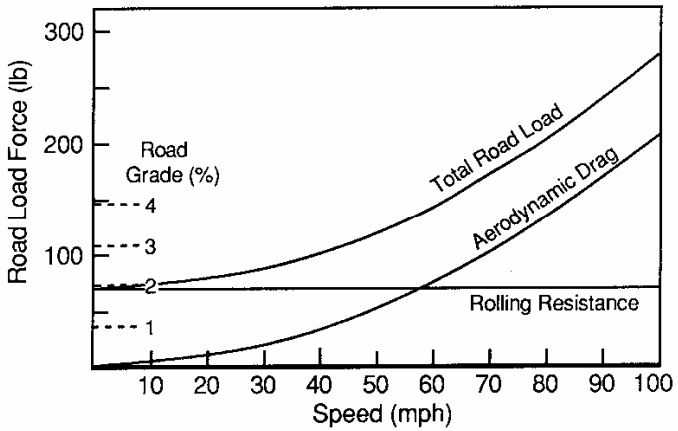

Fig. 4.35 Road load plot for a typical passenger car.

important of the aerodynamic properties. In the decade of the 1970s, drag coefficients of 0.4 to 0.5 were common on relatively large cars. In the 1980s, drag coefficients are commonly less than 0.4 with some cars less than 0.3. In addition, the smaller cross-sectional areas contribute to lower overall drag.

The exact improvements in fuel economy that may be expected from improvements in road loads are difficult to predict because of the uncertainty about the ways cars are used and driven. Figure 4.37 shows an estimate of where the energy is used in EPA driving cycles and in steady highway driving [25].

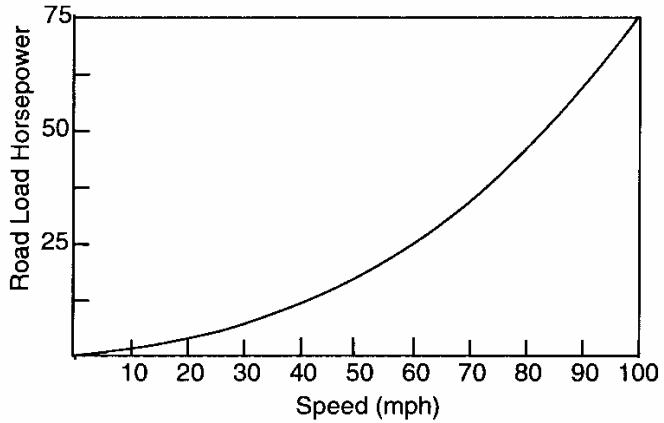

Fig. 4.36 Road load power plot for a typical passenger car.

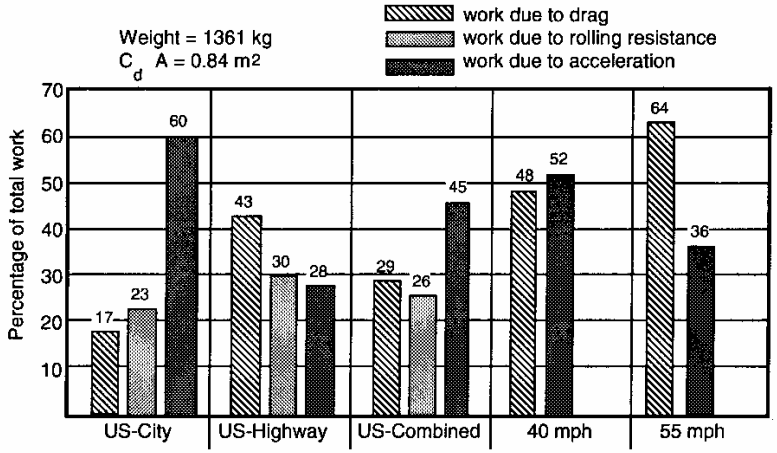

Fig. 4.37 Subdivision of work of a compact car in driving cycles.

EXAMPLE PROBLEMS

1) A heavy truck weighing 72,500 lb rolls along I70 in Denver at a speed of 67 mph. The air temperature is 55°F and the barometric pressure is 26.01 in Hg. The truck is 8' wide by 13.5' high, and has an aerodynamic drag coefficient of 0.65. The truck has radial-ply tires. Calculate the aerodynamic drag, the rolling resistance (according to the SAE equations) and the road load horsepower at these conditions.

Solution:

The aerodynamic drag may be calculated using Eq. (4-2). The temperature and barometric pressure conditions are not standard, so we must first calculate the local air density using Eq. (4-3a).

$$\rho = 0.00236 \frac{P_r}{29.92} \frac{519}{460 + T_r}$$

$$\rho = 0.00236 \frac{26.01}{29.92} \frac{519}{(460 + 55)} = 0.00207 \frac{\text{lb-sec}^2}{\text{ft}^4} = 0.0667 \frac{\text{lb}}{\text{ft}^3}$$

Now the aerodynamic drag can be calculated:

$$D_A = 0.5\ (0.00207 \frac{\text{lb-sec}^2}{\text{ft}^4})\ (\frac{67\ \text{mph}}{0.682\ \text{mph/ft/sec}})^2\ 0.65\ (8\ \text{ft})\ (13.5')\ = 702\ \text{lb}$$

The rolling resistance comes from a combination of Eqs. (4-12) and (4-16a). First from the SAE equation, we calculate the rolling resistance coefficient, assuming a surface coefficient of unity:

$$f_r = [0.0041 + 0.000041\ (67\ \text{mph})] = 0.00685$$

Then the rolling resistance is:

$$R_x = 0.00685\ (72{,}500\ \text{lb}) = 497\ \text{lb}$$

At the speed of 67 mph (98.3 ft/sec) the horsepower required to overcome aerodynamic drag is:

$$HP_A = 702\ \text{lb}\ (98.3\ \text{ft/sec})\ 1\ \text{hp}/(550\ \text{ft-lb/sec}) = 125\ \text{hp}$$

And the horsepower to overcome rolling resistance is:

$$HP_R = 497\ \text{lb}\ (98.3\ \text{ft/sec})\ 1\ \text{hp}/(550\ \text{ft-lb/sec}) = 88.8\ \text{hp}$$

Notes:

a) A total of nearly 215 hp is required to keep the truck rolling at this speed.

b) Highway trucks typically have diesel engines rated at 350 to 600 horsepower. These engines are designed to run continuously at maximum power, so it is not unreasonable for them to run at this output level for mile after mile.

c) At a typical brake specific fuel consumption of 0.35 lb per brake-horsepower-hour, the engine will burn 82.6 lb of diesel fuel per hour (13 gallons/hour) getting about 5.25 miles per gallon. It is not unusual to have a fuel tank capacity of 300 gallons on-board a highway tractor, so they can run for nearly 24 hours or 1500 miles without having to stop for fuel.

2) A passenger car has a frontal area of 21 square feet and a drag coefficient of 0.42. It is traveling along at 55 mph. Calculate the aerodynamic drag and the associated horsepower requirements if it is driving into a 25 mph headwind, and with a 25 mph tailwind.

Solution:

The drag can be calculated from Eq. (4-2), although the relative velocity must take into account the headwinds and tailwinds as given in Eq. (4-4). We will assume that the air temperature and pressure conditions are effectively near standard conditions so that the standard value for air density can be used.

Headwind condition:

$$D_A = 0.5\,(0.00236\frac{\text{lb-sec}^2}{\text{ft}^4})\,(\frac{(55 + 25)\text{ mph}}{0.682\text{ mph/ft/sec}})^2\,0.42\,(21\text{ ft}^2) = 143\text{ lb}$$

Tailwind condition:

$$D_A = 0.5\,(0.00236\frac{\text{lb-sec}^2}{\text{ft}^4})\,(\frac{(55 - 25)\text{ mph}}{0.682\text{ mph/ft/sec}})^2\,0.42\,(21\text{ ft}^2) = 20\text{ lb}$$

Notes:

a) The normal aerodynamic drag on this vehicle in the absence of any headwind or tailwind would be 68 lb.

b) The headwind more than doubles the drag because the drag increases with the square of the relative headwind velocity, which goes from 55 to 80 mph.

c) The tailwind reduces the drag considerably due to the speed square effect.

REFERENCES

1. Li, W.H., and Lam, S.H., Principles of Fluid Mechanics, Addison-Wesley Publishing Company, Inc., Reading, Massachusetts, 1964, 374 p.
2. Shepherd, D.G., Elements of Fluid Mechanics, Harcourt, Brace and World, Inc., New York, 1965, 498 p.
3. Schenkel, F.K., "The Origins of Drag and Lift Reductions on Automobiles with Front and Rear Spoilers," SAE Paper No. 770389, 1977, 11 p.
4. Kramer, C., "Introduction to Aerodynamics," Lecture notes for Short Course 1984-01, von Karman Institute for Fluid Dynamics, Jan. 1984, 60 p.
5. Lay, W.E., "Is 50 Miles per Gallon Possible with Correct Streamlining?" *SAE Journal,* Vol. 32, 1933, pp 144-156, pp 177-186.
6. Hoerner, S., Fluid-Dynamic Drag, Published by the author, Midland Park, NJ, 1965.
7. Kamm, W., "Einfluss der Reichsautobahn auf die Gestaltung von Kraftfahrzeugen," *ATZ,* Vol. 37, 1943, pp 341-354.
8. "SAE Vehicle Dynamics Terminology," SAE J670e, Society of Automotive Engineers, Warrendale, PA (see Appendix A).
9. "Vehicle Aerodynamics Terminology," SAE J1594, Society of Automotive Engineers, Warrendale, PA, June 1987, 5 p.
10. Buchheim, R., Deutenback, K.-R., and Luckoff, H.-J., "Necessity and Premises for Reducing the Aerodynamic Drag of Future Passenger Cars," SAE Paper No. 810185, 1981, 14 p.
11. Hucho, W.-H., and Janssen, L.J., "Beitrage der Aerodynamik im Rahmen einer Scirocco," *ATZ,* Vol. 77, 1975, pp 1-5.
12. Scibor-Rylski, A.J., Road Vehicle Aerodynamics, Second Edition, Pentech Press, London, 1984, 244 p.
13. Sardou - M.S.W.T , M., and Sardou, S.A., "Why to Use High Speed Moving Belt Wind Tunnel for Moving Ground Surface Vehicles Development," Lecture notes for Short Course 1984-01, von Karman Institute for Fluid Dynamics, Jan. 1984, 59 p.
14. Hucho, W.H., Janssen, L.J., and Emmelmann, H.J., "The Optimization of Body Details—A Method for Reducing Aerodynamic Drag of Road Vehicles," SAE Paper No. 760185, 1976, 18 p.

15. Gilhaus, A.M., and Renn, V.E., "Drag and Driving-Stability-Related Aerodynamic Forces and Their Interdependence—Results of Measurement on 3/8-Scale Basic Car Shapes," SAE Paper No. 860211, 1986, 15 p.

16. Cole, D., "Elementary Vehicle Dynamics," course notes in Mechanical Engineering, The University of Michigan, Ann Arbor, MI, 1972.

17. Aerodynamics of Road Vehicles, Wolf-Heinrich Hucho, ed., Butterworths, London, 1987, 566 p.

18. Hogue, J.R., "Aerodynamics of Six Passenger Vehicles Obtained from Full Scale Wind Tunnel Tests," SAE Paper No. 800142, 1980, 17 p.

19. MacAdam, C.C., Sayers, M.W., Pointer, J.D., and Gleason, M., "Crosswind Sensitivity of Passenger Cars and the Influence of Chassis and Aerodynamic Properties on Driver Performance," *Vehicle Systems Dynamics,* Vol. 19, 1990, 36 p.

20. Willumeit, H.P., *et al.*, "Method to Correlate Vehicular Behavior and Driver's Judgment under Side Wind Disturbances," Dynamics of Vehicles on Roads and Tracks, Proceedings, Swets and Zeitlinger B. V. - Lisse, 1988, pp. 509-524.

21. Uffelmann, F., "Influence of Aerodynamics and Suspension on the Cross-Wind Behaviour of Passenger Cars - Theoretical Investigation under Consideration of the Driver's Response," Dynamics of Vehicles on Roads and Tracks, O. Nordstrom, ed., Swets and Zeitlinger B. V. - Lisse, 1986, pp. 568-581.

22. van den Hemel, H., *et al.*, "The Cross-Wind Stability of Passenger Cars: Development of an Objective Measuring Method," Fourth IAVSD Congress, 1987.

23. Clark, S.K., *et al.*, "Rolling Resistance of Pneumatic Tires," The University of Michigan, Interim Report No. UM-010654-3-1, July 1974, 65 p.

24. Fancher, P.S., and Winkler, C.B., "Retarders for Heavy Vehicles: Phase III Experimentation and Analysis; Performance, Brake Savings, and Vehicle Stability," U.S. Department of Transportation, Report No. DOT HS 806 672, Jan. 1984, 144 p.

25. Buchheim, R., "Contributions of Aerodynamics to Fuel Economy Improvements of Future Cars," Fuel Economy Research Conference, Section 2: Technical Presentations.

CHAPTER 5
RIDE

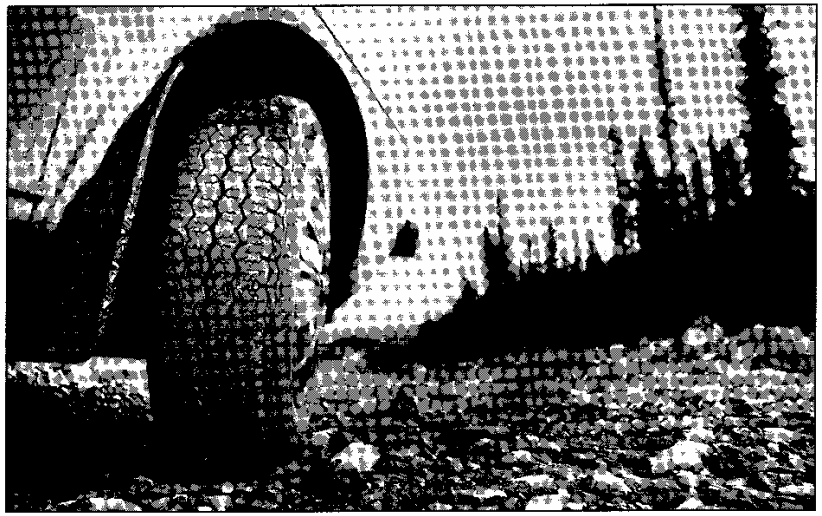

Last segment of Cinturato P3 endurance test. (Photo courtesy of Pirelli Tire Corp.)

Automobiles travel at high speed, and as a consequence experience a broad spectrum of vibrations. These are transmitted to the passengers either by tactile, visual, or aural paths. The term "ride" is commonly used in reference to tactile and visual vibrations, while the aural vibrations are categorized as "noise." Alternatively, the spectrum of vibrations may be divided up according to frequency and classified as ride (0-25 Hz) and noise (25-20,000 Hz). The 25 Hz boundary point is approximately the lower frequency threshold of hearing, as well as the upper frequency limit of the simpler vibrations common to all motor vehicles. The different types of vibrations are usually so interrelated that it may be difficult to consider each separately; i.e., noise is usually present when lower-frequency vibrations are excited.

The vibration environment is one of the more important criteria by which people judge the design and construction "quality" of a car. Being a judgment, it is subjective in nature, from which arises one of the greatest difficulties in developing objective engineering methods for dealing with ride as a performance mode of the vehicle.

The lower-frequency ride vibrations are manifestations of dynamic behavior common to all rubber-tired motor vehicles. Thus, the study of these modes is an important area of vehicle dynamics. As an aid in developing a systematic picture of ride behavior, it is helpful to think of the overall dynamic system as shown in Figure 5.1. The vehicle is a dynamic system, but only exhibits vibration in response to excitation inputs. The response properties determine the magnitude and direction of vibrations imposed on the passenger compartment, and ultimately determine the passenger's perception of the vehicle. Thus, understanding ride involves the study of three main topics:

- Ride excitation sources
- Basic mechanics of vehicle vibration response
- Human perception and tolerance of vibrations

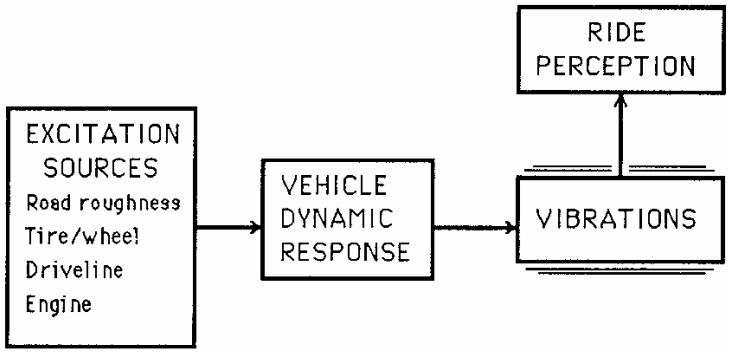

Fig. 5.1 The ride dynamic system.

EXCITATION SOURCES

There are multiple sources from which vehicle ride vibrations may be excited. These generally fall into two classes—road roughness and on-board sources. The on-board sources arise from rotating components and thus include the tire/wheel assemblies, the driveline, and the engine.

Road Roughness

Road roughness encompasses everything from potholes resulting from localized pavement failures to the ever-present random deviations reflecting the practical limits of precision to which the road surface can be constructed and maintained. Roughness is described by the elevation profile along the wheel tracks over which the vehicle passes. Road profiles fit the general

category of "broad-band random signals" and, hence, can be described either by the profile itself or its statistical properties. One of the most useful representations is the Power Spectral Density (PSD) function.

Like any random signal, the elevation profile measured over a length of road can be decomposed by the Fourier Transform process [1] into a series of sine waves varying in their amplitudes and phase relationships. A plot of the amplitudes versus spatial frequency is the PSD. Spatial frequency is expressed as the "wavenumber" with units of cycles/foot (or cycles/meter), and is the inverse of the wavelength of the sine wave on which it is based.

Road elevation profiles can be measured either by performing close interval rod and level surveys [2], or by high-speed profilometers [3]. When the PSDs are determined, plots such as those shown in Figure 5.2 are typically obtained [4,5,6]. Although the PSD of every road section is unique, all roads show the characteristic drop in amplitude with wavenumber. This simply reflects the fact that deviations in the road surface on the order of hundreds of feet in length may have amplitudes of inches, whereas those only a few feet in

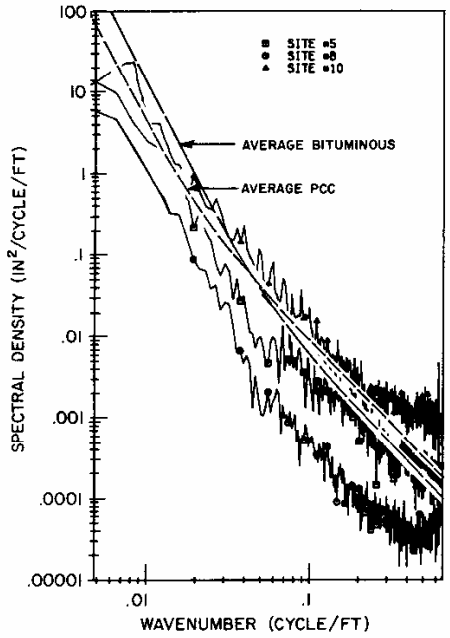

Fig. 5.2 Typical spectral densities of road elevation profiles.

length are normally only fractions of an inch in amplitude. The general amplitude level of the plot is indicative of the roughness level—higher amplitudes implying rougher roads. The wavenumber range in the figure corresponds to wavelengths of 200 feet (61 m) on the left at 0.005 cycle/foot (0.016 cycle/meter), to about 2 feet (0.6 m) on the right at 0.5 cycle/foot (1.6 cycles/meter).

The upper PSD in the figure is a deteriorating Portland Cement concrete (often called "rigid pavement") road surface. Note a marked periodicity in the range of wavenumber between 0.01 cycle/foot (0.03 cycle/meter) and 0.1 cycle/foot (0.3 cycle/meter), which is related to the fixed slab length used in construction of the road. The lowest PSD is a similar road overlaid with a bituminous asphalt surface layer yielding a much smoother surface (the PSD amplitude is reduced by an order of magnitude). The reduction is especially pronounced in the high-wavenumber range. The intermediate PSD is a typical asphalt road (often called "flexible pavement").

Although many ride problems are peculiar to a specific road, or road type, the notion of "average" road properties can often be helpful in understanding the response of a vehicle to road roughness. The general similarity in the spectral content of the roads seen in Figure 5.2 (that elevation amplitude diminishes systematically with increasing wavenumber) has long been recognized as true of most roads [7,8,9]. Consequently, road inputs to a vehicle are often modeled with an amplitude that diminishes with frequency to the second or fourth power approximating the two linear segments of the curve shown in the figure. The average properties shown in the figure are derived from recent studies of a large number of roads [4]. The spectral contents are slightly different for bituminous and Portland Cement concrete (PCC) roads. Other less common road types, such as surface treatment and gravel roads, will have slightly differing spectral qualities [6]. The general level of the elevation of the curve may be raised or lowered to represent different roughness levels, but the characteristic slopes and inflection points are constant. The difference between the bituminous and PCC average curves is the relative magnitude of high- versus low-wavenumber content. For a given overall roughness, more is concentrated in the high-wavenumber (short-wavelength) range with PCC surfaces, causing high-frequency vehicle vibrations, whereas it is in the low-wavenumber range on bituminous surfaces, causing greater excitation in the low-frequency range.

The PSD for average road properties shown in the figure can be represented by the equation as follows:

$$G_z(\nu) = G_o[1+(\nu_o/\nu)^2]/(2\pi\nu)^2 \qquad (5\text{-}1)$$

where:

$G_z(\nu)$ = PSD amplitude (feet^2/cycle/foot)
ν = Wavenumber (cycles/ft)
G_o = Roughness magnitude parameter (roughness level)
= 1.25×10^5 for rough roads
= 1.25×10^6 for smooth roads
ν_o = Cutoff wavenumber
= .05 cycle/foot for bituminous roads
= .02 cycle/foot for PCC roads

The above equation in combination with a random number sequence provides a very useful method to generate road profiles with random roughness having the spectral qualities of typical roads [4] for study of vehicle ride dynamic behavior.

As described above, the roughness in a road is the deviation in elevation seen by a vehicle as it moves along the road. That is, the roughness acts as a vertical displacement input to the wheels, thus exciting ride vibrations. Yet the most common and meaningful measure of ride vibration is the acceleration produced. Therefore, for the purpose of understanding the dynamics of ride, the roughness should be viewed as an acceleration input at the wheels, in which case a much different picture emerges. Two steps are involved. First a speed of travel must be assumed such that the elevation profile is transformed to displacement as a function of time. Thence, it may be differentiated once to obtain the velocity of the input at the wheels, and a second time to obtain an acceleration. Figure 5.3 shows the transformation of road profile elevation to a velocity and then acceleration input to a vehicle. A vehicle speed of 50 mph has been assumed. The conversion from spatial frequency (cycles/foot) to temporal frequency (cycles/second or Hz) is obtained by multiplying the wavenumber by the vehicle speed in feet/second.

Note that the acceleration spectrum has a relatively constant amplitude at low frequency, but begins increasing rapidly above 1 Hz such that it is an order of magnitude greater at 10 Hz. Viewed as an acceleration input, road roughness presents its largest inputs to the vehicle at high frequency, and thus has the greatest potential to excite high-frequency ride vibrations unless attenuated accordingly by the dynamic properties of the vehicle. As will be seen, the vehicle's attenuation of this high-frequency input is an important aspect of the "ride isolation" behavior obtained via the primary suspension commonly used on highway vehicles today.

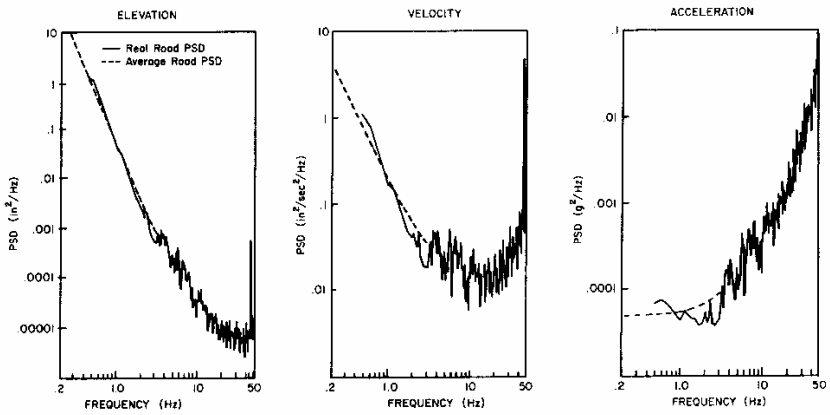

Fig. 5.3 Elevation, velocity and acceleration PSDs of road roughness input to a vehicle traveling at 50 mph on a real and average road.

By viewing road roughness as an acceleration input the primary effect of travel speed can be readily seen. At any given temporal frequency the amplitude of the acceleration input will increase with the square of the speed. This is illustrated by considering a simple sine wave representation of roughness. Then:

$$Z_r = A \sin (2\pi\nu X) \tag{5-2}$$

where:

Z_r = Profile elevation
A = Sine wave amplitude
ν = Wavenumber (cycles/foot)
X = Distance along the road

Now, because the distance, X, equals the velocity, V, times the time of travel, t:

$$Z_r = A \sin (2\pi\nu V t) \tag{5-3}$$

Differentiating twice to obtain acceleration produces:

$$\ddot{Z}_r = - (2\pi\nu V)^2 A \sin (2\pi\nu V t) \tag{5-4}$$

Thus as an acceleration the amplitude coefficient contains the velocity squared. In general, increasing the assumed speed in Figure 5.3 will cause the

acceleration plot to shift upward due to the speed-squared effect just described. It may also be noted that the curve would shift to the left slightly because of the corresponding change in the temporal frequency represented by each roughness wavenumber. This also adds to the acceleration amplitude, although not as strongly as the speed-squared effect.

Thus far the road roughness input has been considered only as a vertical input to the vehicle that would excite bounce and pitch motions. For this purpose the road profile points in the left and right wheeltracks are usually averaged before processing to obtain the PSD, although the PSDs of either wheeltrack will usually appear quite similar to that of the average. The difference in elevation between the left and right road profile points represents a roll excitation input to the vehicle. The PSD for the roll displacement input to a vehicle is typically similar to that for the elevation as was shown in Figure 5.2, although its amplitude is attenuated at wavenumbers below 0.02 to 0.03 cycle/foot. Typical roll excitation characteristics of road roughness are more readily seen by normalizing the roll amplitude (difference between the wheeltracks) by the vertical amplitude (average of the wheeltracks) in each wavenumber band of the PSD, so that roll excitation is seen in relationship to the vertical excitation present in the road.

The PSDs obtained have the characteristics as shown in Figure 5.4. At low wavenumbers (long wavelengths) the roll input from a roadway is much lower in its relative magnitude than that of the vertical input to the vehicle, because the difference in elevation is constrained by requirements to maintain the superelevation of the road.

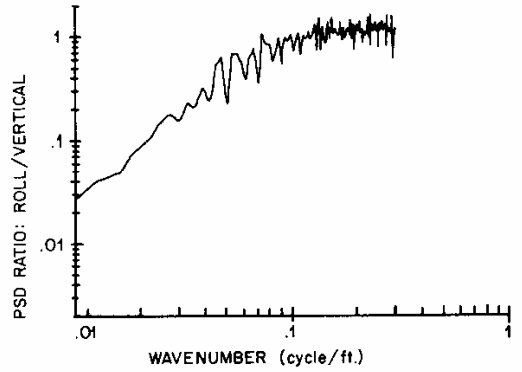

Fig. 5.4 Spectral density of normalized roll input for a typical road.

However, the normalized roll input magnitude grows with wavenumber because of the natural tendency for bumps in the left and right wheeltracks to become less and less correlated at high wavenumbers (short wavelengths). For most vehicles, resonance in roll occurs at a lower frequency (0.5 to 1.0 Hz) than resonance in bounce. Thus of the two, bounce is the more dominant response. At higher frequency, where the bounce and roll inputs are more nearly equal in magnitude, vehicles are less responsive to roll.

As an illustration, consider a vehicle with a roll natural frequency of 1.0 Hz traveling at 60 mph (88 ft/sec). Roll excitation in the road at the 88 ft wavelength (0.011 cycle/ft) will therefore directly excite roll motions. However, the roll amplitude at this wavenumber is only 10 percent of the vertical input, so the vehicle passengers will be more conscious of bounce vibrations rather than roll.

At a low speed, for example at 6 mph, a 1.0 Hz roll resonant frequency would be excited by input from wavenumbers on the order of 0.1 cycle/ft at which the roll and vertical inputs are essentially equal in magnitude. Thus roll and bounce motions would be approximately equal as well. The common case where this is observed is in off-road operation of 4x4 vehicles where the exaggerated ride vibrations are often composed of roll as well as bounce motions.

Tire/Wheel Assembly

Ideally, the tire/wheel assembly is soft and compliant in order to absorb road bumps as part of the ride isolation system. At the same time, it ideally runs true without contributing any excitation to the vehicle. In practice, the imperfections in the manufacture of tires, wheels, hubs, brakes and other parts of the rotating assembly may result in nonuniformities of three major types:

1) Mass imbalance

2) Dimensional variations

3) Stiffness variations

These nonuniformities all combine in a tire/wheel assembly causing it to experience variations in the forces and moments at the ground as it rolls [10]. These in turn are transmitted to the axle of the vehicle and act as excitation sources for ride vibrations [11]. The force variations may be in the vertical (radial) direction, longitudinal (tractive) direction, or the lateral direction [12].

The moment variations in the directions of the overturning moment, aligning torque, and rolling resistance moment generally are not significant as sources of ride excitation, although they can contribute to steering system vibrations.

Imbalance derives from a nonuniform distribution of mass in the individual components of the assembly along or about the axis of rotation [14]. Asymmetry about the axis of rotation is observed as static imbalance. The resultant effect is a force rotating in the wheel plane with a magnitude proportional to the imbalance mass, the radius from the center of rotation, and the square of the rotational speed. Because it is rotating in the wheel plane, this force produces both radial as well as longitudinal excitations. The imbalance force is given by the equation:

$$F_i = (m\ r)\ \omega^2 \qquad (5\text{-}5)$$

where:

F_i = Imbalance force

$m\ r$ = The imbalance magnitude (mass times radius)

ω = the rotational speed (radians/second)

A nonuniform and asymmetric mass distribution along the axis of rotation causes a dynamic imbalance [14]. Dynamic imbalance creates a rotating torque on the wheel, appearing as variations in overturning moment and aligning torque at the wheel rotational frequency. Dynamic imbalance is most important on steered wheels which may experience steering vibrations as a result of the excitation. Static imbalance can exist in the absence of dynamic imbalance, and vice versa. The tires, wheels, hubs and brake drums may all contribute to imbalance effects.

The tire, being an elastic body analogous to an array of radial springs, may exhibit variations in stiffness about its circumference. Figure 5.5 illustrates that tire model. The free length of the springs establishes the dimensional nonuniformities (free radial runout), yet the variations in their compressed length at a nominal load determines the rolling nonuniformities (loaded radial runout).

Dimensional runouts in the wheel or hub on which the tire is mounted do not produce stiffness variations directly, but may contribute to the free- or loaded-radial runouts that are observed.

The significant effect of the nonuniformities in a tire/wheel assembly is the generation of excitation forces and displacements at the axle of the vehicle as

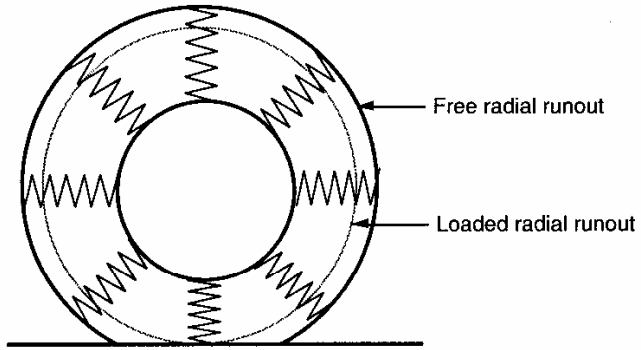

Fig. 5.5 Tire radial spring model.

the wheel rotates. The excitation force observed when the wheel is rolled at constant radius and speed repeats with each revolution of the wheel [15].

Radial force variations measured at constant radius typically take the form illustrated in Figure 5.6. The peak-to-peak magnitude of force variation is called "composite force variation." The force signature may be described in more detail by the amplitude of the harmonics of which it is composed. That is, by a Fourier transform [1], the composition of the signal as a series of sine waves at the fundamental and each multiple frequency can be determined. The amplitude of each harmonic is usually the parameter of primary interest. Although the phase angle of each must also be known to reconstruct the original signal, phase angle information appears to have little relationship to ride phenomena [16].

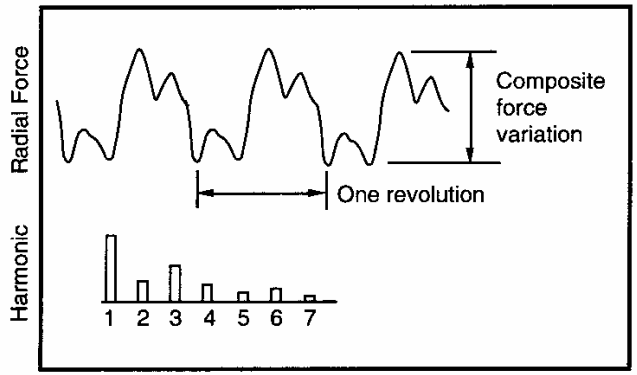

Fig. 5.6 Tire radial force variations.

The first harmonic of the radial force variation tends to be less than that of the composite, and the higher-order harmonics tend to be of diminishing magnitude. For passenger-car tires a decrease of about 30 percent per order has been observed [15], with less of an effect at high speed. Runout of the hub and wheel may also contribute to the radial force variations. The runout may be quantified by finding the point-by-point average radius of the two bead seats around the circumference of the assembled wheel. The first harmonic force variation arising from this source is closely linked to the runout. At first thought, the force variation would be expected to be the runout times the stiffness of the tire mounted on the wheel. Experiments, however, have shown that the force variation is only about 70 percent of that magnitude, indicating that the tire partially masks runout of the wheel [17]. Higher harmonic runouts in the wheel are not as closely related to radial force variations in the overall assembly.

The various harmonics of radial nonuniformities in a tire/wheel assembly are functionally equivalent to imperfections in the shape as shown in Figure 5.7.

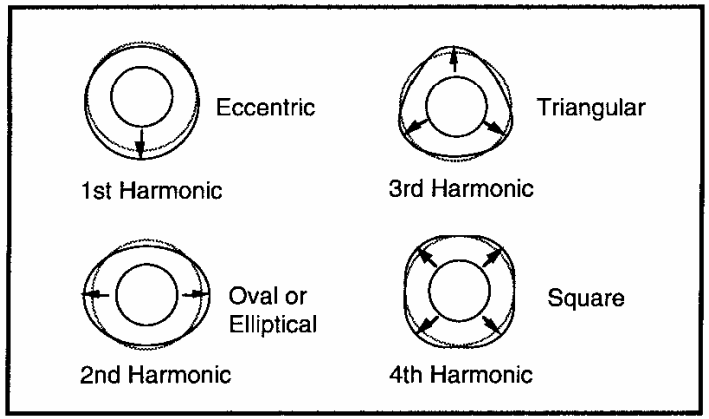

Fig. 5.7 Radial nonuniformities in a tire.

1) Eccentricity—The tires, wheels and hubs individually may exhibit radial eccentricity, resulting in a first-harmonic nonuniformity which produces both radial and tractive excitation on the axle. Since there is one high point and one low point on the assembly, the excitation occurs at the rotational speed of the wheel (10-15 Hz at normal highway speeds). The overall magnitude of the nonuniformity for the assembly depends on the magnitudes in the individual

components and their relative positions when assembled [11]. That is, eccentricity in one component may partially compensate for that in others when the high and low points of the different parts are matched in assembly. The "match-mounting" technique is commonly used in the tire/wheel assemblies for passenger cars to minimize first-harmonic nonuniformities of the assembly. In those cases, wheels may be purposely manufactured with an eccentricity equivalent to the average radial runout of the production tires with which they will be used. The tires and wheels are marked for high/low points to facilitate match mounting.

2) Ovality—Tires and wheels may have elliptical variations that add or subtract depending on the mounting positions [11], although match-mounting is not practical for minimizing this nonuniformity. Because the assembly has two high points and two low points on its circumference, radial and tractive force excitation is produced at twice the wheel rotational frequency (20-30 Hz at normal highway speeds).

3) Higher-order radial variations—Third- and higher-order variations are predominantly of importance in the tire only. Such variations in the wheel are substantially absorbed by the tire [13]. The third harmonic is analogous to a tire with a triangular shape, the fourth harmonic reflects a square shape, and so on. While tires do not purposely have these shapes, the effects may arise from construction methods. For example, in a tire with four plies of fabric material, the overlaps associated with each ply would normally be distributed around the circumference of the tire. The additional stiffness created at each of the overlap positions will then result in a fourth-harmonic stiffness variation and an associated fourth-harmonic force variation. The force variations act in the radial and tractive force directions at the multiple of wheel speed equal to the harmonic number.

Because the magnitude of the radial force variation is relatively independent of speed, low-speed measurements of radial force variations at a constant radius (the method commonly used by tire manufacturers to monitor production) indicate the magnitude of the force tending to excite ride vibrations. Only the frequency is changed with speed. The nonuniformity force can be treated as a direct excitation at the axle. As a point of clarity, it should be noted that the excitation force is not equivalent to the actual force variation experienced at the axle, as the dynamic response of the vehicle can greatly amplify the forces [10]. Nevertheless, the measurement of radial force variations described above is the proper and valid means to characterize the radial excitation potential associated with nonuniformities in the tire and wheel components. Alternatively, measurements of loaded radial runout are also valid and can be transformed to radial force variation by simply multiplying by the radial spring rate of the tire.

Tractive force variations arise from dimensional and stiffness nonuniformities as a result of two effects. The causes are best illustrated by considering a simple eccentric wheel model as shown in Figure 5.8. With eccentricity, even at low speed the axle must roll up and down the "hill" represented by the variation in radius of the wheel assembly. Thus a longitudinal force is involved and a tractive force variation is observed. Its magnitude will be dependent on the load carried and the amount of eccentricity [17]; however, it is independent of speed.

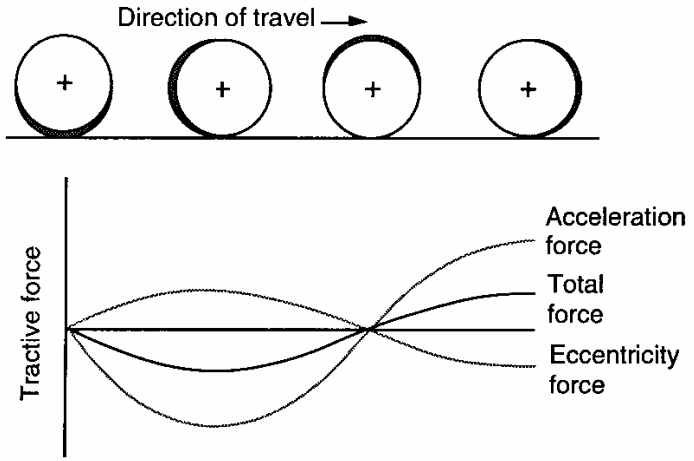

Fig. 5.8 Tractive force variations arising from an eccentric wheel.

On the other hand, at high speed the wheel must accelerate and decelerate in the course of a revolution because of its varying radius. Thus a tractive force at the ground, and accordingly at the hub, must appear in order to produce the acceleration. Quite reasonably, the magnitude of the force will be dependent on the longitudinal stiffness properties of the tire and the rotational moment of inertia of the wheel. Further, the magnitude of the tractive force arising from this mechanism will vary with speed because the acceleration varies with speed, typically increasing by a factor of about 5 over the speed range of 5 to 60 mph. Therefore, the tractive force variation in a tire or tire/wheel assembly

can only be measured validly at high speed, and the rotational inertia properties of the wheel assembly must be closely matched to that of actual vehicles.

Lateral force variations may arise from nonuniformities in the tire, but cannot be readily related to lateral runout effects in the wheel or hub components. They tend to be independent of speed, thus measurements of the force magnitudes at low speed are also valid for high speed [11]. First-order lateral variations in the tires or wheels, or in the way in which they are mounted, will cause wobble. These will affect the dynamic balance of the assembly. The wobble in the wheel may contribute a minor lateral force variation, but may also result in radial and tractive force variations comparable to the effect of ovality [11] because the wheel is elliptical in the vertical plane.

Higher-order lateral variations are predominantly important in the tire only. Wheel variations are substantially absorbed by the tire [11,13]. These sources could potentially cause steering vibrations, but have not been identified as the cause of ride problems.

In general, the imperfections in tires and wheels tend to be highly correlated [18,19], such that radial variations are usually accompanied by imbalance and tractive force variations. Thus it may often be difficult to cure a tire-related ride problem simply by correcting one condition, such as imbalance, without consideration of the other nonuniformities likely to be present.

In order to complete the discussion of the tire/wheel assembly as a ride excitation source, it must be recognized that the assembly itself is a dynamic system influencing the excitation seen at the axle (see Chapter 10). The influence derives from the modal resonance properties of the assembly, which at the low-frequency end are dominated by the tire tread band resonances. The capacity to resonate makes the assembly a vibration absorber at certain modal frequencies, while it accentuates the transmissibility properties at the anti-resonance frequencies [20]. Ultimately, the tire can play a significant role in noise, vibration and harshness (NVH) of a motor vehicle, and in the ride development process the vehicle must be properly tuned to avoid various buzzes and booms that can be triggered by tire response.

Driveline Excitation

The third major source of excitation to the vehicle arises from the rotating driveline. While the driveline is often considered to be everything from the engine to the driven wheels, the engine/transmission package will be treated separately in the discussion.

For purposes of discussion, the driveline therefore consists of the driveshaft, gear reduction and differential in the drive axle, and axle shafts connecting to the wheels. Of these various components, the driveshaft with its spline and universal joints has the most potential for exciting ride vibrations. The rear axle gearing and remainder of the driveline are also capable of generating vibrations in the nature of noise as a result of gear mating reactions and torsional vibration along the drivetrain. However, these generally occur at frequencies above those considered as ride.

The most frequent ride excitations arise from the driveshaft. The driveshaft is normally arranged as shown in Figure 5.9 [21]. On rear-drive passenger cars and short-wheelbase trucks, a single-piece shaft is commonly used, whereas, on long-wheelbase trucks and buses a multiple-piece shaft supported by an intermediate bearing is frequently required. Excitations to the vehicle arise directly from two sources—mass imbalance of the driveshaft hardware, and secondary couples, or moments, imposed on the driveshaft due to angulation of the cross-type universal joints [22,23].

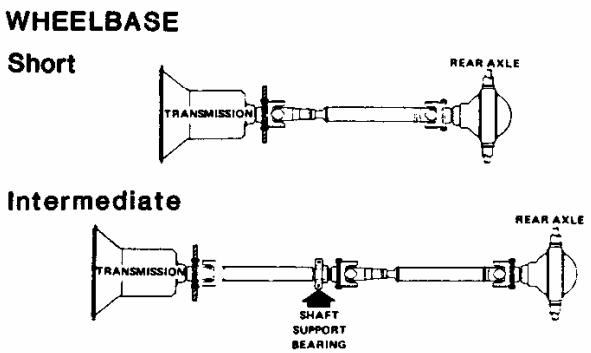

Fig. 5.9 Typical driveline arrangements [39].

Mass Imbalance—Imbalance of the driveshaft may result from the combination of any of the five following factors:

1) Asymmetry of the rotating parts
2) The shaft may be off-center on its supporting flange or end yoke
3) The shaft may not be straight
4) Running clearances may allow the shaft to run off center
5) The shaft is an elastic member and may deflect

An initial imbalance exists as a result of the asymmetry, runouts and looseness in the structure. The imbalance creates a rotating force vector thus imposing forces on the support means in both the vertical and lateral directions. Forces at the front support apply to the transmission. Those at the back exert on the drive axle directly. Where intermediate bearings are employed on trucks, forces may be imposed on the frame via the crossmembers at those points. The force rotates at the speed of the shaft which is always the wheel speed multiplied by the numerical ratio of the final drive, and is equivalent to engine speed when in direct drive. Thus it appears like a harmonic of the wheel of a value equal to the numerical ratio of the rear axle.

In general, the magnitude of the excitation force is equivalent to the product of the imbalance and the square of the rotating speed. However, because the shaft is elastic it may bend in response to the imbalance force allowing additional asymmetry, and an increase in the "dynamic" imbalance. As a result, the apparent magnitude of the imbalance may change with speed, and in theory, the shaft can only be dynamically balanced for one speed [23].

Secondary couples—The use of universal joints in a driveline opens the way for generation of ride excitation forces when they are operated at an angle, due to the secondary couple that is produced. The magnitude and direction of the secondary couple can be determined by a simple vector summation of torques on the universal joint as is illustrated in Figure 5.10.

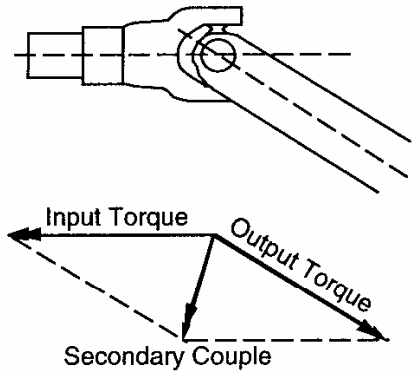

Fig. 5.10 Torque reactions causing a secondary couple.

The magnitude of the secondary torque is proportional to the torque applied to the driveline and the angle of the universal joint. When the torque

varies during rotation due to engine torque pulsations and/or nonconstant-velocity joints, the secondary couple will vary accordingly. The secondary couple reacts as forces at the support points of the driveline on the transmission, crossmembers supporting the driveline intermediate bearings, and at the rear axle. Hence, these forces vary with driveline rotation and impose excitation forces on the vehicle [22].

When cross-type (Cardan or Hooke) universal joints are used and operate at an angle, they are a direct source of torque pulsations in the driveline [40]. The joints do not have a constant relationship between input and output velocity when operated at an angle, but must satisfy the equation:

$$\frac{\omega_o}{\omega_i} = \frac{\cos\theta}{1 - \sin^2\beta \sin^2\theta} \tag{5-6}$$

where:

ω_o = Output speed
ω_i = Input speed
θ = Angle of the U-joint
β = Angle of rotation of the driving yoke

Because of the "$\sin^2\beta$" term in the denominator, the speed variation reaches a maximum twice per revolution (at 90 and 270 degrees). Thus a second-harmonic speed variation occurs as a result of the symmetry of the cross around each arm. It can be shown from the above equation that the maximum speed variation changes with joint angle as:

$$\left|\frac{\omega_o}{\omega_i}\right|_{max} = \frac{1}{\cos\theta} \tag{5-7}$$

Because of the stiffness of the driveline and the accelerations it experiences, torque variations will necessarily arise from the speed variation. These may cause excitation of torsional vibrations in the driveline, as well as be the source of ride excitation forces on the vehicle. The excitation occurs at the second harmonic of the driveline speed, and will vary with the level of torque applied to the driveline. Excitation from the secondary couple can be minimized by proper design of the driveline—maintaining parallel axes on the transmission output shaft and rear axle input shaft, proper phasing of the joints, and keeping angles within the limits recommended by the manufacturers [21, 22, 23].

The torque variations may also act directly at the transmission and the rear

axle. Torque variations at the axle will vary the drive forces at the ground and thus may act directly to generate longitudinal vibrations in the vehicle. The torque variations at the transmission produce excitation in the roll direction on the engine/transmission assembly. In part, these variations must be reacted in the mounting points on the body and thus have a direct path to the interior.

Figure 5.11 illustrates the nature of the vibrations that may be produced as a result of driveline and tire/wheel nonuniformities. In this case the accelerations were measured in a truck cab under carefully controlled conditions (i.e., the vehicle was operated on a smooth road to suppress background vibrations

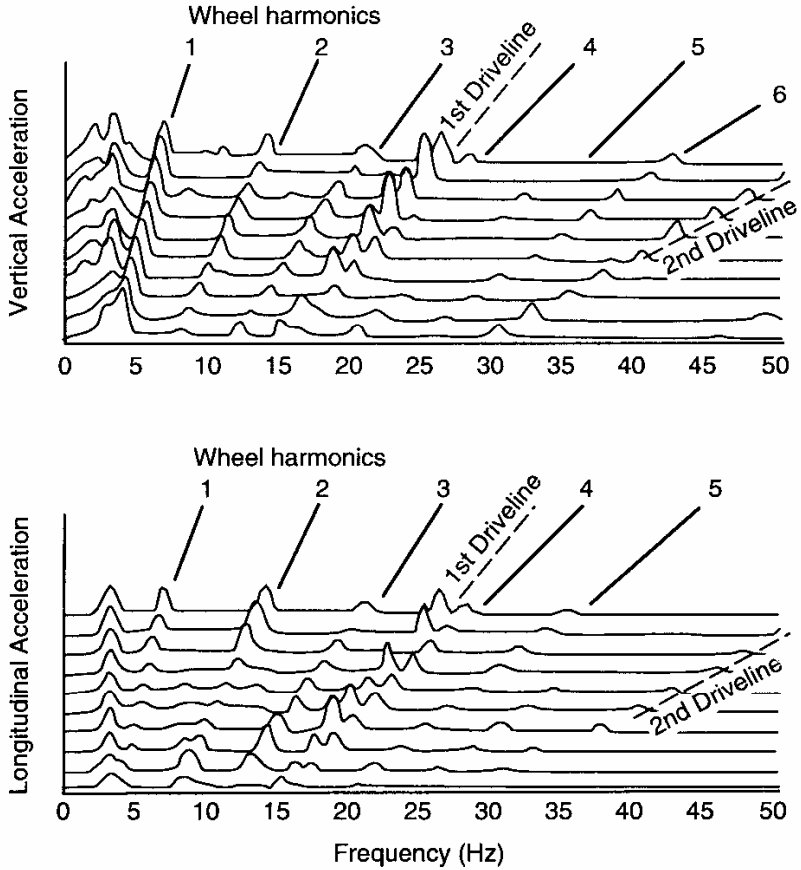

Fig. 5.11 Spectral map of vibrations arising from driveline and tire/wheel nonuniformities.

that would mask the desired effects and all of the tire/wheel assemblies, except for one, were carefully match-mounted to achieve consistency in the tire/wheel excitation).

The figure shows a map of the vibration spectra measured at different vehicle speeds. Excitation from tire/wheel inputs appear as ridges in the spectra moving to higher frequency as the speed increases. The first, second and higher harmonics of the tire/wheel assemblies are evident in the spectra. The ridge at 3.7 times the wheel rotational speed corresponds to first harmonic of the driveline, which is due to imbalance of the driveshaft and other components rotating at this speed. The second harmonic of the driveline at 7.4 times the wheel speed is the result of torque variations in the driveshaft that arise from speed variations caused by the operating angles of the cross-type universal joints.

These or comparable vibrations from the wheels and drivelines will always be present on a vehicle, but are often difficult to recognize in a complex spectrum that includes substantial road roughness excitation. Nevertheless, they constitute one of the factors contributing to the overall ride vibration spectrum and represent one of the areas in which careful design can improve the ride environment of the vehicle.

Engine/Transmission

The engine serves as the primary power source on a vehicle. The fact that it rotates and delivers torque to the driveline opens the possibility that it may be a source for vibration excitation on the vehicle. Further, the mass of the engine in combination with that of the transmission is a substantial part in the chassis, and, if used correctly, can act as a vibration absorber.

Piston engines deliver power by a cyclic process; thus the torque delivered by the engine is not constant in magnitude [24]. At the crankshaft the torque delivered consists of a series of pulses corresponding to each power stroke of a cylinder (see Figure 5.12). The flywheel acts as an inertial damper along with the inertias and compliances in the transmission. Thus the torque output to the driveshaft consists of a steady-state component plus superimposed torque variations. Those torque variations acting through the driveline may result in excitation forces on the vehicle similar to those produced by the secondary couple from the cross-type universal joints explained in the previous sections.

Because of compliance in the engine/transmission mounts, the system will vibrate in six directions—the three translational directions and three rotations

around the translational axes. The axis system for a transverse front-engine configuration is shown in Figure 5.13. The figure also shows a three-point mount typical of those used with most transverse engines today.

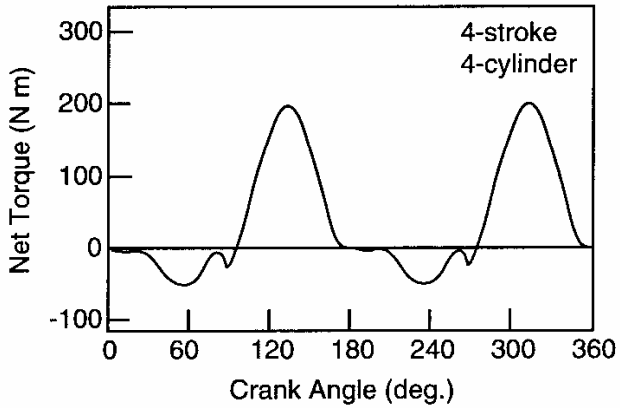

Fig. 5.12 Torque variations at the output of a four-stroke, four-cylinder engine.

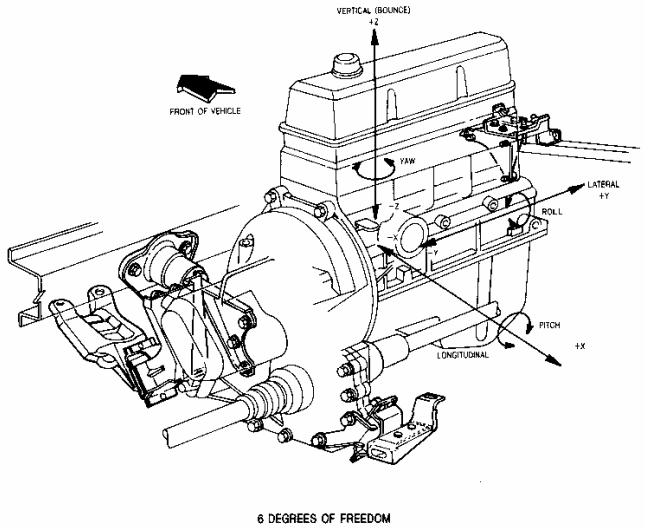

Fig. 5.13 Typical transverse engine and mounting hardware. (Photo courtesy of Ford Motor Company.)

Of all the directions of motion, the most important to vibration is the engine roll direction (about the lateral axis of a transverse engine or about the longitudinal axis of an engine mounted in the north-south direction), which is excited by drive torque oscillations. Torque oscillations occur at the engine firing frequency as well as at sub-harmonics of that frequency due to cylinder-to-cylinder variations in the torque.

A key to isolating these excitations from the vehicle body is to design a mounting system with a roll axis that aligns with the engine inertial roll axis, and provide a resonance about this axis at a frequency that is below the lowest firing frequency. By so doing, torque variations which occur above the resonant frequency are attenuated. In effect, the torque is absorbed in the inertial motion of the engine rather than being transmitted to the vehicle body.

The engine inertial axis of four-cylinder engines will generally be inclined downward toward the transmission because of the contribution from the mass of the transmission. Thus the mounting system must be low at the transmission end and high at the front of the engine. On V-type engines (six- and eight-cylinder) the inertial axis is lower in the front permitting a mounting system more closely aligned with the crankshaft.

The worst-case problem is isolation of idle speed torque variations for a four-cylinder engine with the transmission in drive, which may have a firing frequency of 20 Hz or below. Therefore, successful isolation requires a roll axis resonance of 10 Hz or below. Because the system acts like a simple second-order mass-spring dynamic system [14], torque variations at frequencies below the resonant frequency will be felt directly at the mounts, and near the torsional resonant frequency, excitation amplitudes much greater than the torque variations themselves will occur.

Engines may produce forces and moments in directions other than roll as a result of the inherent imbalances in the reciprocating/rotating masses [24]. These take the form of forces or couples at the engine rotational frequency or its second harmonic, and must be isolated in the same manner as for the roll mode described above. For the more commonly used engine configurations the balance conditions are as follows:

1) Four-cylinder inline—Vertical force at twice engine rotational frequency; can be balanced with counter-rotating shafts.

2) Four-cylinder, opposed, flat—Various forces and moments at rotational frequency and twice rotational frequency depending on crankshaft arrangement.

3) Six-cylinder inline—Inherently balanced in all directions.

4) Six-cylinder inline, two-cycle—Vertical couple generating yaw and pitch moments at the engine rotational frequency; can be balanced.

5) Six-cylinder, 60-degree V—Generates a counter-rotating couple at rotational frequency that can be balanced with counter-rotating shaft.

6) Six-cylinder, 90-degree V (uneven firing)—Generates yaw moment of twice rotational frequency; can be balanced with counter-rotating shaft.

7) Six-cylinder, 90-degree V (even firing)—Generates yaw and pitching moments at crankshaft speed, which can be balanced. Also generates complex yaw and pitching moments at twice rotational speed which are difficult to balance.

8) Eight-cylinder inline—Inherently balanced in all directions.

9) Eight-cylinder, 90-degree V—Couple at primary rotational speed; can be counter-balanced.

With proper design of the mounting system the mass of the engine-transmission combination can be utilized as a vibration absorber attenuating other vibrations to which the vehicle is prone. Most often it is used to control vertical shake vibrations arising from the wheel excitations. For this purpose the mounting system is designed to provide a vertical resonance frequency near that of the front wheel hop frequency (12-15 Hz), so that the engine can act as a vibration damper for this mode of vehicle vibration.

VEHICLE RESPONSE PROPERTIES

A systematic treatment of the vehicle as a dynamic system best starts with the basic properties of a vehicle on its suspension system—i.e., the motions of the body and axles. At low frequencies the body, which is considered to be the sprung mass portion of the vehicle, moves as an integral unit on the suspensions. This is rigid-body motion. The axles and associated wheel hardware, which form the unsprung masses, also move as rigid bodies and consequently impose excitation forces on the sprung mass. Beyond this, one must look to structural modes of vibration and resonances of sub-systems on the vehicle. In addition, there are many individual variables of design and operating condition that are known to affect the vibration response on the vehicle.

The dynamic behavior of a vehicle can be characterized most meaningfully by considering the input-output relationships. The input may be any of the excitations discussed in the preceding section, or combinations thereof. The output most commonly of interest will be the vibrations on the body. The ratio of output and input amplitudes represents a "gain" for the dynamic system. The term "transmissibility" is often used to denote the gain. Transmissibility is the nondimensional ratio of response amplitude to excitation amplitude for a system in steady-state forced vibration. The ratio may be one of forces, displacements, velocities or accelerations. The magnitude ratio of the transfer function is sometimes used in a similar fashion to denote the gain, although this term is normally reserved for use with linear systems.

Suspension Isolation

At the most basic level, all highway vehicles share the "ride isolation" properties common to a sprung mass supported by primary suspension systems at each wheel. The dynamic behavior of this system is the first level of isolation from the roughness of the road. The essential dynamics can be represented by a quarter-car model, as shown in Figure 5.14.

It consists of a sprung mass supported on a primary suspension, which in turn is connected to the unsprung mass of the axle. The suspension has stiffness and damping properties. The tire is represented as a simple spring, although a damper is often included to represent the small amount of damping inherent to the visco-elastic nature of the tire [25]. A more detailed discussion of this model is provided in the SAE Ride and Vibration Data Manual [26].

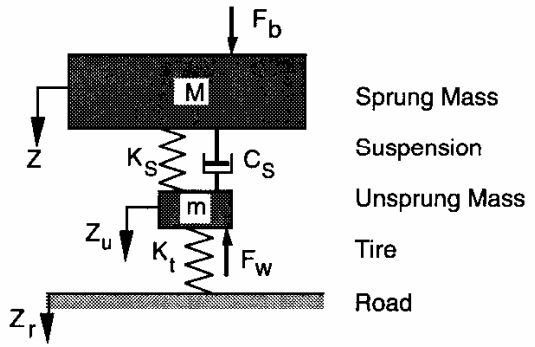

Fig. 5.14 Quarter-car model.

The sprung mass resting on the suspension and tire springs is capable of motion in the vertical direction. The effective stiffness of the suspension and tire springs in series is called the "ride rate" determined as follows:

$$RR = \frac{K_S K_t}{K_S + K_t} \tag{5-8}$$

where:

RR = Ride rate
K_S = Suspension stiffness
K_t = Tire stiffness

In the absence of damping, the bounce natural frequency at each corner of the vehicle can be determined from:

$$\omega_n = \sqrt{\frac{RR}{M}} \quad \text{(radians/sec)} \tag{5-9a}$$

or:

$$f_n = 0.159 \sqrt{\frac{RR}{W/g}} \quad \text{(cycles/sec)} \tag{5-9b}$$

where:

M = Sprung mass
W = M g = Weight of the sprung mass
g = Acceleration of gravity

When damping is present, as it is in the suspension, the resonance occurs at the "damped natural frequency," ω_d, given by:

$$\omega_d = \omega_n \sqrt{1 - \zeta_s^2} \tag{5-10}$$

where:

ζ_s = Damping ratio

$$= C_S / \sqrt{4 K_S M} \tag{5-11}$$

C_S = Suspension damping coefficient

For good ride the suspension damping ratio on modern passenger cars usually falls between 0.2 and 0.4. Because of the way damping influences the resonant frequency in the equation above (i.e., under the square root sign), it

is usually quite close to the natural frequency. With a damping ratio of 0.2, the damped natural frequency is 98% of the undamped natural frequency, and even at 0.4 damping, the ratio is about 92%. Because there is so little difference the undamped natural frequency, ω_n, is commonly used to characterize the vehicle.

The ratio of W/K_S represents the static deflection of the suspension due to the weight of the vehicle. Because the "static deflection" predominates in determining the natural frequency, it is a straightforward and simple parameter indicative of the lower bound on the isolation of a system. Figure 5.15 provides a nomograph relating the natural frequency to static deflection.

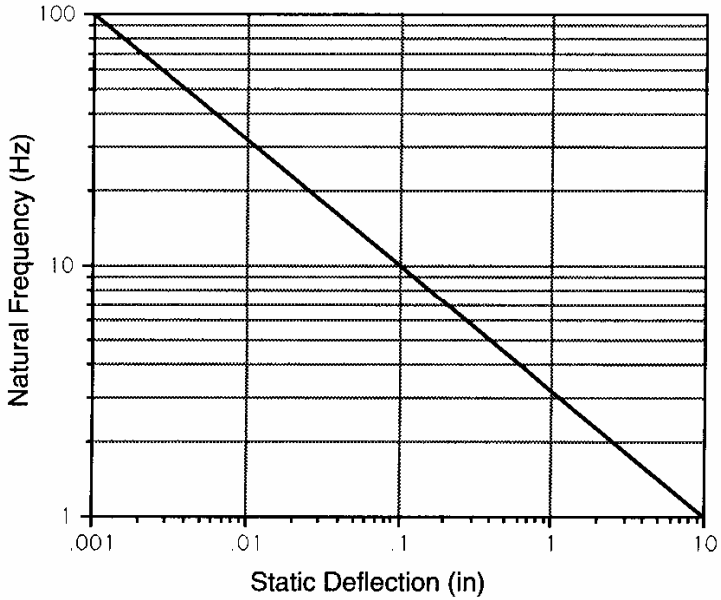

Fig. 5.15 Undamped natural frequency versus static deflection of a suspension.

A static deflection of 10 inches (254 mm) is necessary to achieve a 1 Hz natural frequency—considered to be a design optimum for highway vehicles. A 5-inch (127-mm) deflection results in a 1.4 Hz frequency, and 1 inch (25 mm) equates to a 3.13 Hz frequency. While it is not necessary for the suspension to provide a full 10 inches (254 mm) of travel to achieve the 1 Hz frequency, in general, provisions for larger deflections are necessary with lower frequencies. For example, with a spring rate low enough to yield a 1 Hz frequency, at least

5 inches of stroke must be available in order to absorb a bump acceleration of one-half "g" without hitting the suspension stops. Most large cars have a usable suspension stroke in the range of 7 to 8 inches. On small, compact cars the stroke may be reduced to 5 or 6 inches.

The dynamic behavior for the complete quarter-car model in steady-state vibration can be obtained by writing Newton's Second Law for the sprung and unsprung masses. By considering a free-body diagram for each, the following differential equations are obtained for the sprung and unsprung masses, respectively:

$$M\ddot{Z} + C_s\dot{Z} + K_s Z = C_s\dot{Z}_u + K_s Z_u + F_b \quad (5\text{-}12)$$

$$m\ddot{Z}_u + C_s\dot{Z}_u + (K_s + K_t)Z_u = C_s\dot{Z} + K_s Z + K_t Z_r + F_w \quad (5\text{-}13)$$

where:

Z = Sprung mass displacement
Z_u = Unsprung mass displacement
Z_r = Road displacement
F_b = Force on the sprung mass
F_w = Force on the unsprung mass

While the two equations make solving more complicated, closed-form solutions can be obtained for the steady-state harmonic motion by methods found in classical texts. The solutions of primary interest are those for the sprung mass motion in response to road displacement inputs, forces at the axle, and forces applied directly to the sprung mass. The amplitude ratios for these cases are as follows:

$$\frac{\ddot{Z}}{\ddot{Z}_r} = \frac{K_1 K_2 + \mathbf{j}[K_1 C\omega]}{[\chi\omega^4 - (K_1 + K_2\chi + K_2)\omega^2 + K_1 K_2] + \mathbf{j}[K_1 C\omega - (1+\chi)C\omega^3]} \quad (5\text{-}14)$$

$$\frac{\ddot{Z}}{F_w/M} = \frac{K_2\omega^2 + \mathbf{j}[C\omega^3]}{[\chi\omega^4 - (K_1 + K_2\chi + K_2)\omega^2 + K_1 K_2] + \mathbf{j}[K_1 C\omega - (1+\chi)C\omega^3]} \quad (5\text{-}15)$$

$$\frac{\ddot{Z}}{F_b/M} = \frac{[\mu\omega^4 - (K_1 + K_2)\omega^2] + \mathbf{j}[C\omega^3]}{[\chi\omega^4 - (K_1 + K_2\chi + K_2)\omega^2 + K_1 K_2] + \mathbf{j}[K_1 C\omega - (1+\chi)C\omega^3]} \quad (5\text{-}16)$$

where:

χ = m/M = Ratio of unsprung to sprung mass
C = C_s/M
K_1 = K_t/M
K_2 = K_s/M
$\mathbf{j}$ = Complex operator

The equations above are complex in form consisting of real and imaginary components, the latter denoted by the "j" operator. To obtain the amplitude ratios, the real and imaginary parts of the numerators and denominators must be evaluated at the frequency of interest. The magnitude of the numerator is then determined by taking the square root of the sum of the squares of the real and imaginary parts. The denominator magnitude is determined similarly, and then the ratio of the two may be taken. With appropriate manipulation, the phase angle of the equations may also be determined.

The quarter-car model is limited to study of dynamic behavior in the vertical direction only. Yet, using equations such as those developed above, it can be used to examine vibrations produced on the sprung mass as a result of inputs from road roughness, radial forces arising from tire/wheel nonuniformities, or vertical forces applied directly to the sprung mass from on-board sources. The response properties can be presented by examining the response gain as a function of frequency, as shown in Figure 5.16. The gain is defined differently for each type of excitation input.

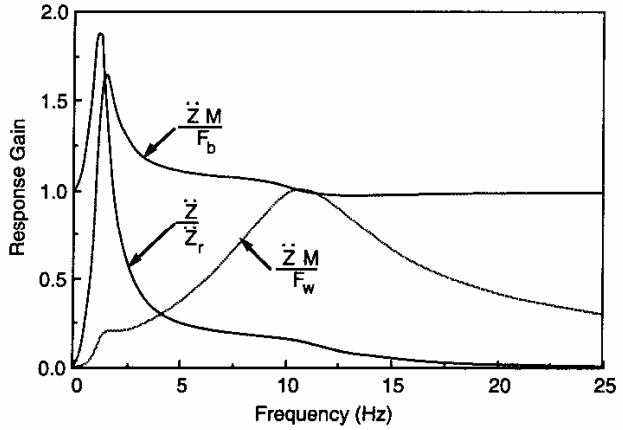

Fig. 5.16 Quarter-car response to road, tire/wheel, and body inputs.

For road roughness input, the gain is the ratio of sprung-mass motion (acceleration, velocity, or displacement) to the equivalent input from the road. At very low frequency the gain is unity (the sprung mass moves in exact duplication of the road input). By classical design of motor vehicles, the sprung mass is chosen to have its natural frequency at or just above 1 Hz. Therefore, at frequencies near 1 Hz the sprung mass is resonating on the suspension and the road inputs are amplified. The amplitude ratio at this peak is very sensitive to damping level, and on typical passenger cars will be in the range of 1.5 to 3. For typical heavy trucks the amplitude ratio is dependent on the road and operating conditions, but in the worst case may reach levels as high as 5 or 6 [27]. Above resonance, the road inputs are increasingly attenuated. In the range of 10 to 12 Hz, the unsprung mass of the tire/wheel assembly goes into a vertical (hop) resonance mode, adding a small bump to the attenuation curve in this region.

The sprung-mass response to tire/wheel excitation is illustrated by choosing an appropriate nondimensional expression for gain of the system. The input is an excitation force at the axle due to the tire/wheel assembly. The output—acceleration of the sprung mass—may be transformed to a force by multiplying by the mass. Thence, the output is the equivalent force on the sprung mass necessary to produce the accelerations. The gain is zero at zero frequency because the force on the axle is absorbed within the tire spring and no sprung-mass acceleration is produced. It rises with frequency through the 1 Hz sprung-mass resonance, but continues to climb until wheel resonance occurs in the 10 to 12 Hz range. Only then does it diminish. This plot tells much about the sensitivity to radial force variations in tires and wheel components that should be expected with conventional motor vehicles. In particular, it illustrates that vehicles will tend to be most responsive to excitation from tire and wheel nonuniformities acting near the resonant frequency of the wheel, and at that frequency the nonuniformity force is transmitted directly to the sprung mass (response gain of unity).

The response gain for direct force excitation on the sprung mass may be expressed nondimensionally by again using the equivalent force on the sprung mass as the output. The response is similar in this case, but shows greater dominance of the sprung-mass resonance. At high frequencies the gain approaches unity because the displacements become so small that suspension forces no longer change and the force is entirely dissipated as acceleration of the sprung mass. By implication, virtually all extraneous forces coming into the body of a vehicle are detrimental to ride vibrations.

The basic isolation properties inherent to a quarter-car model combined with typical spectra of road roughness provide a first picture of the general nature of the ride acceleration spectrum that should be expected on a motor

vehicle because of road inputs. The sprung-mass acceleration spectrum can be calculated for a linear model by multiplying the road spectrum by the square of the transfer function. That is:

$$G_{ZS}(f) = |H_V(f)|^2 G_{ZR} \tag{5-17}$$

where:

$G_{ZS}(f)$ = Acceleration PSD on the sprung mass
$H_V(f)$ = Response gain for road input
G_{ZR} = Acceleration PSD of the road input

The results obtained are illustrated in Figure 5.17. While the road represents an input of acceleration amplitude which grows with frequency, the isolation properties of the suspension system compensate by a decrease in the vehicle's response gain.

The net result is an acceleration spectrum on the vehicle with a high amplitude at the sprung-mass resonant frequency, moderate attenuation out through the resonant frequency of the wheel, and a rapid attenuation thereafter. Note that, even though the road input amplitude increases with frequency, the acceleration response on the vehicle is qualitatively similar to the vehicle's response gain. Thus the acceleration spectrum seen on a vehicle does provide some idea of the response gain of the system even when the exact properties of the road are not known.

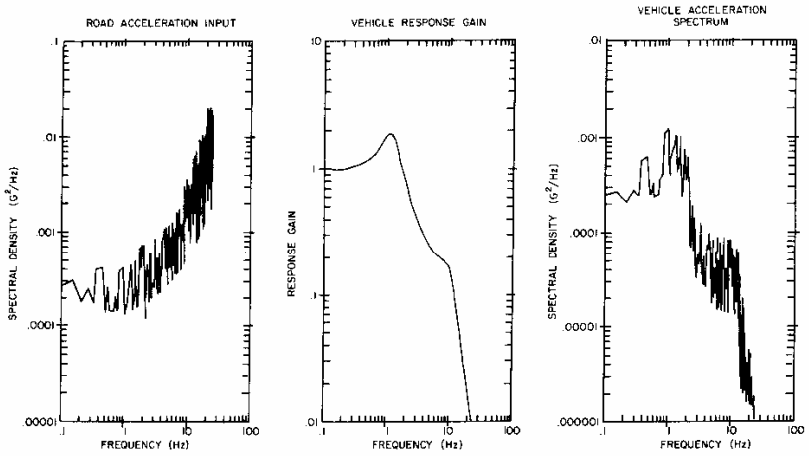

Fig. 5.17 Isolation of road acceleration by a quarter-vehicle model.

Example Problem

Determine the front and rear suspension ride rates for a 5.0 L Mustang given that the tire spring rate is 1198 lb/in. The front suspension rate is 143 lb/in and the rear is 100 lb/in. Also estimate the natural frequencies of the two suspensions when the front tires are loaded to 957 lb and the rear tires are at 730 lb each.

Solution:

The ride rates can be calculated using Eq. (5-8):

$$RR_f = \frac{K_s K_t}{(K_s + K_t)} = \frac{(143)(1198)}{(143 + 1198)} = 127 \frac{lb}{in}$$

$$RR_r = \frac{K_s K_t}{(K_s + K_t)} = \frac{(100)(1198)}{(100 + 1198)} = 92.3 \frac{lb}{in}$$

The natural frequencies for the suspensions can be determined from Eq. (5-9b).

$$f_{nf} = 0.159 \sqrt{\frac{RR_f\, g}{W}} = 0.159 \sqrt{\frac{127 \text{ lb/in} \times 386 \text{ in/sec}^2}{957 \text{ lb}}} = 1.14 \text{ Hz}$$

$$f_{nr} = 0.159 \sqrt{\frac{RR_r\, g}{W}} = 0.159 \sqrt{\frac{92.3 \text{ lb/in} \times 386 \text{ in/sec}^2}{730 \text{ lb}}} = 1.11 \text{ Hz}$$

Suspension Stiffness

Because the suspension spring is in series with a relatively stiff tire spring, the suspension spring predominates in establishing the ride rate and, hence, the natural frequency of the system in the bounce (vertical) mode. Since road acceleration inputs increase in amplitude at higher frequencies, the best isolation is achieved by keeping the natural frequency as low as possible. For a vehicle with a given weight, it is therefore desirable to use the lowest practical suspension spring rate to minimize the natural frequency.

The effect on accelerations transmitted to the sprung mass can be estimated analytically by approximating the road acceleration input as a function that increases with the square of the frequency. Then the mean-square acceleration

can be calculated from Eq. (5-17) as a function of frequency. Figure 5.18 shows the acceleration spectra thus calculated for a quarter-car model in which the suspension spring rate has been varied to achieve natural frequencies in the range of 1 to 2 Hz. Because it is plotted on a linear scale, the area under the curves indicates the relative level of mean-square acceleration over the frequency range shown.

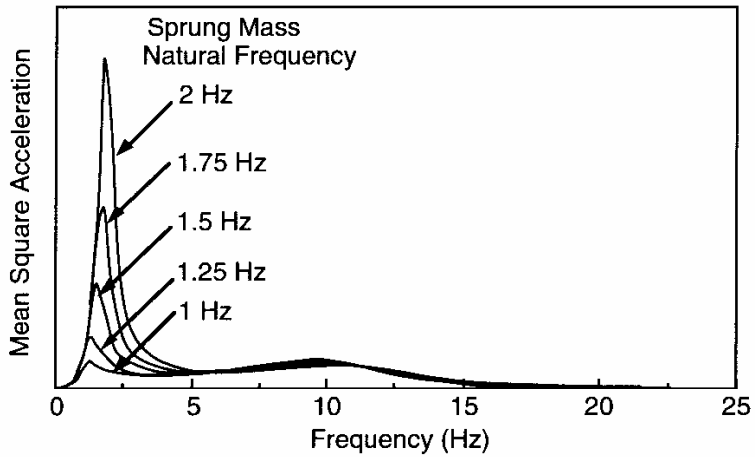

Fig. 5.18 On-road acceleration spectra with different sprung mass natural frequencies.

The lowest acceleration occurs at the natural frequency of 1 Hz. At higher values of natural frequency (stiffer suspension springs), the acceleration peak in the 1 to 5 Hz range increases, reflecting a greater transmission of road acceleration inputs, and the mean square acceleration increases by several hundred percent. In addition, the stiffer springs elevate the natural frequency of the wheel hop mode near 10 Hz, allowing more acceleration transmission in the high-frequency range.

While this analysis clearly shows the benefits of keeping the suspension soft for ride isolation, the practical limits of stroke that can be accommodated within a given vehicle size and suspension envelope constrain the natural frequency for most cars to a minimum in the 1 to 1.5 Hz range. Performance cars on which ride is sacrificed for the handling benefits of a stiff suspension will have natural frequencies up to 2 or 2.5 Hz.

With understeer the angle increases with the square of the speed, reaching twice the initial angle at the characteristic speed. In the oversteer case, the steer angle decreases with the square of the speed and becomes zero at the critical speed value.

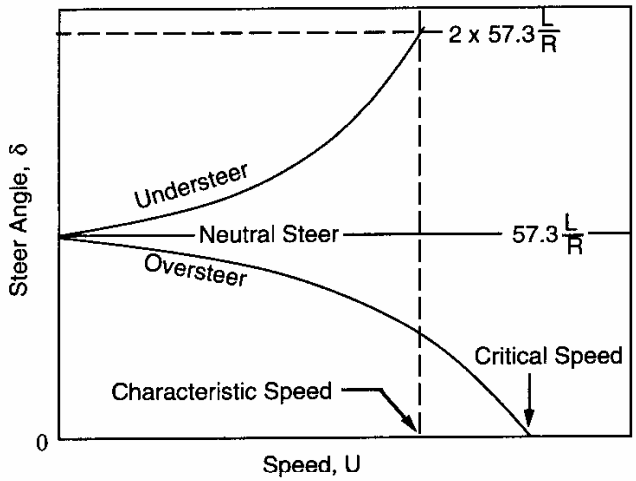

Fig. 6.5 Change of steer angle with speed.

Characteristic Speed

For an understeer vehicle, the understeer level may be quantified by a parameter known as the characteristic speed [8]. Characteristic speed is simply the speed at which the steer angle required to negotiate any turn is twice the Ackerman Angle. This can be seen in Eq. (6-16) when:

$$K\,a_y = 57.3\,L/R \tag{6-17}$$

Since a_y is a function of speed squared, the characteristic speed is:

$$V_{char} = \sqrt{57.3\,L\,g/K} \tag{6-18}$$

Critical Speed

In the oversteer case, a critical speed will exist above which the vehicle will be unstable. The critical speed is given by the expression:

$$V_{crit} = \sqrt{-57.3\,L\,g/K} \tag{6-19}$$

where it must be remembered that K is negative in value, such that the expression under the square root is positive and has a real value. Note that the critical speed is dependent on the wheelbase of the vehicle; for a given level of oversteer, long-wheelbase vehicles have a higher critical speed than short-wheelbase vehicles. An oversteer vehicle can be driven at speeds less than the critical, but becomes directionally unstable at and above the critical speed. The significance of critical speed becomes more apparent through its influence on the lateral acceleration gain and yaw rate gain as discussed in the next sections.

Lateral Acceleration Gain

Inasmuch as one of the purposes for steering a vehicle is to produce lateral acceleration, the turning equation can be used to examine performance from this perspective. Equation (6-16) can be solved for the ratio of lateral acceleration, a_y, to the steering angle, δ. The ratio is the lateral acceleration gain, and is given by:

$$\frac{a_y}{\delta} = \frac{\dfrac{V^2}{57.3\,L\,g}}{1 + \dfrac{K\,V^2}{57.3\,L\,g}} \quad \text{(deg/sec)} \tag{6-20}$$

Note that when K is zero (neutral steer), the lateral acceleration gain is determined only by the numerator and is directly proportional to speed squared. When K is positive (understeer), the gain is diminished by the second term in the denominator, and is always less than that of a neutral steer vehicle. Finally, when K is negative (oversteer), the second term in the denominator subtracts from 1, increasing the lateral acceleration gain. The magnitude of the term is dependent on the square of the speed, and goes to the value of 1 when the speed reaches the critical speed. Thus the critical speed of Eq. (6-19) corresponds to the denominator becoming zero (infinite gain) in the above equation.

Yaw Velocity Gain

A second reason for steering a vehicle is to change the heading angle by developing a yaw velocity (sometimes called "yaw rate"). The yaw velocity, **r**, is the rate of rotation in heading angle and is given by:

$$r = 57.3\ V/R \qquad \text{(deg/sec)} \qquad (6\text{-}21)$$

Substituting this expression into Eq. (6-16) and solving for the ratio of yaw velocity to steering angle produces:

$$\frac{r}{\delta} = \frac{V/L}{1 + \frac{K V^2}{57.3\ L\ g}} \qquad (6\text{-}22)$$

The ratio represents a "gain" which is proportional to velocity in the case of a neutral steer vehicle. This is illustrated in Figure 6.6. It is readily shown that in the oversteer case the yaw velocity gain becomes infinite when the speed reaches the critical speed in accordance with Eq. (6-19). In the case of the understeer vehicle, the yaw velocity increases with speed up to the characteristic speed, then begins to decrease thereafter. Thus the characteristic speed has significance as the speed at which the vehicle is most responsive in yaw.

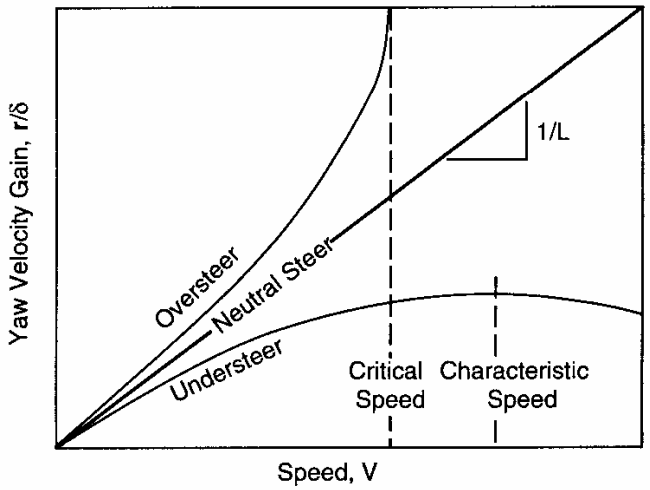

Fig. 6.6 Yaw velocity gain as a function of speed.

Sideslip Angle

From the discussion of turning behavior, it is evident that when the lateral acceleration is negligible, the rear wheel tracks inboard of the front wheel. But

as lateral acceleration increases, the rear of the vehicle must drift outboard to develop the necessary slip angles on the rear tires. At any point on the vehicle a sideslip angle may be defined as the angle between the longitudinal axis and the local direction of travel. In general, the sideslip angle will be different at every point on a car during cornering.

Taking the center of gravity as a case in point, the sideslip angle is defined as shown in Figure 6.7. The sideslip angle is defined as positive for this case because the direction of travel (the local velocity vector) is oriented clockwise from the longitudinal axis (clockwise angles viewed from above are positive in SAE convention). At high speed the slip angle on the rear wheels causes the sideslip angle at the CG to become negative as in Figure 6.8.

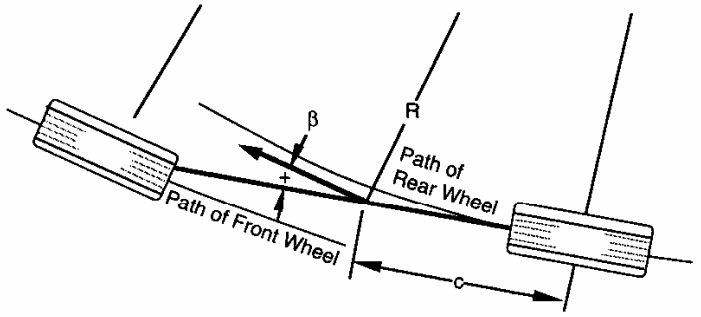

Fig 6.7 Sideslip angle in a low-speed turn.

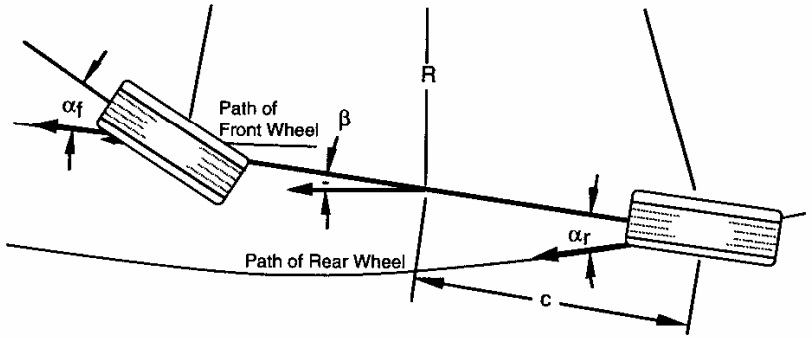

Fig. 6.8 Sideslip angle in a high-speed turn.

For any speed the sideslip angle, β, at the CG will be:

$$\beta = 57.3\, c/R - \alpha_r$$
$$= 57.3\, c/R - W_r\, V^2/(C_{\alpha r}\, g\, R) \qquad (6\text{-}23)$$

Note that the speed at which the sideslip angle becomes zero is:

$$V_{\beta=0} = \sqrt{57.3\, g\, c\, C_{\alpha r}/W_r} \qquad (6\text{-}24)$$

and is independent of the radius of turn.

Static Margin

A term often used in discussions of handling is the static margin and, like understeer coefficient or characteristic speed, provides a measure of the steady-state handling behavior.

Static margin is determined by the point on the vehicle where a side force will produce no steady-state yaw velocity (i.e., the neutral steer point). We may go one step further and define a neutral steer line as shown in Figure 6.9. The neutral steer line is the locus of points in the x-z plane along which external lateral forces produce no steady-state yaw velocity.

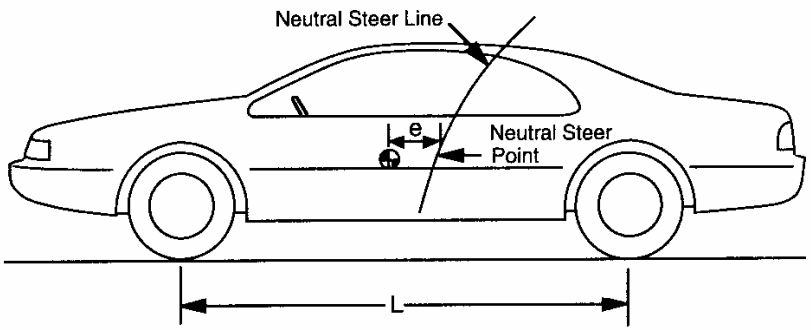

Fig. 6.9 Neutral steer line on a vehicle.

The static margin is defined as the distance the neutral steer point falls behind the CG, normalized by the wheelbase. That is:

$$\text{Static Margin} = e/L \qquad (6\text{-}25)$$

When the point is behind the CG the static margin is positive and the vehicle is understeer. At the CG the margin is zero and the vehicle is neutral steer. When ahead of the CG, the vehicle is oversteer. On typical vehicles the static margin falls in the range of 0.05 to 0.07 behind the CG.

SUSPENSION EFFECTS ON CORNERING

The analysis of turning, thus far, has shown that the behavior is dependent on the ratios of load/cornering coefficient on the front and rear axles ($W_f/C_{\alpha f}$ and $W_r/C_{\alpha r}$). The ratios have the engineering units of deg/g, and have been called the "cornering compliance" [9]. The name arises from the fact that the ratio indicates the number of degrees of slip angle at an axle per "g" of lateral force imposed at that point. Inasmuch as the lateral force in a turn is actually a "D'Alembert" force at the CG, it is distributed at the axles in exact proportions to the weight (as the gravitational force is distributed).

Although the understeer gradient was derived for the case of a vehicle in a turn, it can be shown that the gradient determines vehicle response to disturbances in straight-ahead driving. In particular, an analysis by Rocard [10] demonstrates that oversteer vehicles have a stability limit at the critical speed due to normal disturbances in straight-ahead travel.

When the front axle is more compliant than the rear (understeer vehicle), a lateral disturbance produces more sideslip at the front axle; hence, the vehicle turns away from the disturbance. This is illustrated in Olley's definitions for understeer and oversteer [11] shown in Figure 6.10. If the rear axle exhibits more cornering compliance (oversteer), the rear of the vehicle drifts out, and it turns into the disturbance. The lateral acceleration acting at the CG adds to the disturbance force further increasing the turning response and precipitating instability.

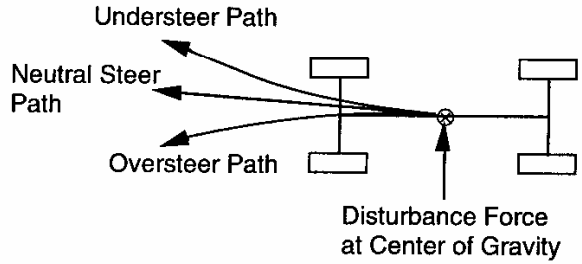

Fig. 6.10 Olley's definitions for understeer/oversteer.

Although tire cornering stiffness was used as the basis for developing the equations for understeer/oversteer, there are multiple factors in vehicle design that may influence the cornering forces developed in the presence of a lateral acceleration. Any design factor that influences the cornering force developed at a wheel will have a direct effect on directional response. The suspensions and steering system are the primary sources of these influences. In this section the suspension factors affecting handling will be discussed.

Roll Moment Distribution

For virtually all pneumatic tires the cornering forces are dependent on, and nonlinear with, load. This is important because load is transferred in the lateral direction in cornering due to the elevation of the vehicle CG above the ground plane. Figure 6.11 shows a typical example of how lateral force varies with vertical load.

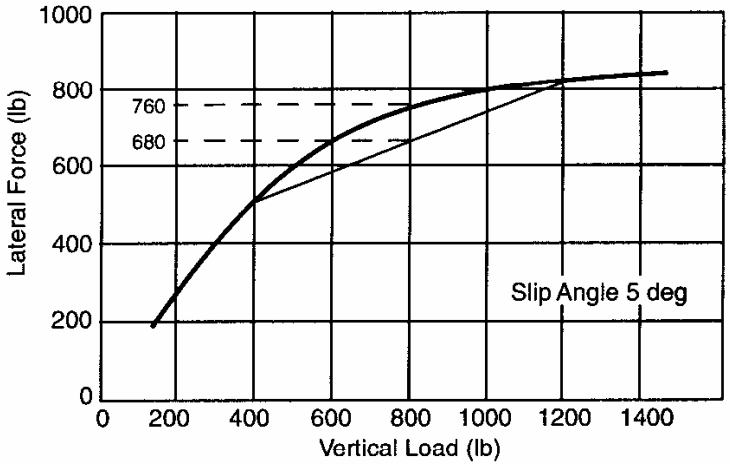

Fig. 6.11 Lateral force-vertical load characteristics of tires.

For a vehicle at 800 lb load on each wheel, about 760 lb of lateral force will be developed by each wheel at the 5-degree slip angle. In hard cornering, the loads might typically change to 400 lb on the inside wheel and 1200 lb on the outside. Then the average lateral force from both tires will be reduced to about

680 lb. Consequently, the tires will have to assume a greater slip angle to maintain the lateral force necessary for the turn. If these are front tires, the front will plough out and the vehicle will understeer. If on the rear, the rear will slip out and the vehicle will oversteer.

Actually, this mechanism is at work on both axles of all vehicles. Whether it contributes to understeer or oversteer depends on the balance of roll moments distributed on the front and rear axles. More roll moment on the front axle contributes to understeer, whereas more roll moment on the rear axle contributes to oversteer. Auxiliary roll stiffeners (stabilizer bars) alter handling performance primarily through this mechanism—applied to the front axle for understeer, and to the rear for oversteer.

The mechanics governing the roll moment applied to an axle are shown in the model of Figure 6.12. All suspensions are functionally equivalent to the two springs. The lateral separation of the springs causes them to develop a roll resisting moment proportional to the difference in roll angle between the body and axle. The stiffness is given by:

$$K_\phi = 0.5\, K_s\, s^2 \qquad (6\text{-}26)$$

where:

K_ϕ = Roll stiffness of the suspension
K_s = Vertical rate of each of the left and right springs
s = Lateral separation between the springs

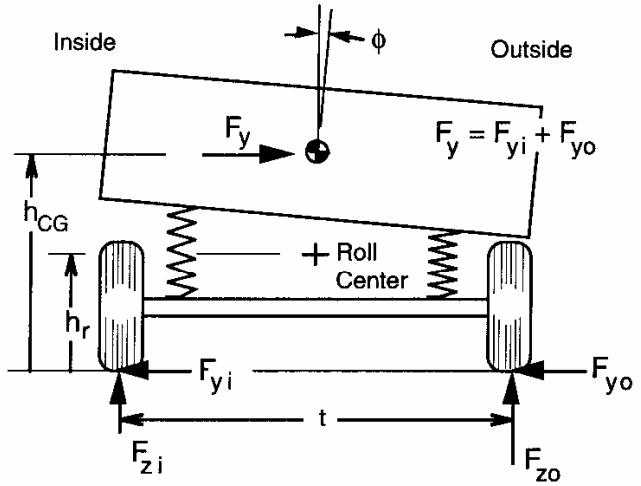

Fig. 6.12 Force analysis of a simple vehicle in cornering.

(In the case of an independent suspension, the above expression can be used by substituting the rate at the wheel for K_s and using the tread as the separation distance. When a stabilizer bar is present, the roll stiffness of the bar must be added to the stiffness calculated above.)

The suspension is further characterized by a "roll center," the point at which the lateral forces are transferred from the axle to the sprung mass. The roll center can also be thought of as the point on the body at which a lateral force application will produce no roll angle, and it is the point around which the axle rolls when subjected to a pure roll moment.

By writing Newton's Second Law for moments on the axle, we can determine the relationship between wheel loads and the lateral force and roll angle. In addition to the vertical forces imposed at the tires there is a net lateral force, F_y (the sum of the lateral forces on the inside and outside wheels), acting to the right on the axle at its roll center. The body roll acting through the springs imposes a torque on the axle proportional to the roll stiffness, K_ϕ, times the roll angle, ϕ. This results in an equation for the load difference from side to side of the form:

$$F_{zo} - F_{zi} = 2 F_y h_r/t + 2 K_\phi \phi/t = 2 \Delta F_z \qquad (6\text{-}27)$$

where:

F_{zo} = Load on the outside wheel in the turn
F_{zi} = Load on the inside wheel in the turn
F_y = Lateral force = $F_{yi} + F_{yo}$
h_r = Roll center height
t = Tread (track width)
K_ϕ = Roll stiffness of the suspension
ϕ = Roll angle of the body

Note that lateral load transfer arises from two mechanisms:

1) $2 F_y h_r/t$—Lateral load transfer due to cornering forces. This mechanism arises from the lateral force imposed on the axle, and is thus an instantaneous effect. It is independent of roll angle of the body and the roll moment distribution.

2) $2 K_\phi \phi/t$—Lateral load transfer due to vehicle roll. The effect depends on the roll dynamics, and thus may lag the changes in cornering conditions. It is directly dependent on front/rear roll moment distribution.

The total vehicle must be considered to obtain the expression for the roll moment distribution on the front and rear axles. In this case, we define a roll axis as the line connecting the roll centers of the front and rear suspensions, as shown in Figure 6.13. Now the moment about the roll axis in this case is:

$$M_\phi = [W h_1 \sin\phi + W V^2/(R g) h_1 \cos\phi] \cos\varepsilon \qquad (6\text{-}28)$$

For small angles, $\cos\phi$ and $\cos\varepsilon$ may be assumed as unity, and $\sin\phi = \phi$. Then:

$$M_\phi = W h_1 [V^2/(R g) + \phi] \qquad (6\text{-}29)$$

But:

$$M_\phi = M_{\phi f} + M_{\phi r} = (K_{\phi f} + K_{\phi r}) \phi \qquad (6\text{-}30)$$

Equations (6-28) and (6-29) can be solved for the roll angle, ϕ:

$$\phi = \frac{W h_1 V^2/(R g)}{K_{\phi f} + K_{\phi r} - W h_1} \qquad (6\text{-}31)$$

The derivative of this expression with respect to the lateral acceleration produces an expression for the roll rate of the vehicle:

$$R_\phi = d\phi/da_y = W h_1/[K_{\phi f} + K_{\phi r} - W h_1] \qquad (6\text{-}32)$$

The roll rate is usually in the range of 3 to 7 degrees/g on typical passenger cars.

Combining the expression for ϕ from Eq. (6-31) with Eq. (6-29) allows solution for the roll moments on the front and rear axles:

$$M'_{\phi f} = K_{\phi f} \frac{W h_1 V^2/(R g)}{K_{\phi f} + K_{\phi r} - W h_1} + W_f h_f V^2/(R g) = \Delta F_{zf} t_f \qquad (6\text{-}33)$$

$$M'_{\phi r} = K_{\phi r} \frac{W h_1 V^2/(R g)}{K_{\phi f} + K_{\phi r} - W h_1} + W_r h_r V^2/(R g) = \Delta F_{zr} t_r \qquad (6\text{-}34)$$

where:

$\Delta F_{zf} = F_{zfo} - W_f/2 = -(F_{zfi} - W_f/2)$
$\Delta F_{zr} = F_{zro} - W_r/2 = -(F_{zri} - W_r/2)$

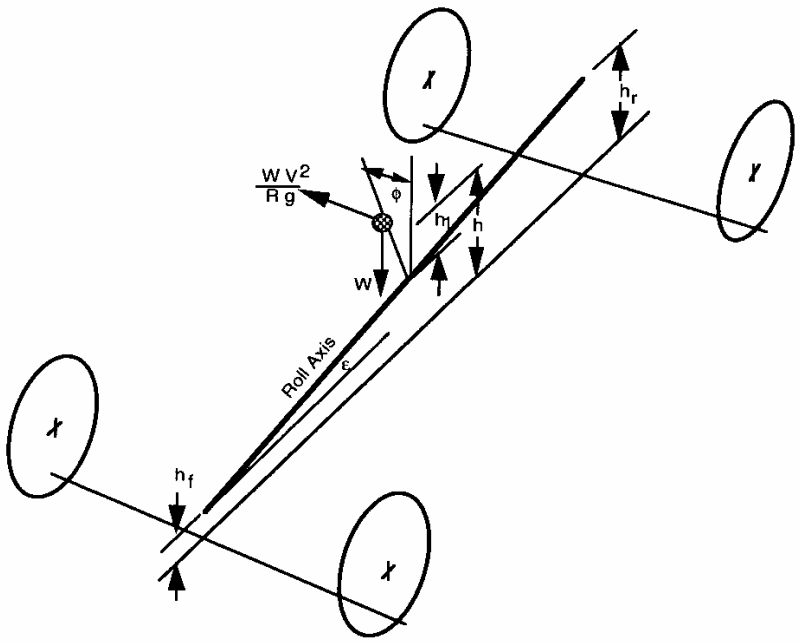

Fig. 6.13 Force analysis for roll of a vehicle.

In general, the roll moment distribution on vehicles tends to be biased toward the front wheels due to a number of factors:

1) Relative to load, the front spring rate is usually slightly lower than that at the rear (for flat ride), which produces a bias toward higher roll stiffness at the rear. However, independent front suspensions used on virtually all cars enhance front roll stiffness because of the effectively greater spread on the front suspension springs.

2) Designers usually strive for higher front roll stiffness to ensure understeer in the limit of cornering.

3) Stabilizer bars are often used on the front axle to obtain higher front roll stiffness.

4) If stabilizer bars are needed to reduce body lean, they may be installed on the front or the front and rear. Caution should be used when adding a stabilizer bar only to the rear because of the potential to induce unwanted oversteer.

We now have the solution for roll moments front and rear, and can calculate the difference in load between the left and right wheels on the axle. To translate the lateral load transfer into an effect on understeer gradient, it is necessary to have data which relates the tire cornering force to slip angle and load. At the given conditions, the slip angle on each axle will change when the load transfer is taken into account. The difference between the change on the front and rear (normalized by the lateral acceleration) represents the understeer effect. The effect can be modeled by expressing the tire load sensitivity as a polynomial. In the first analysis the cornering characteristics of the tires on an axle were described simply by a constant called the cornering stiffness, C_α. The cornering force developed on the axle was given by:

$$F_y = C_\alpha \alpha \tag{6-35}$$

where:

F_y = Lateral force developed on the axle
C_α = Cornering stiffness of two tires, each at one-half the axle load
α = Slip angle

To represent load sensitivity effect, the two tires (inside and outside) must be treated separately. The cornering stiffness of each tire can be represented by a second- or higher-order polynomial, and the lateral force developed by either will be given by:

$$F_y' = C_\alpha' \alpha = (a F_z - b F_z^2) \alpha \tag{6-36}$$

where:

F_y' = Lateral force of one tire
C_α' = Cornering stiffness of one tire
a = First coefficient in the cornering stiffness polynomial (lb_y/lb_z/deg)
b = Second coefficient in the cornering stiffness polynomial (lb_y/lb_z^2/deg)
F_z = Load on one tire (assumed equal on both tires in previous analysis)

For a vehicle cornering as shown in Figure 6.12, the lateral force of both tires, F_y, is given by:

$$F_y = (a F_{zo} - b F_{zo}^2 + a F_{zi} - b F_{zi}^2) \alpha \tag{6-37}$$

Now, let the load change on each wheel be given by ΔF_z.

$$F_{zo} = F_z + \Delta F_z \qquad F_{zi} = F_z - \Delta F_z \tag{6-38}$$

Then:

$$F_y = [a\,(F_z + \Delta F_z) - b\,(F_z + \Delta F_z)^2 + a\,(F_z - \Delta F_z) - b\,(F_z - \Delta F_z)^2\ ]\,\alpha \tag{6-39}$$

This equation reduces to:

$$F_y = [2\,a\,F_z - 2\,b\,F_z^2 - 2\,b\ \Delta F_z^2\ ]\,\alpha \tag{6-40}$$

The equation can be simplified if we recognize that the first two terms in the brackets are equivalent to the cornering stiffness of the tires at their static load conditions (as it has been defined in the previous analysis). Namely:

$$C_\alpha = 2\,a\,F_z - 2\,b\,F_z^2 \tag{6-41}$$

or:

$$F_y = [C_\alpha - 2\,b\ \Delta F_z^2\ ]\,\alpha \tag{6-42}$$

Recall that the steer angle necessary to maintain a turn is given by:

$$\delta = 57.3\ L/R + \alpha_f - \alpha_r \tag{6-43}$$

For the two tires on the front we can write:

$$F_{yf} = [C_{\alpha f} - 2\,b\ \Delta F_{zf}^2\ ]\,\alpha_f = W_f\,V^2/(R\,g) \tag{6-44}$$

and on the rear:

$$F_{yr} = [C_{\alpha r} - 2\,b\ \Delta F_{zr}^2\ ]\,\alpha_r = W_r\,V^2/(R\,g) \tag{6-45}$$

Substituting to eliminate the slip angles in Eq. (6-43):

$$\delta = 57.3\,\frac{L}{R} + \frac{W_f V^2/(R\,g)}{(C_{\alpha f} - 2\,b\,\Delta F_{zf}^2)} - \frac{W_r V^2/(R\,g)}{(C_{\alpha r} - 2\,b\,\Delta F_{zr}^2)} \tag{6-46}$$

This equation can be simplified by utilizing the fact that $C_\alpha >> 2\,b\,\Delta F_z^2$. Then:

$$\frac{1}{(C_\alpha - 2\,b\,\Delta F_z^2)} = \frac{1}{C_\alpha(1 - \dfrac{2\,b\,\Delta F_z^2}{C_\alpha})} \approx \frac{1}{C_\alpha}\left(1 + \frac{2\,b\,\Delta F_z^2}{C_\alpha}\right) \tag{6-47}$$

Equation (6-45) can be rewritten in the form:

$$\delta = 57.3\,\frac{L}{R} + [\,(\frac{W_f}{C_{\alpha f}} - \frac{W_r}{C_{\alpha r}}) + (\frac{W_f}{C_{\alpha f}}\frac{2\,b\,\Delta F_{zf}^2}{C_{\alpha f}} - \frac{W_r}{C_{\alpha r}}\frac{2\,b\,\Delta F_{zr}^2}{C_{\alpha r}})]\frac{V^2}{R\,g}$$

$$\text{<—— 1 ——>} \qquad \text{<———— 2 ————>} \tag{6-48}$$

Term number 1 inside the brackets is simply the understeer gradient arising from the nominal cornering stiffness of the tires, K_{tires}, as was developed earlier. The second term represents the understeer gradient arising from lateral load transfer on the tires; i.e.:

$$K_{llt} = \frac{W_f}{C_{\alpha f}}\frac{2\,b\,\Delta F_{zf}^2}{C_{\alpha f}} - \frac{W_r}{C_{\alpha r}}\frac{2\,b\,\Delta F_{zr}^2}{C_{\alpha r}} \tag{6-49}$$

The values for ΔF_{zf} and ΔF_{zr} can be obtained from Eqs. (6-33) and (6-34) as a function of lateral acceleration. Since all the variables in the above equation are positive, the contribution from the front axle is always understeer; that from the rear axle is always negative, meaning it is an oversteer effect.

Camber Change

The inclination of a wheel outward from the body is known as the camber angle [2]. Camber on a wheel will produce a lateral force known as "camber thrust." Figure 6.14 shows a typical camber thrust curve.

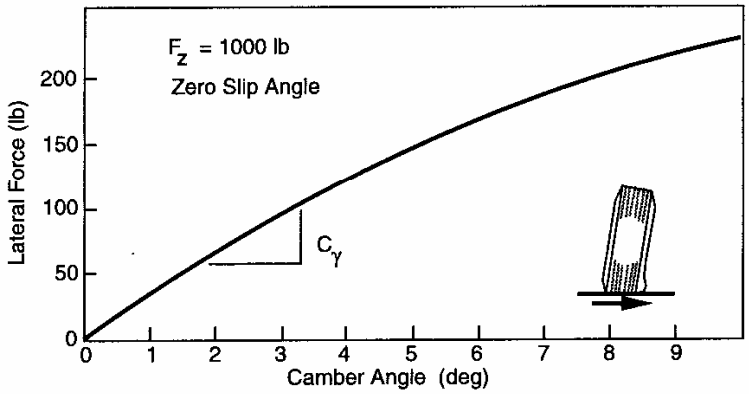

Fig. 6.14 Lateral force caused by camber of a tire.

Camber angle produces much less lateral force than slip angle. About 4 to 6 degrees of camber are required to produce the same lateral force as 1 degree of slip angle on a bias-ply tire. Camber stiffness of radial tires is generally lower than that for bias-ply tires; hence, as much as 10 to 15 degrees are required on a radial. Nevertheless, camber thrust is additive to the cornering force from slip angle, thus affecting understeer. Camber thrust of bias-ply tires is strongly affected by inflation pressure, although not so for radial tires, and it is relatively insensitive to load and speed for both radial and bias tires.

Camber angles are small on solid axles, and at best only change the lateral forces by 10% or less. On independent wheel suspensions, however, camber can play an important role in cornering. Camber changes both as a result of body roll and the normal camber change in jounce/rebound. Figure 6.15 illustrates the mechanisms of camber change as a vehicle rolls in cornering.

The total camber angle during cornering will be:

$$\gamma_g = \gamma_b + \phi \tag{6-50}$$

where:

γ_g = Camber angle with respect to the ground
γ_b = Camber angle of the wheel with respect to the body
ϕ = Roll angle of the vehicle

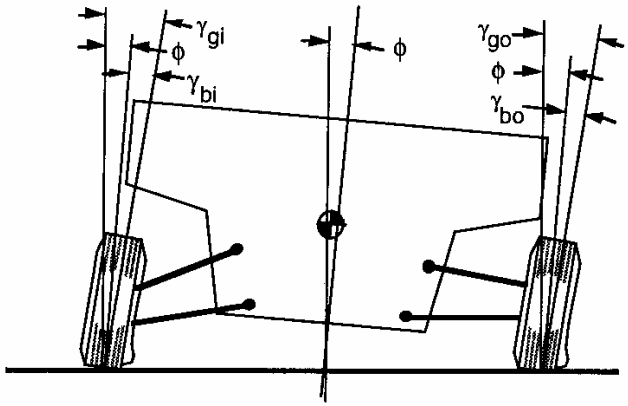

Fig. 6.15 Camber change in cornering of a vehicle.

Now the camber angle arising from the suspension is a function of the roll angle, because the jounce on the inside wheel and the rebound on the outside

wheel relate directly to roll angle. Thus we can obtain the derivative of camber angle with roll angle from analysis of the suspension kinematics. The relationship is dependent on the geometry of the suspension, but for every suspension a kinematic analysis can be performed to develop a camber gradient of the form:

$$\partial\gamma/\partial\phi = f_\gamma(\text{track width, suspension geometry, roll angle}) \tag{6-51}$$

In turn, the roll angle can be related to lateral acceleration through Eq. (6-31) obtained earlier.

The influence on cornering comes about from the fact that the lateral force results not only from slip angle of the tire, but also the camber angle. That is:

$$F_y = C_\alpha \alpha + C_\gamma \gamma \tag{6-52}$$

Thus:

$$\alpha = \frac{F_y}{C_\alpha} - \frac{C_\gamma}{C_\alpha}\gamma \tag{6-53}$$

Now both F_y and γ are related to the lateral acceleration—F_y through Eq. (6-11) and γ through Eq. (6-52). Thus the equations for α_f and α_r take the forms:

$$\alpha_f = \frac{W_f}{C_\alpha} a_y - \frac{C_\gamma}{C_\alpha}\frac{\partial\gamma_f}{\partial\phi}\frac{\partial\phi}{\partial a_y} a_y \quad \text{and} \quad \alpha_r = \frac{W_r}{C_\alpha} a_y - \frac{C_\gamma}{C_\alpha}\frac{\partial\gamma_r}{\partial\phi}\frac{\partial\phi}{\partial a_y} a_y \tag{6-54}$$

When these are substituted into the turning equation (6-14), it takes the form:

$$\delta = 57.3\frac{L}{R} + \left[\left(\frac{W_f}{C_{\alpha f}} - \frac{W_r}{C_{\alpha r}}\right) + \left(\frac{C_{\gamma f}}{C_{\alpha f}}\frac{\partial\gamma_f}{\partial\phi} - \frac{C_{\gamma r}}{C_{\alpha r}}\frac{\partial\gamma_r}{\partial\phi}\right)\frac{\partial\phi}{\partial a_y}\right]\frac{V^2}{R\,g} \tag{6-55}$$

Therefore, the understeer deriving from camber angles on each axle is given by:

$$K_{camber} = \left(\frac{C_{\gamma f}}{C_{\alpha f}}\frac{\partial\gamma_f}{\partial\phi} - \frac{C_{\gamma r}}{C_{\alpha r}}\frac{\partial\gamma_r}{\partial\phi}\right)\frac{\partial\phi}{\partial a_y} \tag{6-56}$$

Roll Steer

When a vehicle rolls in cornering, the suspension kinematics may be such that the wheels steer. Roll steer is defined as the steering motion of the front or rear wheels with respect to the sprung mass that is due to the rolling motion of the sprung mass. Consequently, roll steer effects on handling lag the steer input, awaiting roll of the sprung mass.

The steer angle directly affects handling as it alters the angle of the wheels with respect to the direction of travel. Let "ε" be the roll steer coefficient on an axle (degrees steer/degree roll). Then by reasoning similar to the above, we can derive the understeer gradient contribution from roll steer as:

$$K_{\text{roll steer}} = (\varepsilon_f - \varepsilon_r)\frac{\partial \phi}{\partial a_y} \qquad (6\text{-}57)$$

A positive roll steer coefficient causes the wheels to steer to the right in a right-hand roll. Inasmuch as a right-hand roll occurs when the vehicle is turning to the left, positive roll steer on the front axle steers out of the turn and is understeer. Conversely, positive roll steer on the rear axle is oversteer.

On solid axles the suspension will allow the axle to roll about an imaginary axis which may be inclined with respect to the longitudinal axis of the vehicle. The kinematics of the suspension, regardless of design, may be envisioned as functionally equivalent to leading or trailing arm systems; and the roll axis inclination is equal to that of the arms. Given an initial inclination angle, β, on the arms, as the body rolls, the arm on the inside wheel rotates downward while the arm on the outside wheel rotates upward as illustrated in Figure 6.16.

Fig. 6.16 Roll steer with a solid axle.

If the initial orientation of a rear axle trailing arm is angled downward, as seen in the figure, the effect of the trailing arm angle change is to pull the inside wheel forward while pushing the outside wheel rearward. This produces roll steer of the solid axle contributing to oversteer. The roll steer coefficient is

equal to the inclination angle (ε = β, in radians) of the trailing arms. On a rear trailing arm system, roll understeer is achieved by keeping the transverse pivots of the trailing arms below the wheel center. Figure 6.17 illustrates the effect of trailing arm angle on understeer.

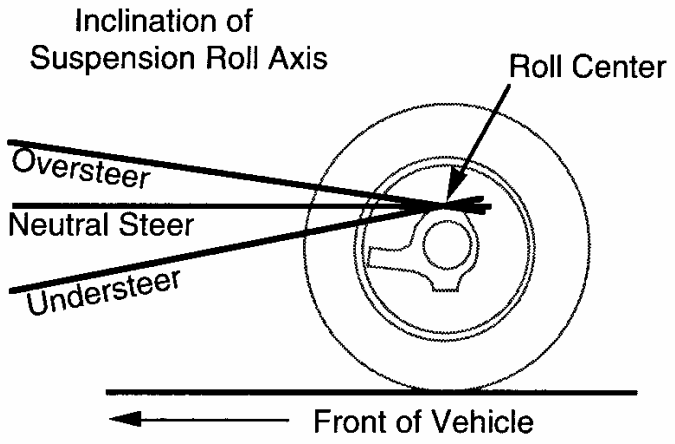

Fig. 6.17 Influence of rear axle trailing arm angle on understeer.

With independent suspensions the roll steer coefficient must be evaluated from the kinematics of the suspension. On steered wheels, the interactions with the steering system must also be taken into account.

Lateral Force Compliance Steer

With the soft bushings used in suspension linkages for NVH reasons, there is the possibility of steer arising from lateral compliance in the suspension. With the simple solid axle, compliance steer can be represented as rotation about a yaw center as illustrated in Figure 6.18.

With a forward yaw center on a rear axle, the compliance allows the axle to steer toward the outside of the turn, thus causing oversteer. Conversely, a rearward yaw center results in understeer. On a front axle, just the opposite is true—a rearward yaw center is oversteer, and a forward yaw center is understeer.

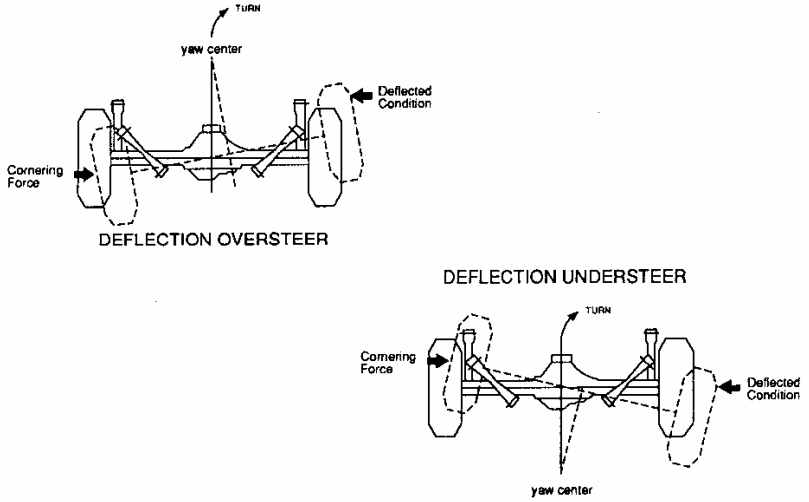

Fig. 6.18 Steer due to lateral compliance in the suspension.

The handling influence of lateral force compliance steer can be quantified by defining an appropriate coefficient as follows:

$$A = \delta_c / F_y \qquad \text{(degrees steer/unit lateral force)} \qquad (6\text{-}58)$$

where:

δ_c = Steer angle
F_y = Lateral force

The lateral force experienced on an axle is simply the load on the axle times the lateral acceleration. Thus on the front axle:

$$\delta_{cf} = A_f W_f a_y \qquad (6\text{-}59)$$

Since the understeer effect is directly related to the steer angles produced on the front and rear axles, the understeer arising from lateral force compliance steer is:

$$K_{lfcs} = A_f W_f - A_r W_r \qquad (6\text{-}60)$$

Of course, the kinematics of linkages must be analyzed and taken into account to determine the coefficients on independent wheel suspensions and on steered wheels.

Aligning Torque

The aligning torque experienced by the tires on a vehicle always resists the attempted turn, thus it is the source of an understeer effect. Aligning torque is the manifestation of the fact that the lateral forces are developed by a tire at a point behind the tire center. The distance is known as the "pneumatic trail (p)."

The direct handling influence can be determined by deriving the turning equations with the assumption that the lateral forces are developed not at the wheels, but at a distance "p" behind each wheel. The understeer term obtained is:

$$K_{at} = W \frac{p}{L} \frac{C_{\alpha f} + C_{\alpha r}}{C_{\alpha f} C_{\alpha r}} \qquad (6\text{-}61)$$

Because the C_α values are positive, the aligning torque effect is positive (understeer) and cannot ever be negative (oversteer).

The understeer due to this mechanism is normally less than 0.5 deg/g. However, aligning torque is indirectly responsible for additional, and more significant, understeer mechanisms through its influence on the steering system. These mechanisms will be discussed with the steering system.

Effect of Tractive Forces on Cornering

The turning analysis developed at the outset of this chapter does not consider the potential effects of drive forces present at the wheels. We will now look at the case of drive forces present at front and rear wheels to develop the general equation showing their influence.

With drive forces, the "bicycle" model for turning is as shown in Figure 6.19. The application of Newton's Second Law in the lateral direction takes the form:

$$W_f V^2/(R\,g) = F_{yf} \cos(\alpha_f + \delta) + F_{xf} \sin(\alpha_f + \delta) \qquad (6\text{-}62)$$

$$W_r V^2/(R\,g) = F_{yr} \cos \alpha_r + F_{xr} \sin \alpha_r \qquad (6\text{-}63)$$

where:

W_f, W_r = Load on the front and rear axles
V = Forward speed
R = Radius of turn
F_{yf}, F_{yr} = Cornering forces on front and rear axles
F_{xf}, F_{xr} = Tractive forces on the front and rear axles
α_f, α_r = Slip angles at front and rear wheels

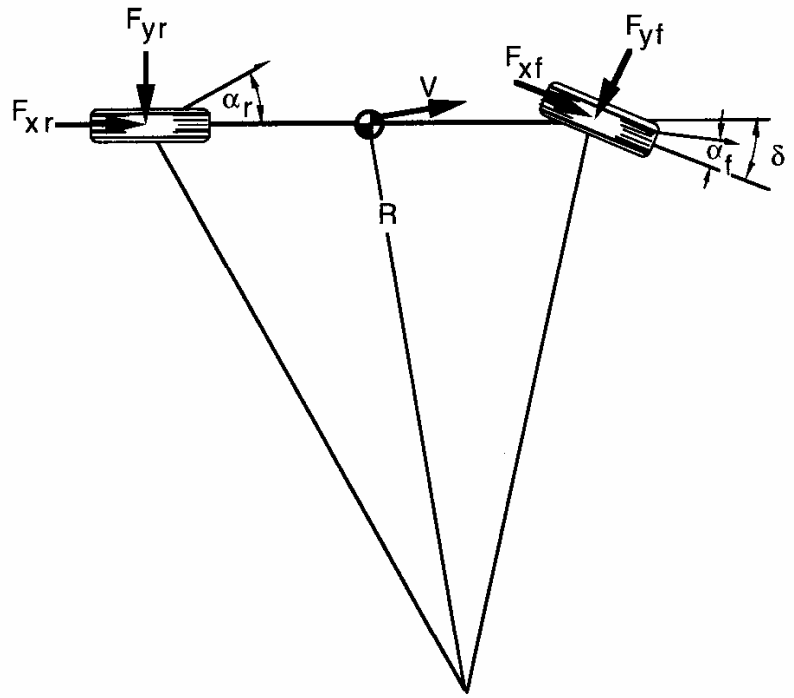

Fig. 6.19 Cornering model with tractive forces.

Now the lateral forces, F_{yf} and F_{yr}, are simply the cornering stiffness on the axle times the slip angle. When that substitution is made in Eqs. (6-62) and (6-63), the right-hand side contains only the tractive forces and the slip angles. Assuming small angles, $\cos \alpha = 1$ and $\sin \alpha = \alpha$, we can then solve for α_f and α_r for substitution into the geometry equation:

$$\delta = 57.3\ L/R + \alpha_f - \alpha_r \tag{6-64}$$

On substitution, δ occurs on both the left- and right-hand sides of the equation, and it is necessary to manipulate to get it only on the left-hand side. Then:

$$\delta = \frac{57.3\ L/R}{1 + F_{xf}/C_{\alpha f}} + \frac{\frac{W_f}{C_{\alpha f}}\frac{V^2}{R\,g}}{1 + F_{xf}/C_{\alpha f}} + \frac{\frac{W_r}{C_{\alpha r}}\frac{V^2}{R\,g}}{1 + F_{xr}/C_{\alpha r}} \tag{6-65}$$

The equation can be gotten into a somewhat more convenient form when we realize that $F_{xf}/C_{\alpha f}$ and $F_{xr}/C_{\alpha r}$ are much less than one. In that case,

$$\frac{1}{1 + F_{xf}/C_{\alpha f}} \approx 1 - F_{xf}/C_{\alpha f} \tag{6-66}$$

The same is true for the rear axle.

Then Eq. (6-65) can be manipulated to the form:

$$\delta = \frac{57.3\ L/R}{1 + F_{xf}/C_{\alpha f}} + [(\frac{W_f}{C_{\alpha f}} - \frac{W_r}{C_{\alpha r}}) - (\frac{W_f}{C_{\alpha f}}\frac{F_{xf}}{C_{\alpha f}} - \frac{W_r}{C_{\alpha r}}\frac{F_{xr}}{C_{\alpha r}})]\frac{V^2}{R\,g}$$

$$\text{<---- 1 ---->} \quad \text{<---- 2 ---->} \quad \text{<---------- 3 ---------->} \tag{6-67}$$

This is the final turning equation for the case where tractive forces are taken into account. Note that though it appears more complicated than that developed earlier, it contains the same basic terms. The three terms on the right-hand side are as follows:

Term 1—This is the Ackerman steer angle altered by the tractive force on the front axle (rear tractive force does not show up here).

- If F_{xf} is positive (drive force applied in a FWD) it reduces the required steer angle for low-speed maneuvers, and accounts for the sense that FWD "pulls" a vehicle around in low-speed maneuvers.
- If F_{xf} is negative (equivalent to rolling resistance on a RWD or engine drag on a FWD) it tends to increase the required steer angle for turning.
- When front wheels spin on snow or ice, tractive force is still produced but $C_{\alpha f}$ goes to zero. In that case the denominator of the term becomes infinite, suggesting that turns of zero radius can be made with virtually no steer angle. This accounts for the "trick" of turning a FWD vehicle within its own length on an icy surface by turning the wheel sharply and making them spin.

Term 2—This is the understeer gradient, unchanged from its earlier form.

Term 3—This term represents the effect of tractive forces on the understeer behavior of the vehicle.

- If F_{xf} is positive it causes an oversteer influence (pulls the front of the vehicle into the turn). Thus this mechanism is an oversteer influence with a FWD in the throttle-on case.

- If F_{xr} is positive it causes an understeer influence by the same reasoning on a RWD.
- On a 4WD these mechanisms would suggest that the rear axle should "over drive" the front axle to ensure understeer behavior.

Anyone familiar with a FWD vehicle may be aware that the throttle-on oversteer mechanism described here is not evident with most vehicles. In discussion of the effects of FWD in the steering section, it will be seen that the modification of tire cornering properties caused by traction forces has a stronger influence on handling than the direct action of the forces on the vehicle.

SUMMARY OF UNDERSTEER EFFECTS

The understeer coefficient, K, for a vehicle is the result of tire, vehicle and steering system parameters. Its total value is computed as the sum of a number of effects as summarized in the following table.

UNDERSTEER COMPONENT	SOURCE
$K_{tires} = \frac{W_f}{C_{\alpha f}} - \frac{W_r}{C_{\alpha r}}$	Tire cornering stiffness
$K_{camber} = (\frac{C_{\gamma f}}{C_{\alpha f}} \frac{\partial \gamma_f}{\partial \phi} - \frac{C_{\gamma r}}{C_{\alpha r}} \frac{\partial \gamma_r}{\partial \phi}) \frac{\partial \phi}{\partial a_y}$	Camber thrust
$K_{roll\ steer} = (\varepsilon_f - \varepsilon_r)\ d\phi/da_y$	Roll steer
$K_{lfcs} = A_f W_f - A_r W_r$	Lateral force compliance steer
$K_{at} = W \frac{p}{L} \frac{C_{\alpha f} + C_{\alpha r}}{C_{\alpha f} C_{\alpha r}}$	Aligning torque
$K_{llt} = \frac{W_f}{C_{\alpha f}} \frac{2\, b\, \Delta F_{zf}^2}{C_{\alpha f}} - \frac{W_r}{C_{\alpha r}} \frac{2\, b\, \Delta F_{zr}^2}{C_{\alpha r}}$	Lateral load transfer
$K_{strg} = W_f \frac{r\, v + p}{K_{ss}}$	Steering system

EXPERIMENTAL MEASUREMENT OF UNDERSTEER GRADIENT

Understeer gradient is defined by the SAE [2] as "The quantity obtained by subtracting the Ackerman steer angle gradient from the ratio of the steering wheel angle gradient to the overall steering ratio." Methods for experimental measurement of understeer gradient [12, 13, 14] are all based on the definition of the gradient reflected in Eq. (6-16). Namely,

$$\delta = 57.3\ L/R + K\ a_y \qquad (6\text{-}16)$$

The derivation of this equation assumes the vehicle to be in a steady-state operating condition; therefore, understeer is defined as a steady-state property. For experimental measurement the vehicle must be placed into a steady-state turn with appropriate measures of the quantities in the above equation so that the value of K can be determined. Four test methods have been suggested as means to measure this property—constant radius, constant speed, constant steer angle and constant throttle. Only the first two reasonably reflect normal driving circumstances, hence, the discussion will be limited to these two.

Constant Radius Method

Understeer can be measured by operating the vehicle around a constant radius turn and observing steering angle versus lateral acceleration. The method closely replicates vehicle operation in many highway situations, such as the constant radius turns in off ramps from limited access highways. At a minimum, instrumentation must be available to measure steering wheel angle and lateral acceleration. Given the radius of turn and some measure of vehicle velocity (from the speedometer, fifth wheel or by lap time), lateral acceleration can be computed using the relationship:

$$a_y = V^2/(Rg) \qquad (6\text{-}68)$$

The recommended procedure is to drive the vehicle around the circle at very low speed, for which the lateral acceleration is negligible, and note the steer angle (Ackerman steer angle) required to maintain the turn. (The experimenter is challenged to develop good technique for this process as cross-slope on the test surface, bumps, etc., will cause the vehicle to drift in and out as it proceeds, complicating the determination of the average steer angle.) Vehicle speed is then increased in steps that will produce lateral accelerations at reasonable increments (typically 0.1 g), noting the steer angle at each speed. The steer angle (divided by the steering ratio to obtain the road wheel angle)

is then plotted as a function of lateral acceleration as illustrated in Figure 6.20.

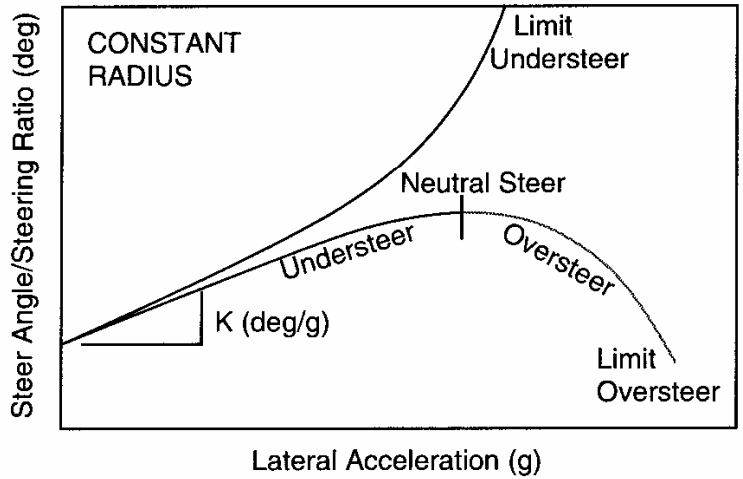

Fig 6.20 Example measurements of understeer gradient by constant radius method.

The meaning of this plot can be seen by taking the derivative of Eq. (6-16):

$$\frac{\partial \delta}{\partial a_y} = \frac{\partial}{\partial a_y}(57.3\,\frac{L}{R}) + K\,\frac{\partial a_y}{\partial a_y} \qquad (6\text{-}69)$$

Since the radius of turn is constant, the Ackerman steer angle is also constant and its derivative is zero. Thus:

$$K = \frac{\partial \delta}{\partial a_y} \qquad (6\text{-}70)$$

The slope of the steer angle curve is the understeer gradient. A positive slope (upward to the right) indicates understeer, zero slope is neutral steer, and a negative slope is oversteer. Typical measurements will take one of the forms shown in Figure 6.20. Some vehicles will be understeer over the entire operating range, remaining so to the limit. Others may be understeer at low lateral acceleration levels but change to oversteer at high lateral acceleration levels and exhibit limit oversteer.

Note that the implied road wheel steer angle (obtained by dividing the steering wheel angle by the steering ratio) is used for characterizing the understeer gradient. While understeer is measured at the steering wheel, it is described by the degrees per g of steer required at the road wheel. As will be seen in the discussion of steering systems, the steering ratio is not a constant because of compliance in the system. This does not invalidate the measurement method, but rather recognizes that those properties in the steering system are a legitimate source of understeer on the vehicle. In cases where the road wheel steer angle is measured directly, a different understeer gradient will be obtained because the steering system effects will not be included. While this method is not incorrect, it fails to fully characterize the understeer properties of the vehicle by excluding contribution from the steering system. Recognizing that the driver must control the vehicle from the steering wheel, the steering system effects should be included in a full characterization of understeer.

The constant radius method has the advantage that minimal instrumentation is required, but has the disadvantage that it is difficult to execute in an objective fashion. Determination of a precise steering wheel angle is difficult because of the deviations necessary to keep the vehicle on the selected radius of turn. This aspect of test technique is not readily controlled.

The minimum radius of turn for this test procedure is normally 30 m (≈100 ft). For two-axle vehicles the understeer gradient is not affected by the radius of the circle. The gradient for multi-axle straight trucks (three axles or more), however, is sensitive to turn radius in this range.

Constant Speed Method

Understeer can be measured at constant speed by varying the steer angle. Measurements by this method closely duplicate many real driving situations since vehicles are normally driven at near constant speed. With this method the radius of turn will vary continuously requiring more extensive data collection to determine the gradient. In addition to measuring speed and steer angle, the radius of turn must be determined for each condition as well. The most practical means to measure radius of turn is either by measuring lateral acceleration or yaw rate. The radius of turn is derived from the measurements using the appropriate form of the relationships below:

$$R = V^2/a_y = V/\mathbf{r} \qquad (6\text{-}71)$$

where:

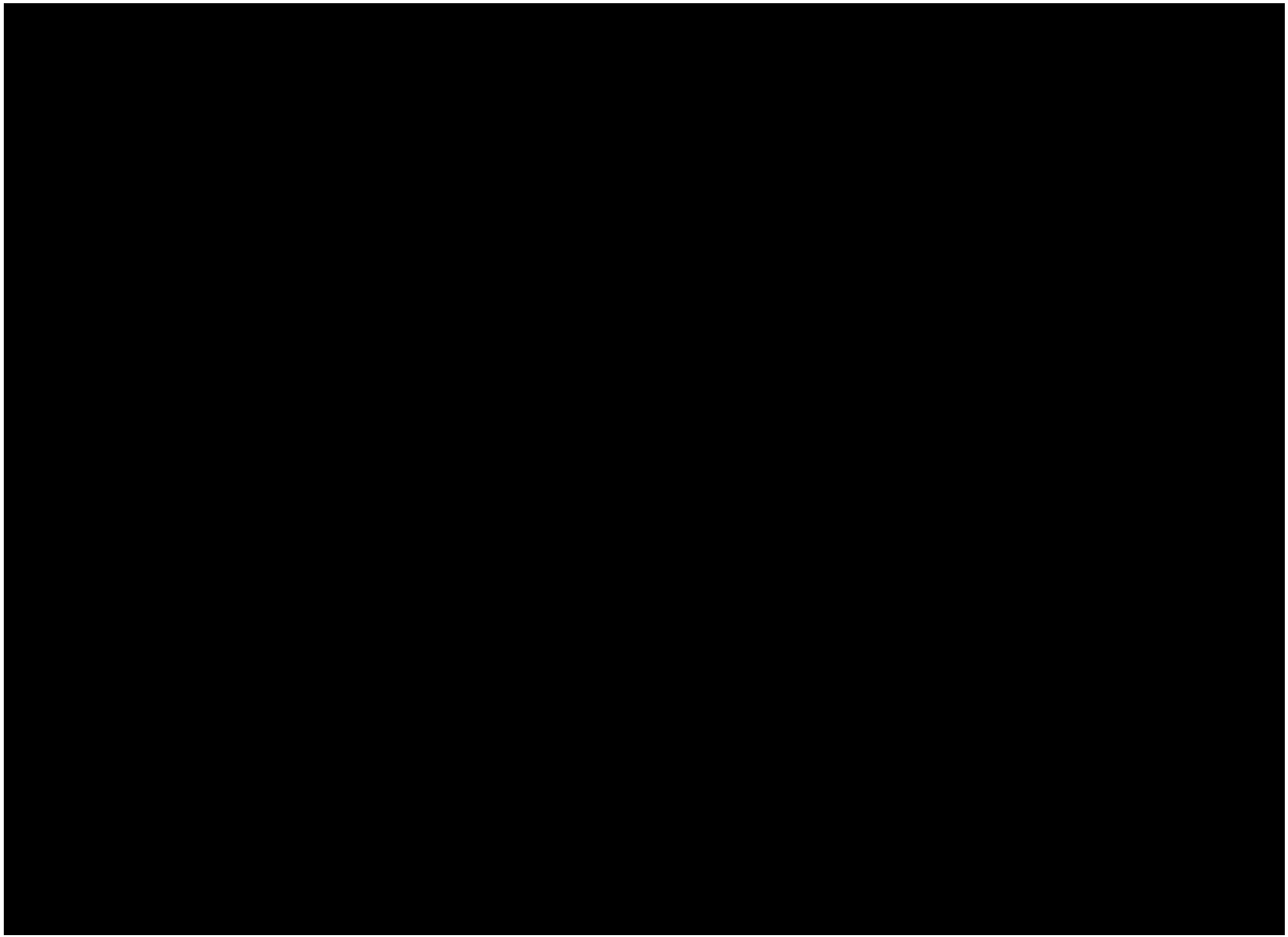

and 1125 lb leads to a stiffness of 232 lb/deg at 950 lb. On the rear axle the load is 776 lb per tire. Again interpolating between the appropriate loads in the tire data, we obtain a cornering stiffness of 195 lb/deg. Now from Eq. (6-15) we get:

$$K = \frac{W_f}{C_{\alpha f}} - \frac{W_r}{C_{\alpha r}} = \frac{950 \text{ lb}}{232 \text{ lb/deg}} - \frac{776 \text{ lb}}{195 \text{ lb/deg}} = (4.09 - 3.98) \text{ deg} = 0.11 \text{ deg(/g)}$$

c) The characteristic speed is determined from Eq. (6-18):

$$V_{char} = \sqrt{57.3 \, L \, g/K} = \sqrt{57.3 \, \frac{\text{deg}}{\text{rad}} \, \frac{110.6 \text{ in}}{12 \text{ in/ft}} \, \frac{32.2 \text{ ft/sec}^2}{0.11 \text{ deg/g}}} = 393 \text{ ft/sec} = 268 \text{ mph}$$

d) The lateral acceleration gain comes from Eq. (6-20):

$$\frac{a_y}{\delta} = \frac{\frac{V^2}{57.3 \, L \, g}}{1 + \frac{K \, V^2}{57.3 \, L \, g}} = \frac{\frac{(88 \text{ ft/sec})^2}{57.3 \text{ deg/rad } (8.38 \text{ ft}) \, (32.2 \text{ ft/sec}^2)}}{1 + \frac{0.11 \text{ deg/g } (88 \text{ ft/sec})^2}{57.3 \text{ deg/rad } (8.38 \text{ ft}) \, (32.2 \text{ ft/sec}^2)}}$$

$$= \frac{0.501 \text{ g/deg}}{1.055} = 0.475 \text{ g/deg}$$

e) The yaw rate gain comes from Eq. (6-22):

$$\frac{r}{\delta} = \frac{V/L}{1 + \frac{K \, V^2}{57.3 \, L \, g}} = \frac{\frac{88 \text{ ft/sec}}{8.38 \text{ ft}}}{1 + \frac{0.11 \text{ deg/g } (88 \text{ ft/sec})^2}{57.3 \text{ deg/rad } (8.38 \text{ ft}) \, (32.2 \text{ ft/sec}^2)}}$$

$$= \frac{10.5 \text{ /sec}}{1.055} = 9.95 \, \frac{\text{deg/sec}}{\text{deg}}$$

f) The sideslip angle is obtained from Eq. (6-23), but first we must find the value for "c," the distance from the CG to the rear axle. This is obtained from a simple moment balance about the front axle.

$$c = \frac{100.6 \text{ in}}{12 \text{ in/ft}} \, \frac{1901 \text{ lb}}{(1901 + 1552) \text{ lb}} = 4.62 \text{ ft}$$

$$\beta = 57.3 \, \frac{c}{R} - \frac{W_r \, V^2}{C_{\alpha r} \, R \, g} = 57.3 \text{ deg/rad } \frac{4.62 \text{ ft}}{800 \text{ ft}} - \frac{1552 \text{ lb } (88 \text{ ft/sec})^2}{390 \text{ lb/deg } (32.2 \text{ ft/sec}^2) \, (800 \text{ ft})}$$

$$= (0.331 - 1.196) \text{ deg} = - 0.865 \text{ deg}$$

g) To find the static margin it is necessary to find the neutral steer point. The neutral steer point (nsp) is the point on the side of the vehicle where one can push laterally and produce the same slip angle at both the front and rear tires. In the solution for part 'a' we determined that the cornering stiffnesses of the front and rear tires are 232 and 195 lb/deg, respectively. From a moment balance in the plan view, we can show that the distance from the nsp to the rear axle (c') must be:

$$c' = WB \, \frac{C_{af}}{C_{af} + C_{ar}} = 8.38 \text{ ft } \frac{232}{232 + 195} = 4.55 \text{ ft}$$

Now c was 4.62 ft, therefore the neutral steer point is 0.07 ft (0.8% of the wheelbase) behind the CG.

Note:

The calculated cornering properties for this vehicle (understeer gradient and static margin) are very close to neutral steer. However, this is a consequence of only the tire properties. Many other systems on the vehicle, particularly the steering and suspension systems, will contribute to the understeer gradient.

2) A passenger car car has an equal arm (parallel) independent front suspension and a conventional solid rear axle with leaf spring suspension. The front suspension has a roll stiffness, $K_{\phi f}$, of 1500 in-lb/deg. The leaf springs have a rate of 115 lb/in and a lateral separation of 40 inches.

a) What is the rear suspension roll stiffness?

b) If the sprung mass is 2750 lb at a CG height 8 inches above the roll axis, what is the roll rate?

c) Assuming a camber stiffness that is 10 percent of the cornering stiffness, estimate the understeer gradient due to camber effects.

d) The rear leaf springs have an effective trailing arm angle of -7 degrees

(the negative sign means that the pivot of the arms is below the wheel center). What is the understeer gradient due to rear roll steer?

Solution:

a) The rear suspension roll stiffness can be computed from Eq. (6-26):

$$K_\phi = 0.5\, K_s\, s^2 = 0.5\,(115\ \text{lb/in})\,(40\ \text{in})^2 = 92{,}000\ \text{in-lb/rad} = 1606\ \text{in-lb/deg}$$

b) The roll rate can be calculated from Eq. (6-32):

$$d\phi/da_y = W\, h_1/[K_{\phi f} + K_{\phi r} - W\, h_1]$$

$$= \frac{2750\ \text{lb (10 in)}}{(1500\ \frac{\text{in-lb}}{\text{deg}} + 1606\ \frac{\text{in-lb}}{\text{deg}} - \frac{2750\ \text{lb (10 in)}}{57.3\ \text{deg/rad}})} = \frac{27500\ \text{in-lb}}{(1500 + 1606 - 480)\ \frac{\text{in-lb}}{\text{deg}}} = 10.5\ \text{deg/g}$$

c) The understeer gradient due to camber effects can be estimated from Eq. (6-56):

$$K_{camber} = \left(\frac{C_{\gamma f}}{C_{\alpha f}}\frac{\partial \gamma_f}{\partial \phi} - \frac{C_{\gamma r}}{C_{\alpha r}}\frac{\partial \gamma_r}{\partial \phi}\right)\frac{\partial \phi}{\partial a_y}$$

Although we know the ratio of camber stiffness to cornering stiffness (given as 0.1), the camber gradients must be determined. For an independent front suspension with parallel equal arms, the wheel does not incline with jounce and rebound. Therefore, the camber angle will change exactly with the roll angle and the gradient for the front axle is 1. The rear axle is a solid axle which does not roll significantly. Therefore, its gradient is zero. Finally, we know the roll gradient from part b, where it was calculated as 10.5 deg/g, and the equation can now be solved.

$$K_{camber} = (0.1 \times 1.0 - 0.1 \times 0)\ 10.5\ \text{deg/g} = 1.05\ \text{deg/g}$$

d) The understeer gradient due to roll steer on the rear axle comes from Eq. (6-57):

$$K_{\text{roll steer}} = (\varepsilon_f - \varepsilon_r)\, d\phi/da_y$$

Since we are concerned only with the rear axle, only the second term must be determined. A solid axle will exhibit roll steer dependent on the effective angle of the imaginary trailing arms, which in this case is -7 degrees (- 0.122 radians). Then:

$$K_{\text{roll steer (rear)}} = +0.122\ \text{radians}\ (10.5\ \text{deg/g}) = 1.28\ \text{deg/g}$$

By SAE convention, the positive sign means that the wheels steer right as the body rolls to the right (left turn). Since the roll steer turns the rear wheels to the right on a left turn, the rear will swing out more in the turn and oversteer is experienced.

REFERENCES

1. Good, M.C., "Sensitivity of Driver-Vehicle Performance to Vehicle Characteristics Revealed in Open-Loop Tests," Vehicle Systems Dynamics, Vol. 6, No. 4, 1977, pp. 245-277.
2. "Vehicle Dynamics Terminology," SAE J670e, Society of Automotive Engineers, Warrendale, PA (see Appendix A).
3. Durstine, J.W., The Truck Steering System from Hand Wheel to Road Wheel, SAE SP-374, 1973, 76 p.
4. Lugner, P., and Springer, H., "Uber den Enfluss der Lenkgeometrie auf die stationare Kurventfahrt eines LKW," (Influence of Steering Geometry on the Stationary Cornering of a Truck), *Automobil-Industrie*, November 1974, pp. 21-25.
5. Pitts, S., and Wildig, A.W., "Effect of Steering Geometry on Self-Centering Torque and 'Feel' During Low-Speed Maneuvers," *Automotive Engineer*, Institution of Mechanical Engineers, June-July 1978, pp. 45-48.
6. Nordeen, D.L., and Cortese, A.D., "Force and Moment Characteristics of Rolling Tires," SAE Paper No. 640028 (713A), 1963, 13 p.
7. 1991 Yearbook, The Tire & Rim Association Inc., Copley, OH, 1991.
8. Bundorf, R.T., "The Influence of Vehicle Design Parameters on Characteristic Speed and Understeer," SAE Paper No. 670078, 1967, 10 p.
9. Bundorf, R.T., and Leffert, R.L.,"The Cornering Compliance Concept for Description of Vehicle Directional Control Properties," SAE Paper No. 760713, 1976, 14 p.
10. Ellis, J.R., Vehicle Dynamics, Business Books Limited, London, 199, 243 p.

11. Olley, M., "National Influences on American Passenger Car Design," Proceedings of The Institution of Automobile Engineers, Vol. 32, 1938, pp. 509-572.

12. "Passenger Car and Light Truck Directional Control Response Test Procedures," SAE XJ266, Proposed Recommended Practice, Society of Automotive Engineers, Warrendale, PA.

13. "Steady-State Circular Test Procedure for Trucks and Buses," SAE J2181, Proposed Recommended Practice, Society of Automotive Engineers, Warrendale, PA.

14. "Road Vehicles - Steady-State Circular Test Procedure," International Standard ISO 4138, International Organization for Standardization, 1982, 14 p.

CHAPTER 7
SUSPENSIONS

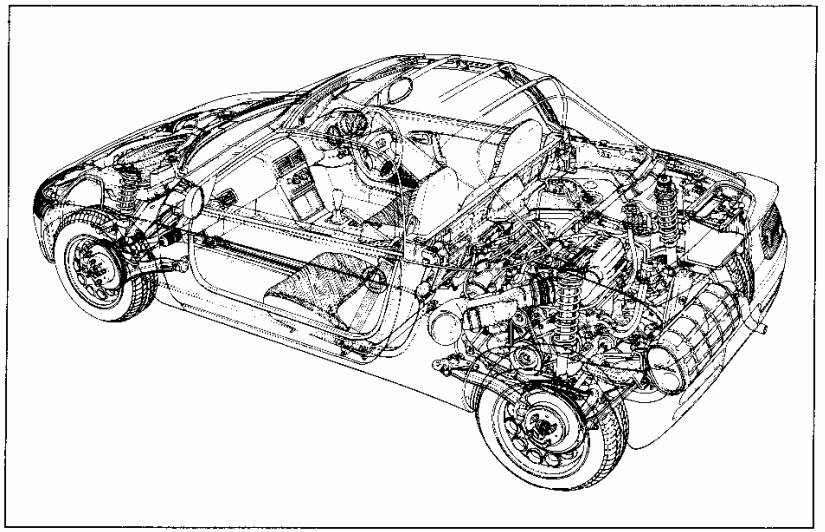

Suspension system of the Beat. (Courtesy of Honda Motor Co., Ltd.)

With a background understanding of suspension properties that affect ride and directional response provided in the previous chapters, it is now appropriate to examine the various types of suspensions used on modern passenger cars.

The primary functions of a suspension system are to:

- Provide vertical compliance so the wheels can follow the uneven road, isolating the chassis from roughness in the road.
- Maintain the wheels in the proper steer and camber attitudes to the road surface.
- React to the control forces produced by the tires—longitudinal (acceleration and braking) forces, lateral (cornering) forces, and braking and driving torques.
- Resist roll of the chassis.
- Keep the tires in contact with the road with minimal load variations.

The properties of a suspension important to the dynamics of the vehicle are primarily seen in the kinematic (motion) behavior and its response to the forces and moments that it must transmit from the tires to the chassis [1, 2, 3, 4]. In addition, other characteristics considered in the design process are cost, weight, package space, manufacturability, ease of assembly, and others.

Suspensions generally fall into either of two groups—solid axles and independent suspensions. Each group can be functionally quite different, and so will be divided accordingly for discussion.

SOLID AXLES

A solid axle is one in which wheels are mounted at either end of a rigid beam so that any movement of one wheel is transmitted to the opposite wheel [5] causing them to steer and camber together. Solid drive (sometimes called "live") axles are used on the rear of many cars and most trucks and on the front of many four-wheel-drive trucks. Solid beam axles are commonly used on the front of heavy trucks where high load-carrying capacity is required.

Solid axles have the advantage that wheel camber is not affected by body roll. Thus there is little wheel camber in cornering, except for that which arises from slightly greater compression of the tires on the outside of the turn. In addition, wheel alignment is readily maintained, minimizing tire wear. The major disadvantage of solid steerable axles is their susceptibility to tramp-shimmy steering vibrations.

Hotchkiss

The most familiar form of the solid drive axle is the Hotchkiss drive [5]. The axle is located by semi-elliptic leaf springs as shown in Figure 7.1, and is driven through a longitudinal driveshaft with universal joints at the transmission and axle. The springs, mounted longitudinally, connect to the chassis at their ends with the axle attached near the midpoint.

Leaf springs are perhaps the simplest and least expensive of all suspensions. While compliant in the vertical direction, the leaf is relatively stiff in the lateral and longitudinal directions, thereby reacting the various forces between the sprung and unsprung masses. The Hotchkiss was used widely on the rear axle of passenger cars into the 1960s, and is still used on most light and heavy trucks. The demise of leaf springs on passenger cars was caused by the inherent

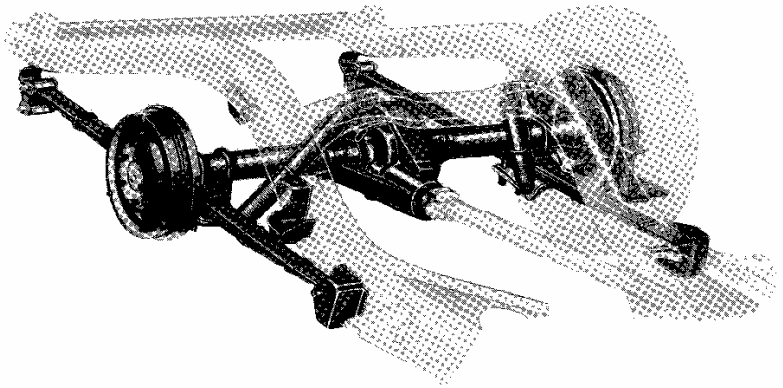

Fig. 7.1 The Hotchkiss rear suspension. (Photo courtesy of Ford Motor Company.)

friction of the springs and the loss in side stability of the springs as they were made longer to achieve lower spring rates [6]. With softer springs, compliance in the windup direction often required the addition of trailing arms to react brake torques and also the greater drive torques coincident with high-power engines popular in the post-war decades.

Four Link

In response to the shortcomings of leaf spring suspensions, the four-link rear suspension, shown in Figure 7.2, evolved as the suspension of choice in recent decades for the larger passenger cars with solid rear-drive axles. The lower control arms provide longitudinal control of the axle while the upper arms absorb braking/driving torques and lateral forces. Occasionally, the two upper arms will be replaced by a single, triangular arm, but it remains functionally similar to the four-link. The ability to use coil springs (or air springs) in lieu of leaf springs provides better ride and NVH by the elimination of the coulomb friction characteristic of leaf springs.

Although more expensive than the leaf spring, the geometric design of the four-link allows better control of roll center location, anti-squat and anti-dive performance, and roll steer properties.

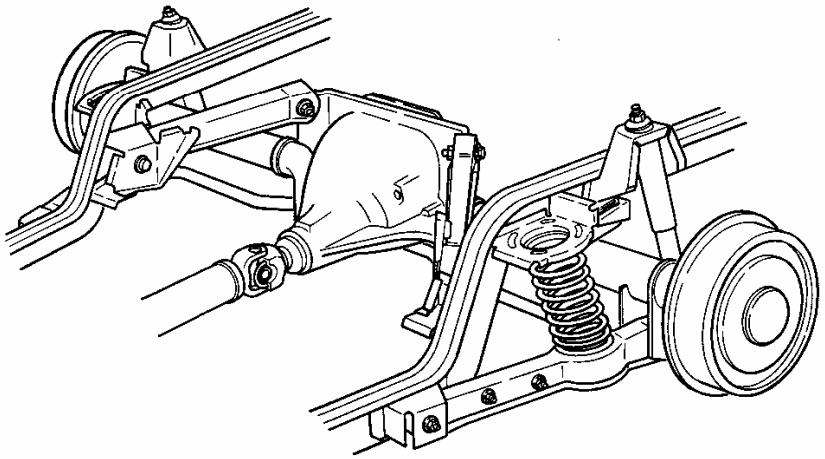

Fig. 7.2 The four-link rear suspension. (Photo courtesy of Ford Motor Company.)

De Dion

A cross between the solid axle and an independent suspension is the classic, but little used, de Dion system (patented in 1894 by Count de Dion and George Bouton), shown in Figure 7.3. It consists of a cross tube between the two driving wheels with a chassis-mounted differential and halfshafts. Like a solid axle, the de Dion keeps the wheels upright while the unsprung weight is reduced by virtue of the differential being removed from the axle. Axle control is provided by any of a variety of linkages from leaf springs to trailing arms. The design also has advantages for interior space because there is no need to provide differential clearance. One of the main disadvantages of the de Dion is the need to have a sliding tube or splined halfshafts, which can add friction to the system.

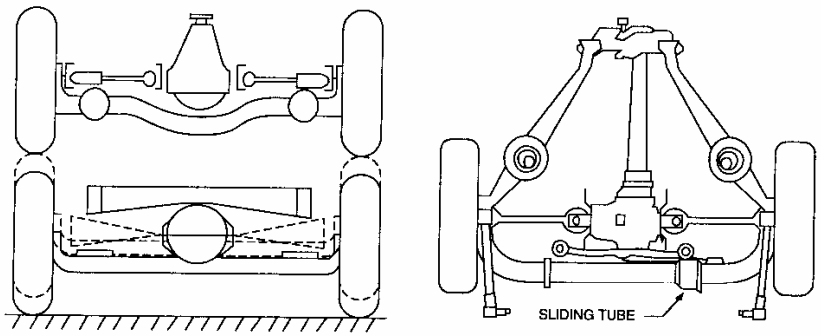

Fig. 7.3 The de Dion rear suspension.

INDEPENDENT SUSPENSIONS

In contrast to solid axles, independent suspensions allow each wheel to move vertically without affecting the opposite wheel. Nearly all passenger cars and light trucks use independent front suspensions, because of the advantages in providing room for the engine, and because of the better resistance to steering (wobble and shimmy) vibrations. The independent suspension also has the advantage that it provides an inherently higher roll stiffness relative to the vertical spring rate.

The first independent suspensions appeared on front axles in the early part of this century. Maurice Olley [7, 8] deserves much of the credit for promoting its virtues, recognizing that it would reduce some of the wobble and shimmy problems characteristic of the solid axles (by decoupling the wheels and interposing the mass of the car between the two wheels). Further advantages included easy control of the roll center by choice of the geometry of the control arms, the ability to control tread change with jounce and rebound, larger suspension deflections, and greater roll stiffness for a given suspension vertical rate.

Trailing Arm Suspension

One of the most simple and economical designs of an independent front suspension is the trailing arm used by Volkswagen and Porsche around the time of World War II. This suspension, shown in Figure 7.4, uses parallel, equal-

length trailing arms connected at their front ends to lateral torsion bars, which provide the springing. With this design the wheels remain parallel to the body and camber with body roll.

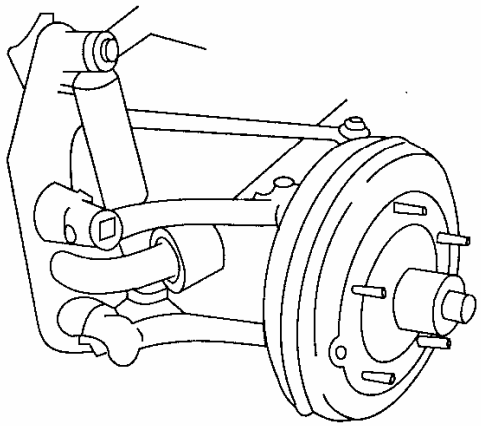

Fig. 7.4 The trailing arm independent front suspension.

SLA Front Suspension

The most common design for the front suspension of American cars following World War II used two lateral control arms to hold the wheel as shown in Figure 7.5. The upper and lower control arms are usually of unequal length from which the acronym SLA (short-long arm) gets its name. The arms are often called "A-arms" in the United States and "wishbones" in Britain. This layout sometimes appears with the upper A-arm replaced by a simple lateral link, or the lower arm replaced by a lateral link and an angled tension strut, but the suspensions are functionally similar.

The SLA is well adapted to front-engine, rear-wheel-drive cars because of the package space it provides for the engine oriented in the longitudinal direction. Additionally, it is best suited to vehicles with a separate frame for mounting the suspension and absorbing the loads.

Design of the geometry for an SLA requires careful refinement to give good performance. The camber geometry of an unequal-arm system can improve camber at the outside wheel by counteracting camber due to body roll, but usually carries with it less-favorable camber at the inside wheel. (Equal-

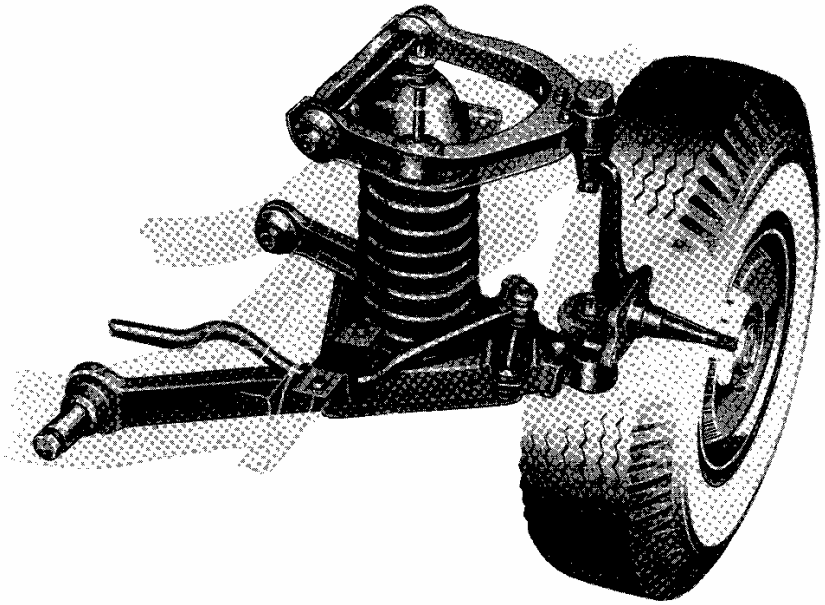

Fig. 7.5 The A-arm front suspension. (Photo courtesy of Ford Motor Company.)

length parallel arms eliminate the unfavorable condition on the inside wheel but at the loss of camber compensation on the outside wheel.) At the same time, the geometry must be selected to minimize tread change in jounce and rebound to avoid excessive tire wear.

MacPherson Strut

Earle S. MacPherson developed a suspension with geometry similar to the unequal-arm front suspensions using a strut configuration (see Figure 7.6). The strut is a telescopic member incorporating damping with the wheel rigidly attached at its lower end, such that the strut maintains the wheel in the camber direction. The upper end is fixed to the body shell or chassis, and the lower end is located by linkages which pick up the lateral and longitudinal forces. Because of the need to offset the strut inboard of the wheel, the wheel loads the strut with an overturning moment which adds to friction in the strut. This is often counteracted by mounting the coil spring at an angle on the strut.

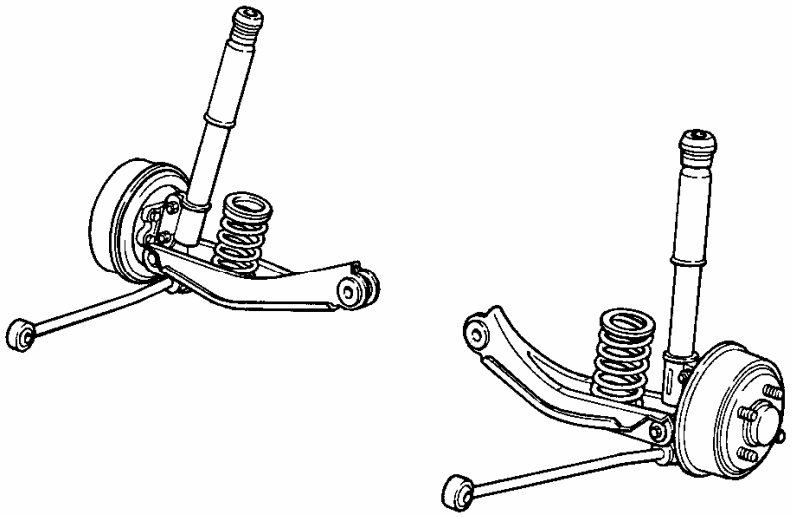

Fig. 7.6 The MacPherson strut suspension. (Photo courtesy of Ford Motor Company.)

The MacPherson strut provides major advantages in package space for transverse engines, and thus is used widely for front-wheel-drive cars. Because of the separation of the connection points on the body, it is well-suited to vehicles with unibody construction. The strut has further advantages of fewer parts and capability to spread the suspension loads to the body structure over a wider area. Among its disadvantages is the high installed height which limits the designer's ability to lower hood height.

Multi-Link Rear Suspension

In recent years, multi-link versions of independent rear suspensions have become quite popular. Figure 7.7 shows that used on the Ford Taurus/Sable cars. The multi-link is characterized by ball-joint connections at the ends of the linkages so that they do not experience bending moments. Generally speaking, four links are required to provide longitudinal and lateral control of the wheels, and react brake torques. Occasionally five links are used, as in the Mercedes Benz rear suspensions. The additional link over-constrains the wheel, but capitalizes on compliances in the bushings to allow more accurate control of toe angles in cornering. The use of linkages provides flexibility for the designer to achieve the wheel motions desired.

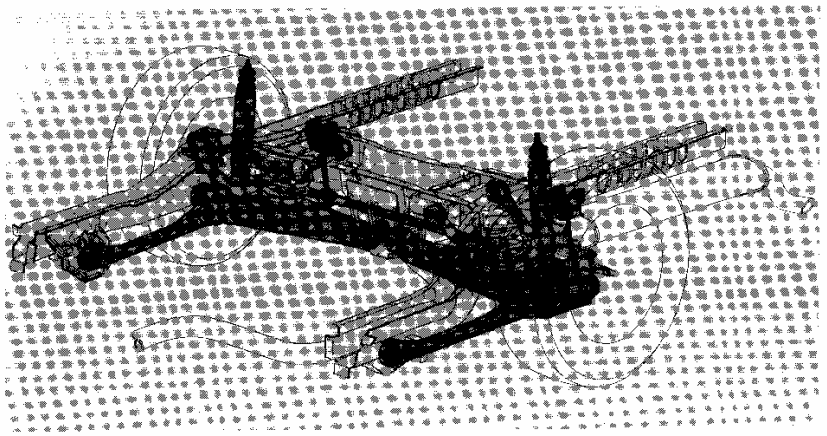

Fig. 7.7 Multi-link rear suspension of the Ford Taurus and Sable. (Photo courtesy of Ford Motor Company.)

Trailing-Arm Rear Suspension

Suspensions of this type are often used on more expensive and high-performance cars. A popular American car example is the Corvette rear suspension shown in Figure 7.8. The control arms (trailing arms) absorb longitudinal forces and braking moments, and control squat and lift. In the Corvette design the U-jointed halfshafts serve as an upper lateral control arm with a simple strut rod serving as the lower lateral arm. The independent suspension has the advantage of reducing unsprung weight by mounting the differential on the body.

Semi-Trailing Arm

The semi-trailing arm rear suspension was popularized by BMW and Mercedes Benz. This design, as shown in Figure 7.9, gives rear wheel camber somewhat between that of a pure trailing arm (no camber change relative to the body) and a swing axle. Its pivot axis is usually about 25 degrees to a line running across the car. The semi-trailing arm produces a steering effect as the wheels move in jounce and rebound. The steer/camber combination on the outside wheel acts against the direction of cornering, thus generating roll understeer on the rear axle, but lateral force compliance steer will contribute oversteer if not controlled.

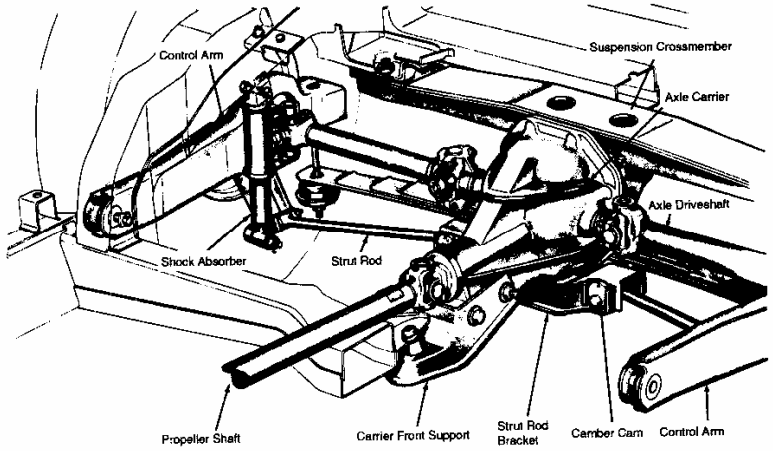

Fig. 7.8 The Corvette independent rear suspension. (Courtesy of Chevrolet Motor Division.)

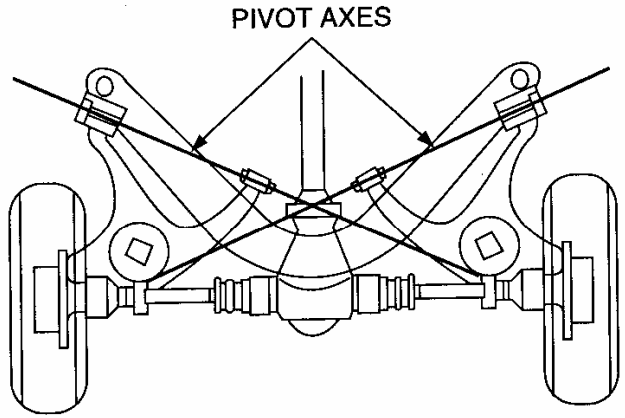

Fig. 7.9 The semi-trailing arm rear suspension.

Swing Axle

The easiest way to get independent rear suspension is by swing axles as shown in Figure 7.10. Edmund Rumpler is credited with inventing this system around the turn of the century, and by 1930 they were used on several European cars, most notably the Volkswagen "Beetle."

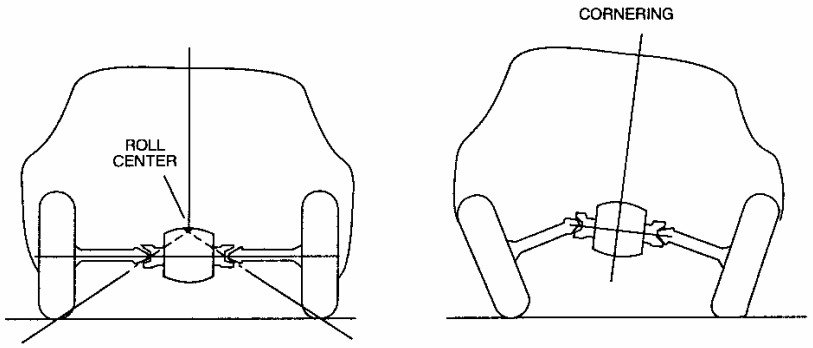

Fig. 7.10 The swing-axle rear suspension.

The camber behavior is established entirely by the axle shafts pivoting at the U-joint adjacent to the differential. The swing radius is small and thus the camber change with jounce and rebound movements can be large. As a result, it is difficult to get consistent cornering performance from swing-axle arrangements.

Critical to any independent suspension, but especially with the swing axle and semi-trailing arm, is a phenomenon known as "jacking." Jacking occurs during cornering when both tires are developing cornering forces but with the outside (more heavily loaded tire) contributing the greater cornering force. The inward direction of the cornering force attempts to lift the vehicle such that the wheels "tuck under." This has the effect of elevating the vehicle body (reducing its rollover resistance) and causing loss of cornering force on the axle due to camber thrust, leading to the possibility that the vehicle will spin out and roll over. Unless an additional control arm is included in the suspension to limit wheel travel under high lateral acceleration conditions, serious directional control problems are likely. This property of swing axle suspensions received much publicity as a result of its use on the Corvair passenger car in the 1960s [9].

ANTI-SQUAT AND ANTI-PITCH SUSPENSION GEOMETRY

In earlier chapters it was observed that under acceleration the load on the rear wheels increases due to longitudinal weight transfer. The load on the rear axle is:

$$W_r = W\left(\frac{b}{L} + \frac{a_x}{g}\frac{h}{L}\right) \tag{7-1}$$

The second term on the right side of this equation is the weight transfer effect. The weight is transferred to the axle and wheels principally through the suspension. Therefore, there is an implied compression in the rear suspension which, in the case of rear-drive vehicles, has been called "Power Squat." Concurrently, there is an associated rebound in the front suspension. The combination of rear jounce and front rebound deflections produces vehicle pitch. Suspension systems may be designed to counteract the weight transfer and minimize squat and pitch.

Equivalent Trailing Arm Analysis

Anti-squat forces can be generated on a rear-drive axle by choice of the suspension geometry. The mechanics of the system can be understood most easily by recognizing that all suspensions are functionally equivalent to a trailing arm with regard to the reaction of forces and moments onto the vehicle. For analysis purposes consider a drive axle restrained by upper and lower control arms as shown in Figure 7.11. The horizontal drive force at the ground is F_x. The force F_z is the vertical reaction at the ground caused by the vertical components of the control arm forces. Static vertical loads may be neglected in the analysis. Thus, writing Newton's Second Law for the horizontal and vertical directions and for the moments around the point "o" yields:

$$F_x + P_1 \cos\theta_1 - P_2 \cos\theta_2 = 0 \tag{7-2}$$

$$F_z - P_1 \sin\theta_1 - P_2 \sin\theta_2 = 0 \tag{7-3}$$

$$F_x z_2 - P_1 \cos\theta_1 z_1 = 0 \tag{7-4}$$

From Eq. (7-4) we can solve for P_1:

$$P_1 = \frac{F_x z_2}{z_1 \cos\theta_1} \tag{7-5}$$

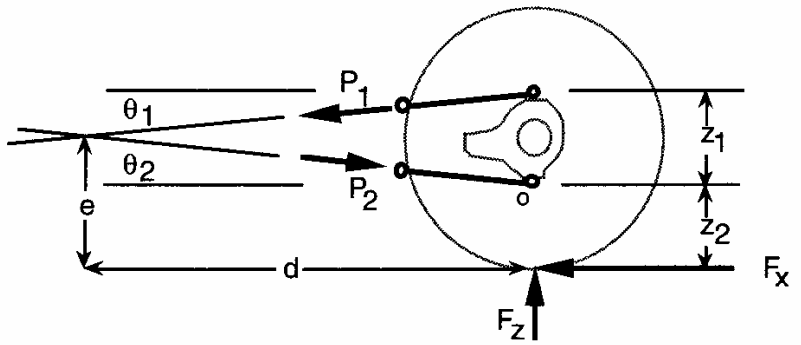

Fig. 7.11 Forces acting on a drive axle suspension system.

Assuming small angles and combining Eqs. (7-2) and (7-5):

$$P_2 = \frac{F_x (1 + z_2/z_1)}{\cos\theta_2} \tag{7-6}$$

Then using Eq. (7-3) to solve for F_z:

$$F_z = P_1 \sin\theta_1 + P_2 \sin\theta_2 = F_x \frac{z_2}{z_1} \tan\theta_1 + F_x \left(1 + \frac{z_2}{z_1}\right) \tan\theta_2 \tag{7-7}$$

From the geometry it is seen that:

$$\tan\theta_1 = \frac{z_2 + z_1 - e}{d} \quad \text{and} \quad \tan\theta_2 = \frac{e - z_2}{d} \tag{7-8}$$

When this is substituted into Eq. (7-7), the ratio of forces is seen to be:

$$\frac{F_z}{F_x} = \frac{e}{d} \tag{7-9}$$

The expression given in Eq. (7-9) is identical to that which would be obtained if the control arms were replaced with a single (trailing) arm pivoting on the body at the projected intersection of the control arm axes. The intersection represents a "virtual reaction point" where the torque reaction of the suspension control arms can be resolved into equivalent longitudinal and vertical forces imposed on the vehicle body.

Given that any suspension is functionally equivalent to a trailing arm, the anti-squat performance can be quantified by analyzing the free-body diagram of a rear-drive axle as shown in Figure 7.12. In the figure, point "A" is the imaginary pivot on the vehicle body. Since the arm is rigidly fastened to the axle (resisting axle windup), it has the ability to transmit a vertical force to the sprung mass which can be designed to counteract squat.

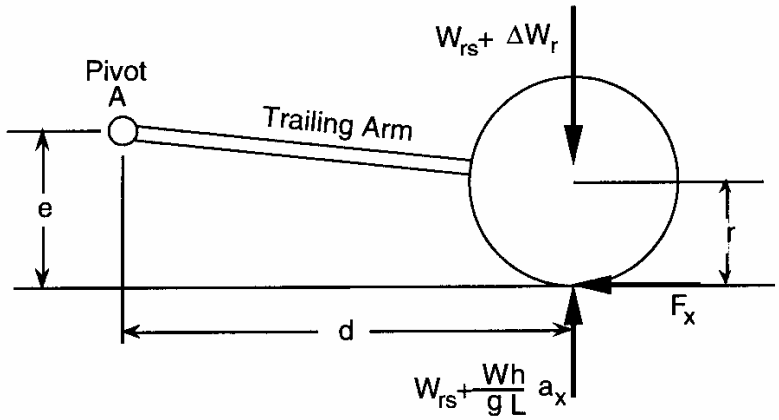

Fig. 7.12 Forces acting on a rear-drive axle during acceleration.

Rear Solid Drive Axle

The system is analyzed by applying NSL for the torques around the pivot point "A." The sum of these torques must be zero when the system is in equilibrium. Note that the wheel load is shown as consisting of a static component plus the dynamic component arising from longitudinal load transfer during acceleration. Also, for simplicity in the analysis, the rear axle weight will be neglected. Taking counterclockwise torques to be positive:

$$\Sigma M_A = W_{rs}\, d + \frac{W}{g}\frac{h}{L} a_x\, d - W_{rs}\, d - \Delta W_r\, d - F_x\, e = 0 \qquad (7\text{-}10)$$

where:

W_{rs} = Static load on the axle = Static load in the suspension

ΔW_r = Change in the suspension load under acceleration

This equation can be solved for the change in rear suspension load.

$$\Delta W_r = \frac{W}{g}\frac{h}{L} a_x - F_x \frac{e}{d} = K_r \delta_r \qquad (7\text{-}11)$$

where:

K_r = Rear suspension spring rate

δ_r = Rear suspension deflection (positive in jounce)

The front suspension is undergoing a rebound deflection because of the longitudinal load transfer, and has a magnitude of:

$$\Delta W_f = -\frac{W}{g}\frac{h}{L} a_x = K_f \delta_f \qquad (7\text{-}12)$$

The pitch angle of the vehicle, θ_p, during acceleration is simply the sum of the suspension deflections divided by the wheelbase. Thus we can write:

$$\theta_p = \frac{\delta_r - \delta_f}{L} = \frac{1}{L}\frac{W}{g}\frac{h}{L}\frac{a_x}{K_r} - \frac{1}{L}\frac{F_x}{K_r}\frac{e}{d} + \frac{1}{L}\frac{W}{g}\frac{h}{L}\frac{a_x}{K_f} \qquad (7\text{-}13)$$

Since F_x is simply the mass times the acceleration, $(W/g)a_x$, the equation can be rewritten:

$$\theta_p = \frac{1}{L}\frac{W}{g}\frac{h}{L}\frac{a_x}{K_r} - \frac{1}{L}\frac{W}{g}\frac{a_x}{K_r}\frac{e}{d} + \frac{1}{L}\frac{W}{g}\frac{h}{L}\frac{a_x}{K_f}$$

$$= \frac{1}{L}\frac{W}{g} a_x \left(\frac{1}{K_r}\frac{h}{L} - \frac{1}{K_r}\frac{e}{d} + \frac{1}{K_f}\frac{h}{L}\right) \qquad (7\text{-}14)$$

From this equation it is easy to show that zero pitch angle is achieved when the following condition is satisfied:

$$\frac{e}{d} = \frac{h}{L} + \frac{h}{L}\frac{K_r}{K_f} \qquad (7\text{-}15)$$

The first term on the right-hand side corresponds to the condition by which anti-squat is achieved on the rear suspension. That is, if e/d = h/L, the rear suspension will not deflect (jounce) during acceleration. The degree to which this is achieved is described as the percent anti-squat. For example, if e/d = 0.5 h/L, the suspension is said to be 50% anti-squat. Since h/L is in the vicinity of 0.2 for most passenger cars, full anti-squat generally requires an effective trailing arm length of about five times the elevation of "e."